



STUDIA UNIVERSITATIS
BABEŞ-BOLYAI

Volume 68, No. 1 (2023)

Engineering



UNIVERSITATEA BABEŞ-BOLYAI
BABEŞ-BOLYAI TUDOMÁNYEGYETEM
BABEŞ-BOLYAI UNIVERSITÁT
BABEŞ-BOLYAI UNIVERSITY
TRADITIO ET EXCELLENTIA



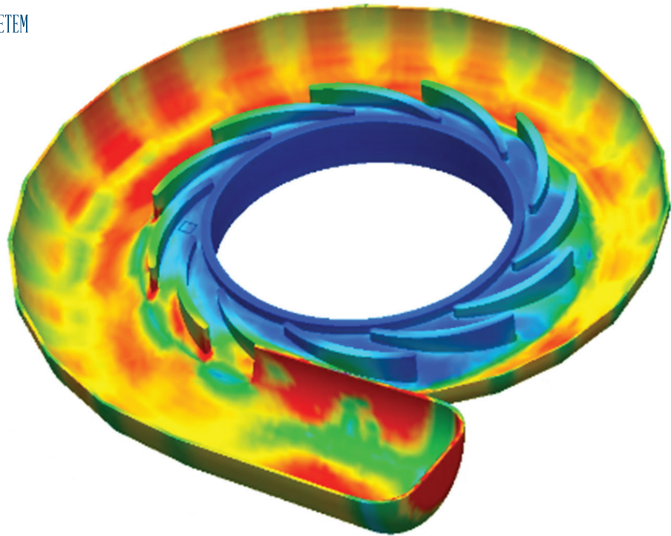
STUDIA UNIVERSITATIS
BABEŞ-BOLYAI
www.studia.ubbcluj.ro
51 B.P. Hasdeu Street, 400371
Cluj-Napoca, ROMANIA



CLUJ UNIVERSITY PRESS
www.editura.ubbcluj.ro

ISSN: 2734-7680

ISSN-L: 2734-7680





Studia Universitatis Babeş-Bolyai **ENGINEERING**

The Journal of the Faculty of Engineering at Reşiţa
Babeş-Bolyai University from Cluj-Napoca

Volume 68, No. 1, 2023

doi:10.24193/subbeng.2023.1

Published Online: 2023-11-15

ISSN (Online): 2734-7680

EDITORIAL OFFICE:

Piața Traian Vuia, Nr. 1-4, 320085, Reșița,
Caraș-Severin, România
http://studia.ubbcluj.ro/serii/engineering/index_en.html

EDITOR-IN-CHIEF:

Nicoleta GILLICH

BBU University Center in Reșița – Romania
Faculty of Engineering
nicoleta.gillich@ubbcluj.ro

© Studia Universitatis Babeș-Bolyai, Babeș-Bolyai University
B.P. Hasdeu str. no. 51, 400371 Cluj-Napoca, Romania
Phone: +40-264-405300 *6452; Fax: +40-264-591906
e-mail: office@studia.ubbcluj.ro

Hybrid Soft Computing System for Student Performance Evaluation

Victor Eguavoen*, Emmanuel Nwelih

Abstract. *Education Institutions have deployed technology accelerated learning systems and innovations for effective learning outcomes. Evaluating student's performance in these systems must align with the cognitive, affective, and psychomotor learning domains. In this research, a Hybrid soft computing system comprising of the Clustering Algorithm, Machine learning technique, and Optimization algorithm were hybridized and implemented to evaluate student academic performance using academic, social, and economic data of students. The proposed model demonstrated the best results with the lowest mean square error (MSE) and root mean square error (RMSE) values of 0.17 and 0.41, respectively. Additionally, the GANFIS model achieved values of 0.25 and 0.50, respectively, which slightly outperformed the proposed FCM-PSOAN-FIS model. The proposed model works better with bigger datasets, and it delivers higher predictive findings under settings that depict student learning capacities while assessing student academic achievement.*

Keywords: *Hybrid; Soft Computing; Clustering Algorithm; Machine learning; Optimization Algorithm.*

1. Introduction

Several stakeholders, including educators, organizations, and communities, are concerned about how understudies are presented [1]. As a result, graduates must study harder for excellent reviews to progress to the desire for enlistment offices. Student assessment is critical in the education sector because it allows individual schools to monitor their student achievement, which aids university entrance commissions in evaluating individual students' abilities and results [2]. The term "evaluation" refers to the method of assessing a program critically. It comprises acquiring and analyzing data on a program's features, operations, and results. It aims to analyze



programs, increase their efficiency, and/or provide programming advice. In education, performance evaluation (PE) is a common mechanism for determining the degree or extent of a student's successful learning outcomes. It includes a wide range of tasks, from writing a brief response to conducting and analyzing a laboratory investigation, all of which involve students creating an original response that demonstrates their abilities and reasoning. They are used to evaluate high-level reasoning and problem-solving skills, as well as emotions or behaviors, environmental or psychological experiences, and the ability to apply learning to real-world problems [3].

Student Performance Evaluation (SPE) is a type of testing that allows students to complete a task rather than choose a response from a pre-determined list, after which experienced raters (either teachers or other professional staff) assess the quality of the student's work using a collection of established specifications. Traditional evaluation use CGPA as an output attribute for evaluating student success, which educational psychology and similar disciplines contend is unreliable in evaluating students' academic performance [4]. Without having to employ their long-term logical thinking abilities, students react to each question individually. Despite their ignorance of the topic at hand, they frequently pass up chances to demonstrate their logical thinking. This method does not allow for simple adjustment of student learning development because it does not allow for collaborative and innovative thinking, which has been shown to improve technical and professional skills. Since, to enhance learning processes, most educational institutions use Technological Accelerated Learning (TAL) systems in the form of e-learning, distance learning, m-learning, or online learning. When it comes to conventional learning programs, student success is often assessed using the cognitive domain, which includes understanding, comprehension, implementation, interpretation, and synthesis. Feelings, thoughts, behaviors, beliefs, motivations, physical expression, balance, motor, and sensory abilities are frequently overlooked in the Affective and Psychomotor domain. Performance Evaluation of students in TALs should envelop the learning domain such as the cognitive, affective, and psychomotor [5].

Soft Computing (SC) refers to a class of machine learning approaches that use AI and evolutionary theory to provide a simple and effective solution to extremely tough problems when analytical (hard computing) formulations are not possible. SC techniques like the Particle Swarm Optimization (PSO) and the bacterial foraging optimization (BFO) now incorporate swarm intelligence and biological population foraging behavior. [6]. Particle Swarm Optimization is a strategy that involves a group of particles moving together in order to maximize results. Researchers claim that while a bunch of particles migrates, the velocity vectors known as the vector are used to shift the positions of the particles. Real-world samples and social models were examined in the early stages of particle swarm optimization [7] [8]. Since PSO is part of Swarm Intelligence, swarms or neurons cooperate to find the best solution [9]. Since PSO's concept is based on natural phenomena like bird flocking and fish schooling, it is a population algorithm.

The existing approach of evaluating student performance/examinations from juvenile (first year) to the peak year (final year) focused solely on the cognitive learning domain. It evaluates learners using CGPA as an output attribute for measuring student success, which educational psychology and similar disciplines contend is unreliable in assessing students' academic performance. The emotional intelligence (affective), environmental conditions of institutions, and student mental well-being (psychomotor) were not been factored into use. In other to overcome this drawback, we factor in some affective and psychomotor constraints such as the learning material type used, the economic and social background of the learner, and the environmental conditions of the learning institution and the student. To solve this issue, we use the Fuzzy Clustering approaches to group students as cognitive, affective, and psychomotor domains. The output variable would be the classified outcome, making the proposed model stable and dynamic enough to be used in any educational framework. Supervised learning has many drawbacks, such as dimensions, and it took many training trials to determine the best parameter to use. However, due to the excessive use of data, measuring student performance is becoming more difficult [10]. Fashioning how best to implement this process will assist the department to make a viable learning environment that will address the poor level of attaining specialized skills in computer science. Hence the need for a scientific approach called soft computing to tackle the drawbacks of using an existing approach is required.

The imprecision or ambiguity associated with assessing student success that combines most of the drawbacks/constraints mentioned above can only be significant if they are well incorporated. Assume that linguistic categories such as high, medium, low, and so on would be used to express these shortcomings. These types of measurements are vague, necessitating the use of a Fuzzy Inference System (FIS). Furthermore, machine learning model that collects these parameters must be adaptive to reveal secret information that could be useful in decision-making. As a result, an Adaptive Neuro-Fuzzy Inference System (ANFIS) was introduced. Despite an impressive and robust power of ANFIS, determining better solutions that best predict the test dataset based on the training model requires many experiments (training) and model parameter reconfiguration, such as category of stimulation utilities, learning rate etc. This will necessitate a significant amount of time and space. These parameters can be tweaked to yield better performance. A more robust derivative, the Particle Swarm Optimization (PSO) is considered in this analysis.

The goal of this study is to create a Soft Computing Clustering Expert Framework, the Fuzzy C-Means - Particle Swarm Optimization ANFIS (FCM-PSOANFIS) for evaluating students' overall performance utilizing computer science from the University of Benin (UNIBEN) as an evaluator. The goals are to:

1. Propose Soft Computing Clustering Expert Framework (FCM-PSO-ANFIS) for the evaluation of student performance
2. Implement and evaluate the feasibility of the proposed model using both simulated and department of computer science datasets.

This research reveals a perception of the various issues associated with the current form of evaluating student academic performances.

2.1. Related Work

Several previous pieces of research based on the mathematical and predictive models developed for the prediction of student's success. [11]. [12] Proposed the Neural Network (NN) to develop a technique of predicting student performance in mathematics courses that assists educators in identifying disadvantaged kids. They use four separate training algorithms to assess the classification potential of neural networks: Broyden-Fletcher-Goldfarb-Shanno (BFGS), LevenbergMarquardt (LM), Resilient Backpropagation (RRBP) and modified spectral Perry (MSP). In comparison to the other classification techniques, the MSP-trained FNNs exhibit more consistent behavior and have greater generalization accuracy. [13] Used Artificial Neural Networks (ANN) to create a framework that utilized the Multilayer Perceptron Topology to determine why some Nigerian colleges have low student performance. The academic achievement of over 70 percent of incoming freshmen may be reliably predicted by the model using ANN, according to test data analysis, which took several factors into account.

[14] Developed a system based on fuzzy logic to estimate the threat progress of the students based on some basic knowledge about academic achievement to assess the risk level of students. The simulated model reveals that prior academic achievement is associated with a level of risk. The study's results showed that in order to enhance a student's learning ability, an instructor must pay more attention to their weaknesses [15] introduces a novel approach to performance evaluation that is based on fuzzy logic. It takes into account three factors for a single academic course and evaluates student performance using the Mamdani approach. The findings indicate that this method may be used to evaluate students' performance at universities.

Numerous academics have used neural networks to forecast student outcomes, and one of these researchers [16] proposed a decision-support tool based on the NN that identifies "at-risk" students who do not continue their academic progress in the next year. About 70% of pupils' permanence was appropriately predicted by the program. [17] Proposed the model that predict e-learning outcome indicators using the Balanced Scorecard and Neural Networks. The study addresses the problem of small sample size data by using interpolation and principal component analysis, and the

proposed method is shown to be effective and applicable through numerical experiments on real data. The author has obtained an error in the prognosis of 3-4 percent which is appropriate from a realistic perspective. [13] Used a NN to evaluate variables influencing pupils' performance. According to their conclusions, they classified the pupils into three classes. The forecast accuracy that the paper's authors were able to achieve was around 74%. [18] Used a three-layer MLPN with back propagation training to predict graduation levels for graduates. The network model builds of authors had 70.27 percent precision for competent learners and 66.29 percent accuracy for incompetent graduates. [19], a genetic algorithm was used to select highly influential attributes associated with student success. The author compared two classification algorithms: Bayesian Network (BN) and Decision Tree (DT). The findings showed that BN outperformed DT due to its greater precision rating, with student attendance and GPA in the first semester being among the best among all classification algorithms. [20] Focuses on the creation of predictive models using multivariate linear regression, multilayer perceptron neural networks, radial basis function neural networks, and support vector machines to forecast the academic performance of students in an introductory engineering course titled Engineering Dynamics. This course is made up of 239 undergraduate students. The findings demonstrate that, with an average prediction accuracy of 89.0%-90.9% and good predictions of 62.3%-69.0%, the support vector machine model gives the overall best forecasts.

From the studies it revealed that most of the researcher focuses on the cognitive domain in the evaluation of student performance using soft computing as cited by [21], [11], and [19]. Some attribute to attendance, previous knowledge or results as cited by [19], [13]. [22], [23] attributed it to size, dataset, teachers, environmental, personal, social, [24], [20]. The majority of these studies appear to concentrate on a particular topic or course as the factors that influence academic success [11], [19], and [13]. To improve prediction accuracy, [11] suggested that future studies should focus on other variables that may influence student academic performance, such as temperament, intellect, and psychological factors. While many research have been carried out to assess students' academic achievement globally, there are insufficient studies to assess students' performance based on the cognitive, emotional, and psychomotor domains. The vacuum in the literature must be filled. Hence, the study aims to evaluate student performance using a soft computing model called FCM-PSOANFIS in the cognitive, affective, and psychomotor domains of students.

3. 1. Methodology

The proposed hybrid soft-computing model aims to incorporate multiple models of both conventional and technology-based learning systems that will solve several of the problems affecting the predictive and reasoning models. A hybrid of the

FCM-PSOANFIS model was used in this research to design an expert model of a multi-neuro-fuzzy system. The proposed model consists of knowledge databases, which stores pre-entrance, constraints, and academic records of students and stores optimized data. The PSO was integrated to identify solutions and parameters that best train the ANFIS model. The ANN in ANFIS streamlines the set of existing rules use for predicting academic achievement of the student grouping from FCM with necessary parameters and constraints retrieved from the learner database to solve a given new problem while the fuzzy logic part was adopted as a means for implying the imprecision in both constraint and education/academic records. These parameters, therefore, constitute the fuzzy parameter of the adaptive education mining system.

3.2. Proposed system’s dataset components and attributes

A specific record description contains three classes of data attributes which are Pre-entrance attributes; Constraint attributes and Academic data attributes. The reason for splitting the definition of the attributes into these classes is that it allows various constraints and requirements to be applied to particular entities and these constraints have to be met to conduct an effective mining operation. It also diminishes the effect of irrelevant or less-relevant attributes on the system performance and decomposes complex information in a more comprehensible manner. Table 1 and Table 2 show the pre-entrance attributes and academic data attributes.

Table 1. Pre-entrance attributes

S/N	Variable Name	Linguistic Variable Format	Variable Type
1	UTME Score (UTME)	3(Above 250), 2(200-250), 1(Below 200)	Categorical
2	Average Pre-Entrance or SSCE Result (Mathematics, English, Physics, Biology, Chemistry, etc.)	7(70 and Above), 6(60-69), 5(55-59), 4(50-54), 3(45-49), 2(40-44), 1(Below 40)	Categorical
3	SSCE Sitings (SS)	2(One sitting), 1(two Sitings)	Categorical
4	SSCE Exam Type (SST)	3(WAEC), 2(NECO), 1(NABTEB)	Categorical
5	Age of student at admission (Age)	3(Below 18 years), 2(18-23 years), 1(Above 23)	Categorical
6	Gender (Sex)	2(Male), 1(Female)	Categorical

Table 2. Academic data attributes

SN	Attributes/Variables	Description	Values	Type of attributes
1	Level	Level of student	100, 200, 300, 400, 500, 600, 700,800	Categorical
2	Subj1, Subj2 Subj3, Subj4, Subj5, Subj6, Subj7, Subj8, Subj9, Subj10	1 st Semester subjects scores	0 to 100	Continuous
3	Subj11, Subj12 Subj13, Subj14, Subj15, Subj16, Subj17, Subj18, Subj19, Subj20	2 nd Semester subjects scores	0 to 100	Continuous
4	Class	Class of Degree	1(Distinction), 2(upper Credit), 3(Lower Credit), 4(3 rd Class), 5(Fail)	Categorical

3.3. Component of particle swarm optimization (PSO)

Particles in the PSO algorithm move around the problem space, guided by their strongest prior position and the best prior position of the entire swarm or maybe a nearby neighbor. Every loop is modified by the particle's velocity in equation (1):

$$u_i(p + 1) = u_i(p) + \left(W_1 \times rand() \times (s_i^{best} - s_i(p)) \right) + \left(W_2 \times rand() \times (s_{gbest} - s_i(p)) \right) \quad (1)$$

Where W_1 and W_2 are the weight coefficients of the absolute best and universal positions, $u_i(p + 1)$ the current velocity of the i th particle, $s_i(p)$ is the location of an i th particle at time p , s_{gbest} is the renowned swarm position and s_i^{best} is the famous i th particle location. The function $rand()$ generates a variable $[1,0]$ which is uniformly random. Variants on this update equation take into account the best locations of a particle in time t within the local neighborhood. The particle Position is updated using the equation (2)

$$s_i(p + 1) = u_i(p) + s_i(p) \quad (2)$$

Fuzzy Logic (FL) and Neural Network (NN), two powerful data mining approaches, are combined to create the Adaptive Neuro-Fuzzy Inference System, or ANFIS for short. The Adaptive Neuro-Fuzzy Inference System combines FL and NN as its FL

and NN elements. This mechanism is under the control of FL and NN intensity. ANFIS have six layers, each of which has a unique property. The architectural layers of ANFIS are as follows.

3.3.1. Input/entering layer: Users can access ANFIS through this layer, which also accepts pre-entrance numerical vectors, undergraduate information, and constraints in various language qualities as inputs. These vectors serve as representations of the significant parameter values and training cycle variables for the model. The letter “Z” stands in for the fuzzy word for parameters (also known as attributes) and has a collection of linguistic or continuous values that guarantee the appropriate evaluation of the constraints/attributes. The Z_{ni} ‘scale is written as shown in equation (3)

$$Z_{ni} = \{M_{n1}..M_{ni}, R_{n1}..R_{ni}, P_{n1}..P_{ni}\} \quad (3)$$

Where:

$M1...Mi$ are linguistic variables for restriction values, and n is a significant indication in the datasets i , such as LMC, PSC, e.t.c, $R1...Ri$ is continuous values for Academic data parameters i such as ACA, TCE, and $P1...Pi$ are linguistic values for pre-entrance parameters i such as Sex, Age, e.t.c

Equation (4) illustrates how this can be described numerically.

$$A_i^1 = c_i \quad (4)$$

Where:

A_i^1 is the i^{th} contribution from the first layer of neurons

x_i = Each parameter’s input value

3.3.2. Layer of membership-function: The affiliate function, which maps inputs to fuzzy sets, is included in this layer. The Gaussian membership feature was used to assign parameters to the fuzzy scheme, Figure 1. Membership function with a Gaussian distribution can be mathematically represented as equation (5)

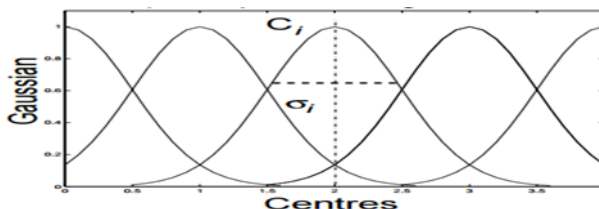


Figure 1. Membership function with a Gaussian distribution

$$\mu(v) = \exp\left(-\frac{(c_i - v)^2}{2A_i^2}\right) \quad (5)$$

Where:

C_i is the i th fuzzy set's center or mean

A_i = the i th fuzzy set's variance/width

V = each input parameter's value

$\mu(v)$ = v 's membership function

Membership function with a Gaussian distribution was used to map linguistic variables (constraint, academic data, and pre-entrance data) to a collection of members in this layer.

The Rule layer specifies the result for each set of inputs. A second layer with an input value is added to such layers. This layer implemented the Takagi-Sugeno inference model, which can be represented mathematically as formula (6).

$$A_i^3 = \mu(c_1) * \mu(c_2) * \dots * \mu(c_n) \quad (6)$$

Where:

$\mu(c_n)$ = variable n 's membership function

A_i^3 is the i^{th} neuron's layer 3 output.

In the Layer of normalization, each neuron is paired exclusively with a rule-layer neuron. The standardization layer verifies the input from the preceding layer. Equation (7) illustrates how this can be interpreted mathematically.

$$A_i^4 = \frac{A_i^3}{A_1^3 + A_2^3 + \dots + A_n^3} \quad (7)$$

Where:

A_i^4 is the i^{th} neuron production from layer 4.

A_i^3 is the i^{th} neuron production from layer 3.

n is the cumulative number of neurons in the third layer.

The normalization layer's input is all supplied into one neuron in the layer of defuzzification.

Defuzzification is the process of converting fuzzy values to actual values. Equation (8) illustrates how this may be expressed numerically.

$$A_i^5 = A_i^4(d_i(c_i) + d_2(c_2) + \dots + d_n(c_n) + u) \quad (8)$$

Where:

c_i is the vector n 's resultant parameter.

u = bias

A_i^5 is the i^{th} neuron production from layer 5.

c_i, d_i = subordinate parameters

Layer of output generated results, and the number of neurons within the said layer decides how many outputs the system produces. Equation (9) illustrates how it can be expressed mathematically.

$$A_i^6 = \sum_i^n A_i^5 \quad (9)$$

Where:

A_i^5 is the i^{th} neuron production from layer 5

A_i^6 is the i^{th} neuron production from layer 6 respectively.

Creating student profile module allow the educationist to generate a student profile comprising of all attributes captured from the student information record submitted to the department either from the hardcopy form or from the online application. This ensures that appropriate data are captured for the ANFIS component. The database will hold information about the student in their respective departments and will also provide a mechanism for storage and result retrieval. While the view student profile component allow the student to view their results based on the FCM-PSO-ANFIS model.

3.4 Model performance validation function

The fitness function is the root mean square error (RMSE) or mean square error (MSE), a particular method used for classification. Equation (10) was utilized to validate model findings. A predictive model with a smaller root mean square error (RMSE) can provide more data.

$$RMSE = \sqrt{\frac{1}{m} \sum_{j=1}^m (S_j^{real} - S_j^{prediction})^2} \quad (10)$$

Where:

m denotes the total number of samples to be analyzed.

j = sample index for research, $j = 1, 2, 3, \dots, n$,

S_j^{real} denotes the current situation,

$S_j^{prediction}$ denote the expected condition/outcome.

4.1. Results and Discussions

MATLAB was used in the development of the PSO component and ANFIS to optimize and store datasets. The APACHE HTTP server was used to distribute the user interfaces, which were developed using PHP and HTML. Datasets and tables were stored in MySQL. The suggested solution made use of MATLAB and includes the Adaptive Machine Learning (ANFIS), Particle Swarm Optimization, and Fuzzy Clustering-Means algorithms. 91 and 31 datasets were utilized/used for training. Root mean square error (RMSE) findings for ANFIS, GANFIS, and FCM-PSOANFIS were 0.65, 0.50, and 0.41, and 0.74, 0.41, and 0.44 respectively. When these data were compared, FCM-PSOANFIS showed more convergence than ANFIS and GANFIS.

4.2. ANFIS Model Training and Testing.

The performance of different models was evaluated using a training dataset of 91 students (Table 1). The proposed FCM-PSOANFIS model demonstrated the best results with the lowest mean square error (MSE) and root mean square error (RMSE) values of 0.17 and 0.41, respectively. These values indicate that the FCM-PSOANFIS model performed optimally on the training dataset. Similarly, the models were tested on a separate dataset of 39 students in the 200 level (Table 2). In terms of MSE and RMSE, the GANFIS model achieved values of 0.25 and 0.50, respectively, which slightly outperformed the proposed FCM-PSOANFIS model with values of 0.19 and 0.44. This suggests that the proposed algorithm can effectively handle both small and large datasets, meeting the required standards.

Table 1. Model Performance for Training Dataset

MODEL TYPE	MEAN SQUARE ERROR (MSE)	ROOT MEAN SQUARE ERROR (RMSE)	NO OF TRAINING DATA
ANFIS	0.42	0.65	91
GANFIS	0.25	0.50	91
FCM-PSOANFIS	0.17	0.41	91

Table 2. Model Performance for Testing Dataset

MODEL TYPE	MEAN SQUARE ERROR (MSE)	ROOT MEAN SQUARE ERROR (RMSE)	NO OF TRAINING DATA
ANFIS	0.54	0.74	39
GANFIS	0.172	0.41	39
FCM-PSOANFIS	0.19	0.44	39

5. Conclusion

The aim of evaluating student performance is to assist teachers and students in strengthening their teaching and learning processes. In this study, we developed a hybrid software model that will help educators and administrators evaluate students' academic success based on both academic outcomes and economic and social status. We used the Fuzzy Clustering Algorithm (Fuzzy C-Means), Optimization algorithms (Particle Swarm Optimization), and Adaptive Machine Learning (ANFIS). The results from training and testing using root mean square error (RMSE) for ANFIS, GANFIS and FCM-PSOANFIS where 0.65, 0.50, 0.41 and 0.74, 0.41, 0.44 respectively which show a higher convergence for the FCM-PSOANFIS when compare with ANFIS and GANFIS. The proposed model will provide more predictive results in any conditions that portray the student learning abilities and when used in assessing student academic performance. Future research should explore the application and verification of a combined bootstrap educational mining model by utilizing contemporary nature-inspired optimization algorithms like Grey Wolf, Artificial Bees, and Whale Optimization Techniques. Furthermore, an advisory mechanism should be established to enhance students' learning patterns through specialized learning techniques, employing an SMS alert system.

References

- 1 Kharola A., A hybrid ANFIS techniques for effective performance evaluation., *PM World Journal*, 4(9), 2015, pp. 21-39.
- 2 Mertens D., *Research and Evaluation in Education and Psychology: Integrating Diversity With Quantitative, Qualitative, and Mixed Methods*, SAGE Publications.
<https://books.google.com.ng/books?id=6RR7DwAAQBAJ>, 9781544333748, 2019

- 3 Liu O.L., Bridgeman B., Adler M.R., Measuring Learning Outcomes in Higher Education: Motivation Matters., *Educational Researcher* 41(9), 2012, <https://doi.org/10.3102/0013189X12459679>, pp. 352–362.
- 4 Tang J., Liu G. Pan i Q., A Review on Representative Swarm Intelligence Algorithms for Solving Optimization Problems: Applications and Trends, *IEEE/CAA Journal of Automatica Sinica*, 8(10), 2021, pp. 1627-1643.
[doi: 10.1109/JAS.2021.1004129](https://doi.org/10.1109/JAS.2021.1004129)
- 5 Zajmi L., Ahmed F.Y.H., Jaharadak A.A., Concepts, Methods, and Performances of Particle Swarm Optimization, Backpropagation, and Neural Networks, *Applied Computational Intelligence and Soft Computing Hindawi*, 2018, <https://doi.org/10.1155/2018/9547212>
- 6 Thandavaraj E., Gani N., Nasir M., A Review of Psychological Impact on Students Online Learning during Covid-19 in Malaysia, *Creative Education*, 12(6), 2021, [doi: 10.4236/ce.2021.126097](https://doi.org/10.4236/ce.2021.126097). pp. 1296-1306.
- 7 Boutakidis I, Rodriguez J. L., Academic motivation and engagement across three generations of Latino/a junior high school students, *Journal of Latinos and Education*, 21(5), 2022, <https://doi.org/10.1080/15348431.2019.1674147>
- 8 Udeni J., Ajantha S., Anuja D., *Student's Performance Evaluation in Online Education System vs Traditional Education system*, International Conference on Remote Engineering and Virtuak Instrumentation. Bangkok, Thailand: IEEE, 2015, pp. 127-131.
- 9 Lin C., Optimization of Bearing Locations for Maximizing First Mode Natural Frequency of Motorized Spindle-Bearing Systems Using a Genetic Algorithm., *Applied Mathematics*, 5, 2014, [doi: 10.4236/am.2014.514208](https://doi.org/10.4236/am.2014.514208)., pp. 2137-2152.
- 10 Faiz M. Al, Sadeq S., Particle Swarm Optimization Based Fuzzy-Neural Like PID Controller for TCP/AQM Router, *Intelligent Control and Automation*, 3(1), 2012, [doi: 10.4236/ica.2012.31009](https://doi.org/10.4236/ica.2012.31009)., pp. 71-77.
- 11 Amirah M.S., Wahidah H., Nur'aini A.R., A Review on Predicting Student's Performance Using Data Mining Techniques, *Procedia Computer Science*, 72, 2015, <https://doi.org/10.1016/j.procs.2015.12.157>. <https://www.sciencedirect.com/science/article/pii/S1877050915036182>, pp. 414-422.
- 12 Livieris I.E., Drakopoulou K., Pintelas P., Predicting students' performance using artificial neural networks, *8th PanHellenic Conference with International Participation Informaion and Communication Technologies*, 2012, pp. 321-328.
- 13 Rao G., Kumar K., Students Performance Prediction in Online Courses Using Machine Learning Algorithms, *United International Journal for Research&Technology (UIJRT)*, 2(11), 2021, pp. 74-79.

- 14 Oladokun V., Adebajo A., Charles-Owaba O., Predicting Students Academic Performance using Artificial Neural Network: A Case Study of an Engineering Course, *The Pacific Journal of Science and Technology*. 9(1). http://www.akamaiuniversityhttps://www.researchgate.net/publication/228526441_Predicting_Students_Academic_Performance_using_Artificial_Neural_Network_A_Case_Study_of_an_Engineering_Course, 2008.
- 15 Yao B., Hagrais H., Alhaddad M.J., Al-Ghazzawi D.M., A fuzzy logic-based system for the automation of human behavior recognition using machine vision in intelligent environments, *Soft Computing*, 19, 2015, <https://doi.org/10.1007/s00500-014-1270-4>, pp. 499-506.
- 16 Petrudi S.H.J., Pirouz M., Pirouz B., *Application of fuzzy logic for performance evaluation of academic students*, 13th Iranian Conference on Fuzzy Systems (IFSC), 2013, doi: 10.1109/IFSC.2013.6675615.
- 17 Petar H., Prediction of e-Learning Efficiency by Neural Networks, *Cybernetics and Information Technologies*, 12(2), 2012, DOI: 10.2478/cait-2012-0015
- 18 Cooper C., *Students At Risk: The Impacts of Self-Efficacy and Risk Factors on Academic Achievement*, 2015.
- 19 Khasanah A.U., Havarti, A Comparative Study to Predict Student's Performance Using Educational Data Mining Techniques, *IOP Conference Series: Materials Science and Engineering*, 215, 2017.
- 20 Karamouzis S.T., Vrettos A., *An Artificial Neural Network for Predicting Student Graduation Outcomes*, Proceedings of the World Congress on Engineering and Computer Science, Oct. 22-24, 2008, San Francisco https://www.academia.edu/67409477/An_Artificial
- 21 Huang S., Fang N., *Work in progress - Prediction of students' academic performance in an introductory engineering course*, Frontiers in Education Conference (FIE), S4D-1-S4D-3., 2011. DOI:10.1109/FIE.2011.6142729
- 22 Mrinal P., Taruna S., Towards the integration of multiple classifier pertaining to the Student's performance prediction, *Perspectives in Science*, 8, Available online at www.sciencedirect.com ScienceDirect, 2016, pp. 364-366,
- 23 Al-Hmouz A., Shen J., Al-Hmouz R., Yan J., Modeling and Simulation of An Adaptive Neuro-Fuzzy Inference System (ANFIS) for mobile learning, *IEEE Transactins on Learning Technologies*, 5(3), 2012, pp. 226-237.
- 24 Asif R., a.o., Analyzing undergraduate students' performance using educational data mining, *Journal of Comput. Educ.* 113, 2017, pp. 177-194.

Addresses:

- Osasu Victor Eguavoen, Wellspring University, College of Science & Computing, Department of Computer Science & Software Engineering, Irhirhi, Benin City, Edo State, Nigeria
victor_eguavoen@wellspringuni.edu.ng, eguavoenvictor@gmail.com
(* *corresponding author*)
- Dr. Emmanuel Nwelih, University of Benin, Faculty of Physical Sciences, Department of Computer Science, Benin City, Edo State, Nigeria.
emmanuel.nwelih@uniben.edu

Hall effect on unsteady MHD flow along vertical plate with variable temperature and mass diffusion in the presence of porous medium and chemical reaction

Manish Kumar, Gaurav Kumar*, Abdul Wadood Khan

Abstract. *The effects of chemical reaction and Hall current on the unsteady magneto hydrodynamic flow along a vertical plate with variable temperature and mass diffusion in the presence of a porous medium is studied here. The fluid flow model of this paper contains governing partial differential equations of the motion, energy, and diffusion equation. To simplify the analysis, the governing equations are transformed into dimensionless form using non-dimensional variables. The Laplace-transform technique is employed to obtain an exact solution for the flow equations of the MHD model. The results of the analysis are presented using graphical representations of the velocity profiles. With the help of graphs, we discussed the behavior of fluid velocities with different parameters, including the chemical reaction parameter, Hall currents parameter, accelerated parameter, magnetic field parameter, and permeability parameter, and the numerical values of Sherwood number have been tabulated. We found that the values obtained for velocity, concentration and temperature are in concurrence with the actual flow of the fluid.*

Keywords: *MHD flow, chemical reaction, Hall current*

1. Introduction

The influence of chemical reaction and Hall current on magneto hydrodynamic (MHD) flow has been extensively studied in various scientific and technological fields, including chemical engineering, mechanical engineering, biological science, and petroleum engineering. Researchers have investigated different aspects of MHD flow problems associated with these factors, focusing on diverse scenarios and phenomena. Raptis and Kafousias [4] examined MHD free convection flow and mass transfer through a porous medium bounded by an infinite vertical porous plate with



a constant heat flux. They aimed to understand the behavior of the flow and its interaction with the porous medium in the presence of MHD effects, chemical reactions, and heat transfer. Abo-Eldahab et al. [1] explored the impact of Hall current on MHD free-convection flow past a semi-infinite vertical plate with mass transfer. Their investigation sought to comprehend how the Hall current influenced the convective flow patterns and the transfer of mass between the fluid and the plate. Youn [10] focused on the heat and mass transfer in MHD micro polar flow over a vertical moving porous plate in a porous medium. Attia [2] analyzed the ion slip effect on unsteady Coquette flow with heat transfer under an exponential decaying pressure gradient. The investigation aimed to understand how the ion slip phenomenon influenced the flow behavior, heat transfer, and the overall fluid dynamics. The influence of chemical reaction and Hall current on MHD flow was also explored by Ibrahim and Makinde [3], they investigated the chemically reacting MHD boundary layer flow of heat and mass transfer over a moving vertical plate with suction. The study aimed to uncover the effects of these factors on the boundary layer flow, heat transfer, and mass transfer processes. Sahin and Chamkha [8] studied the effects of chemical reaction, heat and mass transfer, and radiation on MHD flow along a vertical porous wall in the presence of an induced magnetic field. Their investigation aimed to comprehend the combined impact of these factors on the flow characteristics, heat transfer, and mass transfer mechanisms occurring within the porous medium. Rajput and Kumar [6] focused on unsteady MHD flow past an impulsively started inclined plate with variable temperature and mass diffusion in the presence of Hall currents. By considering the effects of unsteadiness, variable temperature, mass diffusion, and Hall currents, they aimed to analyze the complex interactions and their influence on the flow behavior and heat and mass transfer. Further, they [5] have worked on chemical reaction effect on unsteady MHD flow past an impulsively started oscillating inclined plate with variable temperature and mass diffusion in the presence of Hall current. Sharma et al. [9] studied Influence of chemical reaction and radiation on unsteady MHD free convection flow and mass transfer through viscous incompressible fluid past a heated vertical plate immersed in porous medium in the presence of heat source. The study aimed to understand how the chemical reaction, radiation, and MHD effects influenced the convective flow patterns, heat transfer, and mass transfer in the presence of a porous medium. Rajput and Kumar [7] examined the effects of radiation and chemical reaction on MHD flow past a vertical plate with variable temperature and mass diffusion. Their investigation aimed to analyze the combined influence of radiation, chemical reaction, and MHD effects on the flow behavior, heat transfer, and mass transfer occurring near the vertical plate.

In this paper, we have investigate the influence of chemical reaction and Hall current on unsteady MHD flow along a vertical plate with variable temperature and mass diffusion in the presence of a porous medium. The present study provides

insights into how these factors affect the flow characteristics, heat transfer, and mass transfer processes. The results of their investigation are presented using graphical representations and tabulated data, which help visualize and summarize the findings.

2. Mathematical Analysis.

In this paper, consider unsteady MHD flow past on vertical plate with no electrical conductivity. The plate's x axis and z normal are taken along the flow of fluid. Fluid flow has a primary velocity u along the plate, while fluid has a secondary velocity v along the z -axis. The uniform strength magnetic field B_0 is applied perpendicular to the surface at angled φ . The plate and the fluid were first assumed to be at the same temperature T_∞ . It is assumed that C is the species concentration in the fluid. The temperature of the plate is increased to T_w at time $t > 0$ when the plate suddenly starts to rise vertically upward in its own plane in the positive x -direction with a velocity of $u_0 f(t)$. The concentration C near the plate is raised linearly with respect to time. The induced magnetic field can be ignored because the fluid has a relatively low Reynolds number value. So, under above assumptions, the flow model is as under.

Momentum equations

$$\frac{\partial u}{\partial t} = \nu \frac{\partial^2 u}{\partial z^2} + g\beta(T - T_\infty) + g\beta^*(C - C_\infty) - \frac{\sigma B_0^2 \text{Cos}^2 \varphi (u + mv \text{Cos} \varphi)}{\rho(1 + m^2 \text{Cos}^2 \varphi)} - \frac{\nu u}{K}, \quad (1)$$

$$\frac{\partial v}{\partial t} = \nu \frac{\partial^2 v}{\partial z^2} + \frac{\sigma B_0^2 \text{Cos}^2 \varphi (mu \text{Cos} \varphi - v)}{\rho(1 + m^2 \text{Cos}^2 \varphi)} - \frac{\nu v}{K}, \quad (2)$$

Diffusion equation

$$\frac{\partial C}{\partial t} = D \frac{\partial^2 C}{\partial z^2} - K_c (C - C_\infty), \quad (3)$$

Energy equation

$$\rho C_p \frac{\partial T}{\partial t} = k \frac{\partial^2 T}{\partial z^2} \quad (4)$$

Following are the initial and boundary conditions:

$$\left. \begin{aligned} t \leq 0 : u = 0, v = 0, T = T_\infty, C = C_\infty, \text{ for every } z, \\ t > 0 : u = u_0 f(t), v = 0, T = T_\infty + (T_w - T_\infty) \frac{u_0^2 t}{\nu}, C = C_\infty + (C_w - C_\infty) \frac{u_0^2 t}{\nu}, \text{ at } z=0, \\ u \rightarrow 0, v \rightarrow 0, T \rightarrow T_\infty, C \rightarrow C_\infty \text{ as } z \rightarrow \infty. \end{aligned} \right\} \quad (5)$$

Here u and v are the primary and the secondary velocities along x and z respectively, ν - the kinematic viscosity, ρ - the density, C_p - the specific heat at constant pressure, k - thermal conductivity of the fluid, D - the mass diffusion coefficient, g - gravitational acceleration, β - volumetric coefficient of thermal expansion, t - time, m - the Hall current parameter, T - temperature of the fluid, β^* - volumetric coefficient of concentration expansion, C - species concentration in the fluid, T_w - temperature of the plate, C_w - species concentration, ϕ - Angle of inclination, B_0 - the uniform magnetic field, σ - electrical conductivity.

To convert equations (1), (2), (3), and (4) into dimensionless form, the following non-dimensional quantities are introduced:

$$\left. \begin{aligned} \bar{z} &= \frac{zu_0}{v}, \quad \bar{u} = \frac{u}{u_0}, \quad \bar{v} = \frac{v}{u_0}, \quad S_c = \frac{v}{D}, \quad \mu = \rho\nu, \quad M = \frac{\sigma B_0^2 \nu}{\rho u_0^2}, \\ K_0 &= \frac{\nu K_c}{u_0^2}, \quad P_r = \frac{\mu C_p}{k}, \quad G_r = \frac{g\beta\nu(T_w - T_\infty)}{u_0^3}, \quad \theta = \frac{(T - T_\infty)}{(T_w - T_\infty)}, \\ G_m &= \frac{g\beta^* \nu(C_w - C_\infty)}{u_0^3}, \quad \bar{C} = \frac{(C - C_\infty)}{(C_w - C_\infty)}, \quad \bar{t} = \frac{tu_0^2}{v}, \end{aligned} \right\} \quad (6)$$

The symbols in dimensionless form are as under:

b - Acceleration parameter, θ - the temperature, \bar{C} - the concentration, G_r - thermal Grashof number, \bar{u} - the primary velocity, \bar{v} - the secondary velocity, μ - the coefficient of viscosity, P_r - the Prandtl number, S_c - the Schmidt number, \bar{t} - time, G_m - mass Grashof number, K_0 - The chemical reaction parameter, \bar{K} - permeability parameter of the medium, Ha - the magnetic parameter.

As a result, the model is:

$$\frac{\partial \bar{u}}{\partial \bar{t}} = \frac{\partial^2 \bar{u}}{\partial \bar{z}^2} + G_r \theta + G_m \bar{C} - \frac{(Ha)^2 \text{Cos}^2 \varphi (\bar{u} + m\bar{v} \text{Cos} \varphi)}{(1 + m^2 \text{Cos}^2 \varphi)} - \frac{1}{\bar{K}} \bar{u}, \quad (7)$$

$$\frac{\partial \bar{v}}{\partial \bar{t}} = \frac{\partial^2 \bar{v}}{\partial \bar{z}^2} + \frac{(Ha)^2 \text{Cos}^2 \varphi (m\bar{u} \text{Cos} \varphi - \bar{v})}{(1 + m^2 \text{Cos}^2 \varphi)} - \frac{1}{\bar{K}} \bar{v}, \quad (8)$$

$$\frac{\partial \bar{C}}{\partial \bar{t}} = \frac{1}{S_c} \frac{\partial^2 \bar{C}}{\partial \bar{z}^2} - K_0 \bar{C}, \quad (9)$$

$$\frac{\partial \theta}{\partial \bar{t}} = \frac{1}{P_r} \frac{\partial^2 \theta}{\partial \bar{z}^2}. \quad (10)$$

with the aforementioned boundary constraints:

$$\left. \begin{aligned} \bar{t} \leq 0 : \bar{u} = 0, \bar{v} = 0, \theta = 0, \bar{C} = 0, \text{ for every } \bar{z}, \\ \bar{t} > 0 : \bar{u} = f(\bar{t}), \bar{v} = 0, \theta = \bar{t}, \bar{C} = \bar{t}, \text{ at } \bar{z} = 0. \\ \bar{u} \rightarrow 0, \bar{v} \rightarrow 0, \theta \rightarrow 0, \bar{C} \rightarrow 0, \text{ as } \bar{z} \rightarrow \infty. \end{aligned} \right\} \quad (11)$$

When we drop bars from the equations above, we obtain:

$$\frac{\partial u}{\partial t} = \frac{\partial^2 u}{\partial z^2} + G_r \theta + G_m C - \frac{(Ha)^2 \text{Cos}^2 \varphi (u + mv \text{Cos}^2 \varphi)}{(1 + m^2 \text{Cos}^2 \varphi)} - \frac{1}{K} u, \quad (12)$$

$$\frac{\partial v}{\partial t} = \frac{\partial^2 v}{\partial z^2} + \frac{(Ha)^2 \text{Cos}^2 \varphi (mu \text{Cos} \varphi - v)}{(1 + m^2 \text{Cos}^2 \varphi)} - \frac{1}{K} v, \quad (13)$$

$$\frac{\partial C}{\partial t} = \frac{1}{S_c} \frac{\partial^2 C}{\partial z^2} - K_0 C, \quad (14)$$

$$\frac{\partial \theta}{\partial t} = \frac{1}{P_r} \frac{\partial^2 \theta}{\partial z^2}. \quad (15)$$

with the boundary conditions:

$$\left. \begin{aligned} t \leq 0 : u = 0, v = 0, \theta = 0, C = 0, \text{ for every } z, \\ t > 0 : u = f(t), v = 0, \theta = t, C = t, \text{ at } z = 0, \\ u \rightarrow 0, v \rightarrow 0, \theta \rightarrow 0, C \rightarrow 0, \text{ as } z \rightarrow \infty. \end{aligned} \right\} \quad (16)$$

Combining equations (12) and (13) in the following form:

$$\frac{\partial q}{\partial t} = \frac{\partial^2 q}{\partial z^2} + G_r \theta + G_m C - \frac{(Ha)^2 \text{Cos}^2 \varphi (1 - im \text{Cos} \varphi) q}{1 + m^2 \text{Cos}^2 \varphi} - \frac{q}{K}, \quad (17)$$

$$\frac{\partial C}{\partial t} = \frac{1}{S_c} \frac{\partial^2 C}{\partial z^2} - K_0 C, \quad (18)$$

$$\frac{\partial \theta}{\partial t} = \frac{1}{P_r} \frac{\partial^2 \theta}{\partial z^2}. \quad (19)$$

the boundary conditions:

$$\left. \begin{aligned} t \leq 0 : q = 0, \theta = 0, C = 0, \text{ for every } z, \\ t > 0 : q = f(t), \theta = t, C = t, \text{ at } z=0, \\ q \rightarrow 0, \theta \rightarrow 0, C \rightarrow 0, \text{ as } z \rightarrow \infty. \end{aligned} \right\} \quad (20)$$

The standard Laplace-transform method is used to solve the dimensionless governing equations (17) to (19), subject to the boundary conditions (20). The found solutions are as follows:

$$\begin{aligned} C = & \frac{1}{4\sqrt{K_0}} \exp(-z\sqrt{S_c K_0}) \left\{ \operatorname{erfc}\left[\frac{1}{2\sqrt{t}}(z\sqrt{S_c} - 2t\sqrt{K_0})\right](-z\sqrt{S_c} \right. \\ & + 2t\sqrt{K_0}) + \exp(2z\sqrt{S_c K_0}) \operatorname{erfc}\left[\frac{1}{2\sqrt{t}}(z\sqrt{S_c} + 2t\sqrt{K_0})\right](z\sqrt{S_c} \\ & \left. + 2t\sqrt{K_0}) \right\}. \end{aligned}$$

$$\theta = t \left\{ \left(1 + \frac{z^2 P_r}{2t}\right) \operatorname{erfc}\left[\frac{z\sqrt{P_r}}{2\sqrt{t}}\right] - \frac{z\sqrt{P_r}}{\sqrt{\pi\sqrt{t}}} \exp\left(-\frac{z^2}{4t}\right) P_r \right\}.$$

Case 1: In this case, we considered the motion of the surface with uniform velocity, and the velocity is

$$\begin{aligned} q = & \frac{e^{-\sqrt{a}z}}{2} \left(1 + \operatorname{erf}\left[\frac{2\sqrt{at} - z}{2\sqrt{t}}\right] + e^{2\sqrt{a}z} \operatorname{erfc}\left[\frac{2\sqrt{at} + z}{2\sqrt{t}}\right] \right) + \frac{1}{4a^2} G_r \{ z\chi_{11} \\ & + 2 \exp(-\sqrt{a}z) \chi_2 P_r + 2 \chi_{14} \chi_4 (1 - P_r) \} + \frac{G_m}{4(a - K_0 S_c)^2} \{ z\chi_{11} + 2 \chi_{13} \chi_5 \\ & (1 - S_c) + 2 \exp(-\sqrt{a}z) \chi_2 S_c (1 - tK_0) - \frac{1}{\sqrt{a}} z \exp(-\sqrt{a}z) \chi_3 K_0 S_c \} \\ & - \frac{1}{2a^2 \sqrt{\pi}} G_r \{ 2za \exp\left(-\frac{z^2 P_r}{4t}\right) \sqrt{tP_r} + \sqrt{\pi} \chi_{14} (\chi_6 + \chi_7 P_r) + \sqrt{\pi} \chi_{12} \\ & (az^2 P_r - 2 + 2at + 2P_r) \} + \frac{G_m \sqrt{S_c}}{2\sqrt{\pi} (a - K_0 S_c)^2} \left\{ \frac{1}{2\sqrt{K_0}} \exp(-z\sqrt{K_0 S_c}) \right. \\ & \left. \chi_9 \sqrt{\pi S_c} (S_c K_0 - az) + \chi_{13} \sqrt{\pi} A_{10} (S_c - 1) + \exp(-z\sqrt{K_0 S_c}) \sqrt{\pi} \chi_8 (1 \right. \\ & \left. - at - S_c + tK_0 S_c) \right\} \end{aligned}$$

Case 2: In this case, we studied the motion of the surface with exponentially accelerating, after which the fluid's velocity is

$$\begin{aligned}
q &= \frac{1}{2} \exp(bt - \sqrt{a+bz})(1 + \operatorname{erfc}[\frac{2\sqrt{a+bt} - z}{2\sqrt{t}}] + \exp(2\sqrt{a+bz}) \\
&\operatorname{erfc}[\frac{2\sqrt{a+bt} + z}{2\sqrt{t}}]) + \frac{1}{4a^2} G_r \{z\chi_{11} + 2\exp(-\sqrt{az})\chi_2 P_r + 2\chi_{14}\chi_4 \\
&(1 - P_r)\} + \frac{G_m}{4(a - K_0 S_c)^2} \{z\chi_{11} + 2\chi_{13}\chi_5(1 - S_c) + 2\exp(-\sqrt{az})\chi_2 \\
&S_c(1 - tK_0) - \frac{1}{\sqrt{a}} z \exp(-\sqrt{az})\chi_3 K_0 S_c\} - \frac{1}{2a^2 \sqrt{\pi}} G_r \{2za \exp(\frac{-z^2 P_r}{4t}) \\
&\sqrt{tP_r} + \sqrt{\pi}\chi_{14}(\chi_6 + \chi_7 P_r) + \sqrt{\pi}\chi_{12}(az^2 P_r - 2 + 2at + 2P_r)\} \\
&+ \frac{G_m \sqrt{S_c}}{2\sqrt{\pi}(a - K_0 S_c)^2} \{ \frac{1}{2\sqrt{K_0}} \exp(-z\sqrt{K_0 S_c})\chi_9 \sqrt{\pi S_c} (S_c K_0 - az) \\
&+ \chi_{13} \sqrt{\pi} A_{10} (S_c - 1) + \exp(-z\sqrt{K_0 S_c})\sqrt{\pi}\chi_8(1 - at - S_c + tK_0 S_c)\}
\end{aligned}$$

where,

$$q = u + iv, \quad a = \frac{(Ha)^2 \operatorname{Cos}^2 \varphi (1 - im \operatorname{Cos} \varphi)}{1 + m^2 \operatorname{Cos}^2 \varphi} + \frac{1}{K}.$$

$$\chi_1 = 1 + \chi_{16} + \exp(2\sqrt{az})(1 - \chi_{17}), \quad \chi_2 + \chi_1 = 0,$$

$$\chi_3 + \exp(2z\sqrt{a})(1 - \chi_{17}) = 1 + \chi_{16}, \quad \chi_4 + 1 = \chi_{22} + \chi_{18}(\chi_{23} - 1),$$

$$\chi_5 + 1 = \chi_{24} + \chi_{19}(\chi_{25} - 1), \quad \chi_6 + \chi_{26} + 1 = \chi_{18}(\chi_{27} - 1),$$

$$\chi_7 + \chi_6 = 0, \quad \chi_8 + \chi_{20} + 1 = \chi_{30}(\chi_{21} - 1),$$

$$\chi_9 = 1 + \chi_{20} + \chi_{30}(\chi_{21} - 1), \quad \chi_{10} + \chi_{28} + 1 = \chi_{19}(\chi_{29} - 1),$$

$$z\chi_{11} = \exp(-\sqrt{az})(2\chi_1 + 2at\chi_2 + \sqrt{a}\chi_3), \quad \chi_{12} + 1 = \operatorname{erfc}[\frac{z\sqrt{P_r}}{2\sqrt{t}}],$$

$$\chi_{13} = \exp(\frac{at - tK_0 S_c}{S_c - 1} - z\chi_{31}\sqrt{S_c}), \quad \chi_{14} = \exp((\chi_{32})^2 t - z\chi_{32}\sqrt{P_r}),$$

$$\chi_{15} = 1, \quad \chi_{16} = \operatorname{erfc}[\frac{2\sqrt{at} - z}{2\sqrt{t}}] \quad \chi_{17} = \operatorname{erfc}[\frac{2\sqrt{at} + z}{2\sqrt{t}}],$$

$$\begin{aligned}
\chi_{18} &= \exp(-2z\chi_{32}\sqrt{P_r}), \chi_{19} = \exp(-2z\chi_{31}\sqrt{S_c}), \\
\chi_{20} &= \operatorname{erf}[\sqrt{tK_0} - \frac{z\sqrt{S_c}}{2\sqrt{t}}], \chi_{21} = \operatorname{erf}[\sqrt{tK_0} + \frac{z\sqrt{S_c}}{2\sqrt{t}}], \\
\chi_{22} &= \operatorname{erf}[\frac{1}{2t}(z - 2t\chi_{32}\sqrt{P_r})], \chi_{23} = \operatorname{erf}[\frac{1}{2t}(z + 2t\chi_{32}\sqrt{P_r})], \\
\chi_{24} &= \operatorname{erf}[\frac{1}{2t}(z - 2t\chi_{31}\sqrt{S_c})], \chi_{25} = \operatorname{erf}[\frac{1}{2t}(z + 2t\chi_{31}\sqrt{S_c})], \\
\chi_{26} &= \operatorname{erf}[\frac{1}{2\sqrt{t}}(2t\chi_{32} - z\sqrt{P_r})], \chi_{27} = \operatorname{erf}[\frac{1}{2\sqrt{t}}(2t\chi_{32} + z\sqrt{P_r})], \\
\chi_{28} &= \operatorname{erf}[\sqrt{t}\chi_{31} - \frac{zS_c}{2\sqrt{t}}], \chi_{29} = \operatorname{erf}[\sqrt{t}\chi_{31} + \frac{zS_c}{2\sqrt{t}}], \\
\chi_{30} &= \exp(2z\sqrt{K_0}\sqrt{S_c}), (\chi_{31})^2 = \frac{(a-K_0)}{S_c-1}, (\chi_{32})^2 = \frac{a}{P_r-1}
\end{aligned}$$

2.1. Sherwood Number

The dimensionless Sherwood number is given by

$$\begin{aligned}
S_h = \left(\frac{\partial C}{\partial z} \right)_{z=0} &= \operatorname{erfc}[-\sqrt{tK_0}] \left(-\frac{1}{4\sqrt{K_0}} \sqrt{S_c} - \frac{t\sqrt{S_c K_0}}{2} \right) + \sqrt{S_c} \operatorname{erfc}[\sqrt{tK_0}] \left(\frac{1}{4\sqrt{K_0}} \right. \\
&\quad \left. + t\sqrt{K_0} \right) - \frac{e^{-tK_0} \sqrt{tS_c K_0}}{\sqrt{\pi K_0}},
\end{aligned}$$

The numerical values of S_h are given in table-1 for different parameters.

3. Results and Discussion

In this paper, graphical representations of the analytical solution obtained for the MHD fluid velocity, which has two components-primary velocity u and secondary velocity v in the transverse direction and along the direction of motion of the surface, are shown in figures 1 to 14. Here, two cases are discussed thought graph: Figures 1 to 6 show the velocity profile for the first case's various parameters, such as the magnetic field parameter (Ha), Hall parameter (m), chemical reaction

parameter (K_0), acceleration parameter (b), and permeability parameter (K), while additional figures are shown for the second case of the solution. It is observed that in both situations, primary velocity and secondary velocity each reach an extreme value in the area close to the plate before gradually decreasing to reach free stream value. Figures 1 and 7 show that as the angle of inclination φ increases, the primary fluid velocity rises and the secondary fluid velocity falls. From figures 2 and 10, it can be concluded that as permeability parameter K increases, then rise the velocities. This is because a decrease in the resistance of the porous medium, as indicated by an increase in the permeability parameter K , tends to accelerate primary and secondary velocities in the boundary layer region. It seems that the velocities decrease as the chemical reaction parameter K_0 increases (Figures 3, 4, and 11, 12). It can be seen from figures 5 and 13 that speeds rise as the Hall current parameter m is raised. Additionally, figures 6 and 14 show that increasing values of the parameter Ha have the opposite effect on u and v . Figures 8 and 9 show that when velocities increase, the acceleration parameter b also increases.

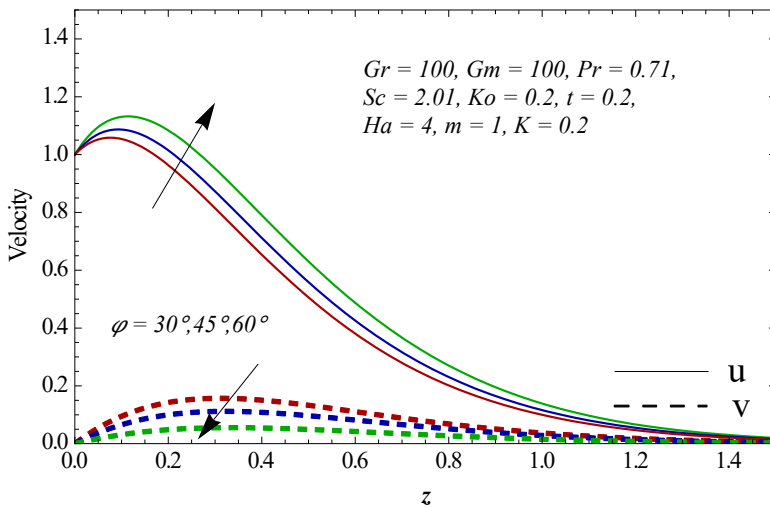


Figure 1. Velocity u and v for different values of φ

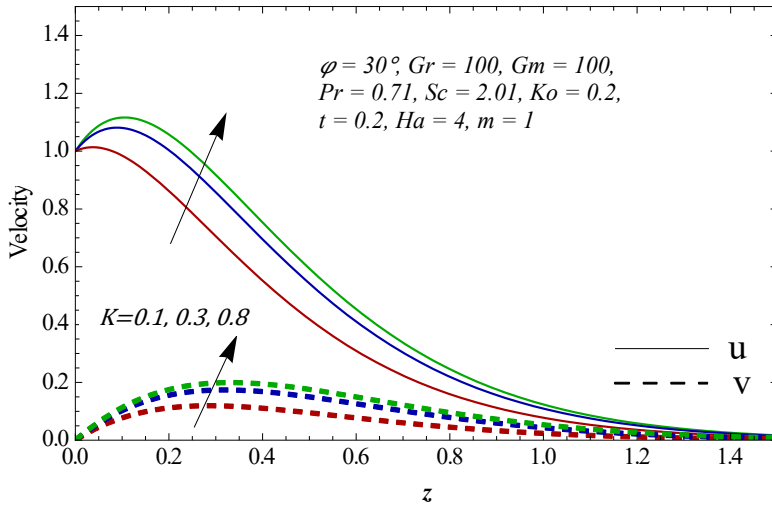


Figure 2. Velocity u and v for different values of K

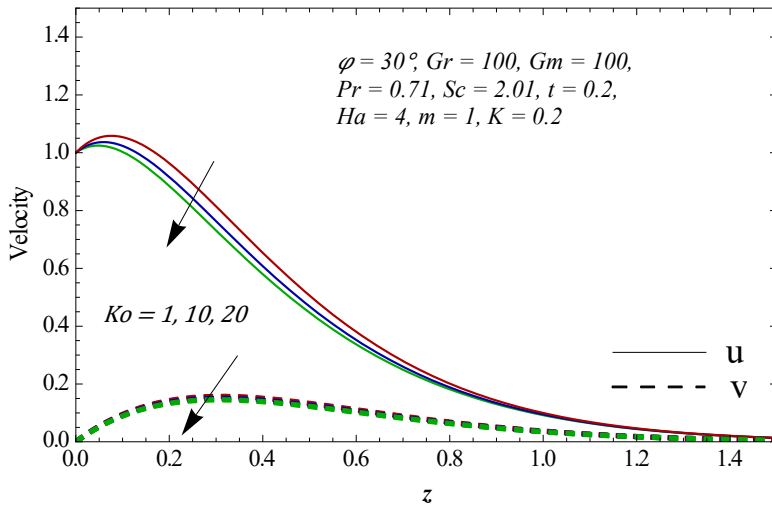


Figure 3. Velocity u and v for different values of Ko

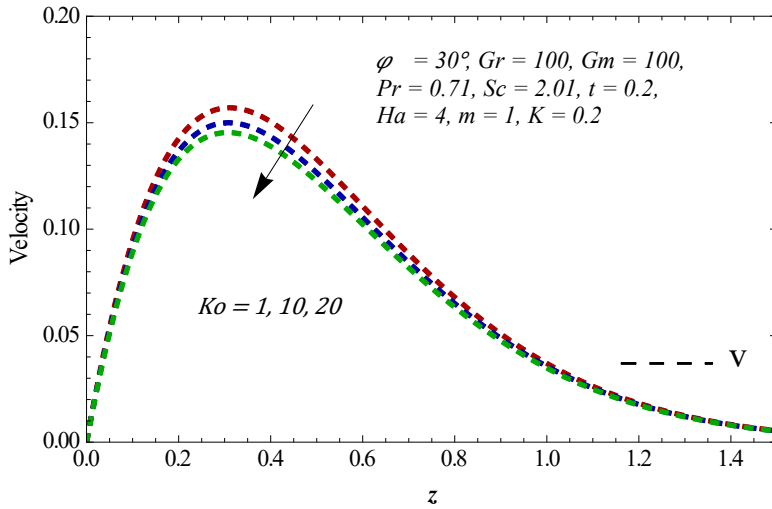


Figure 4. Velocity v for different values of Ko

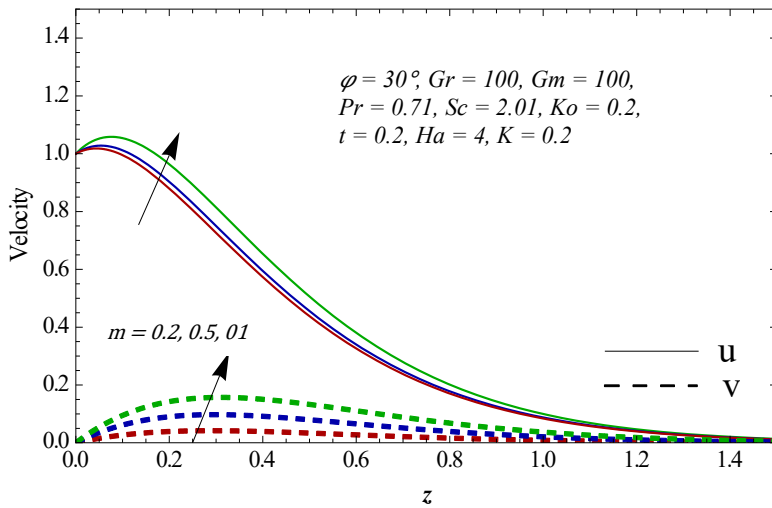


Figure 5. Velocity u and v for different values of m

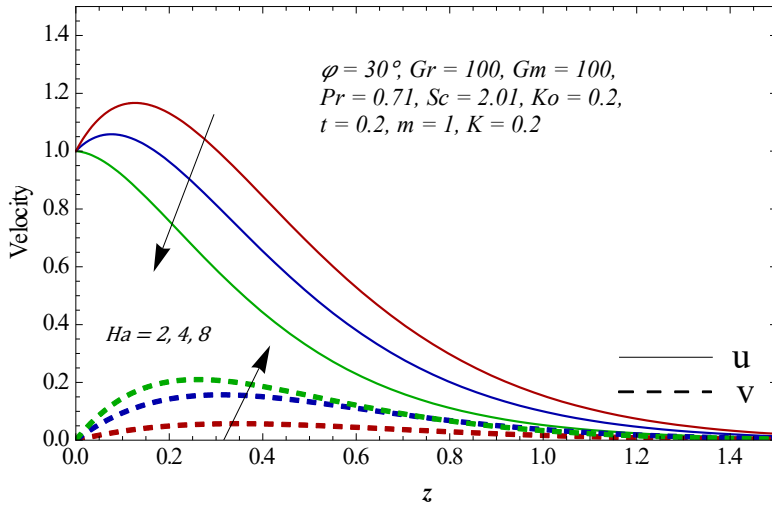


Figure 6. Velocity u and v for different values of Ha

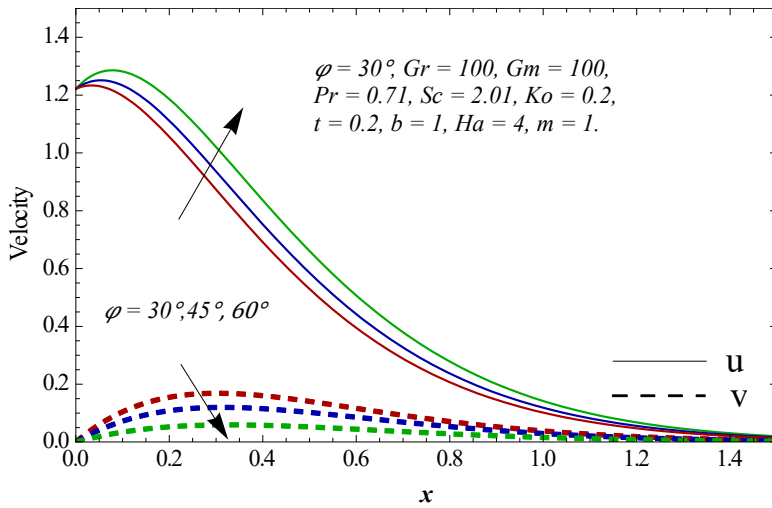


Figure 7. Velocity u and v for different values of φ

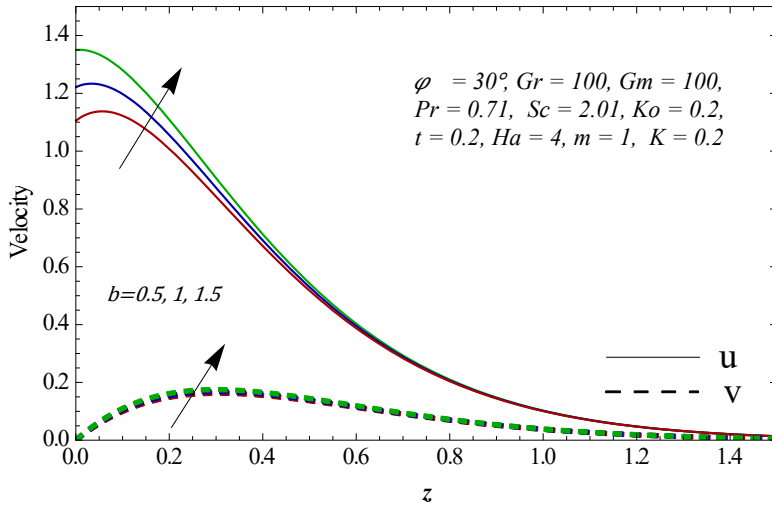


Figure 8. Velocity u and v for different values of b

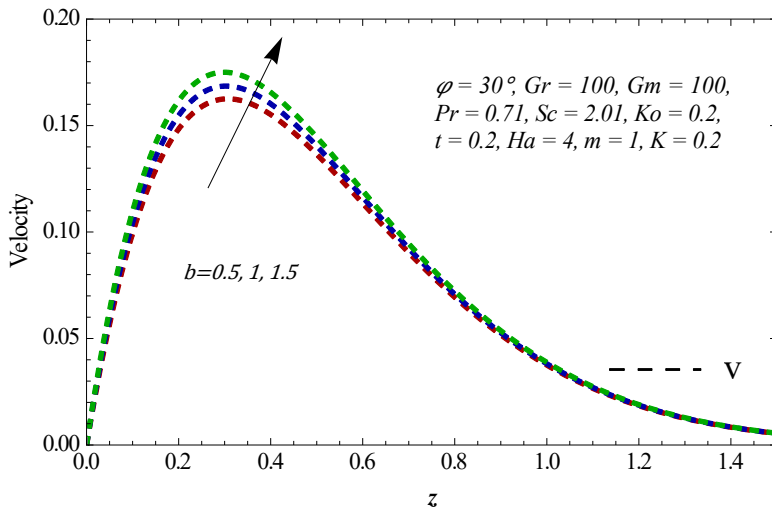


Figure 9. Velocity v for different values of b

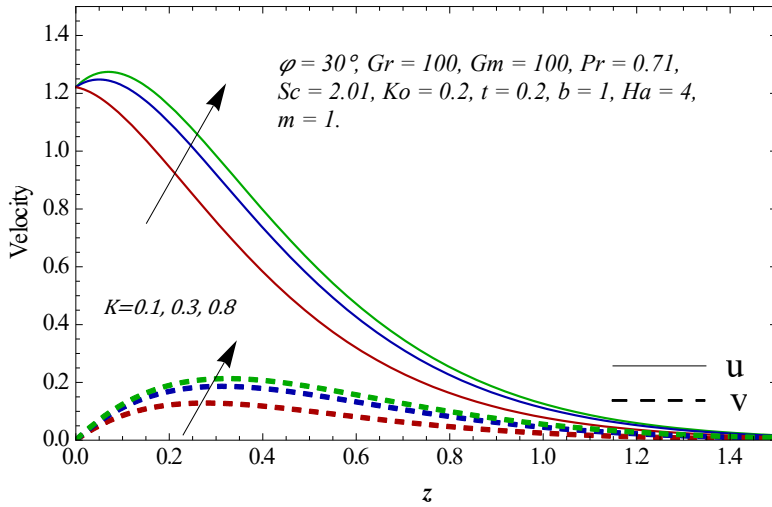


Figure 10. Velocity u and v for different values of K

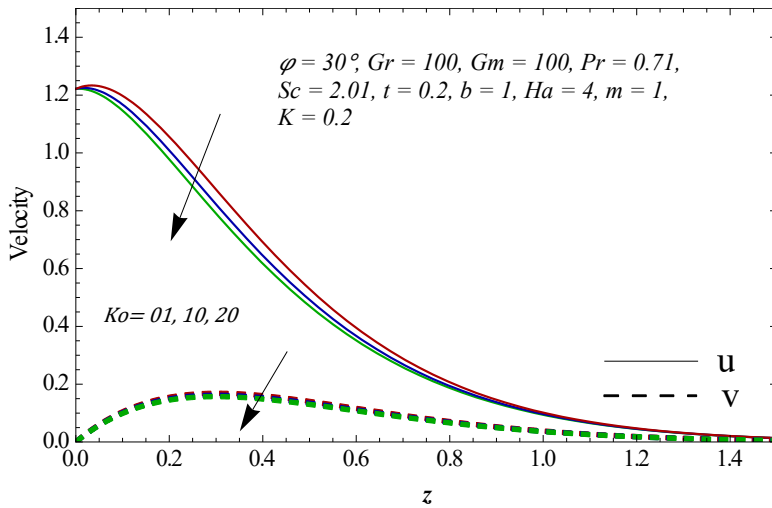


Figure 11. Velocity u and v for different values of Ko

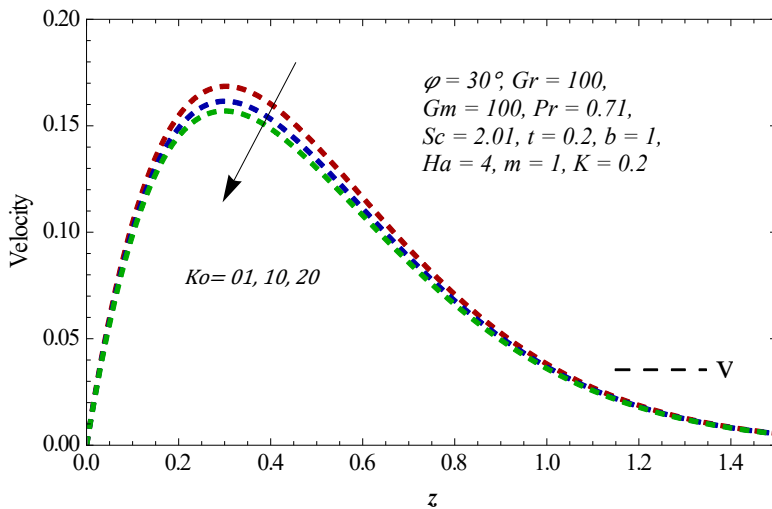


Figure 12. Velocity v for different values of Ko

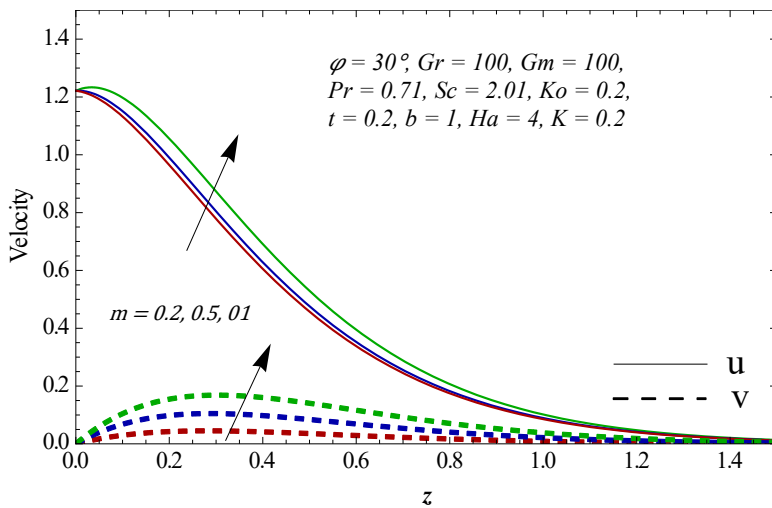


Figure 13. Velocity u and v for different values of m

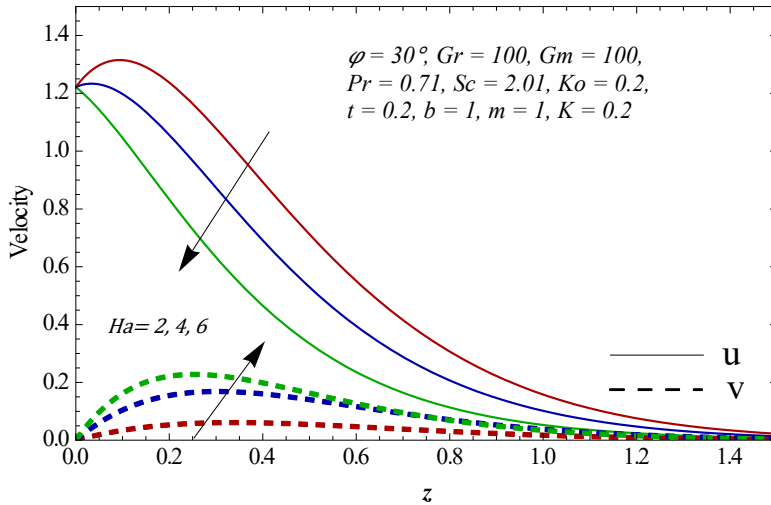


Figure 14. Velocity u and v for different values of Ha

Table 1. Sherwood number for different Parameters

K_0	Sc	t	S_h
01	2.01	0.2	-0.7622
10	2.01	0.2	-1.1182
20	2.01	0.2	-1.4264
05	3.00	0.2	-1.1399
05	4.00	0.2	-1.3162
05	2.01	0.3	-1.2602
05	2.01	0.4	-1.5814

4. Conclusion

An analytical investigation has been conducted for the MHD fluid flow model under the consideration by converting the governing linear partial differential equations into non dimensional form. It has been observed that raising the chemical reaction parameter causes a decrease in boundary layer velocity. The velocity of

fluid close to the surface increase as the acceleration parameter increases. It has been noted that Hall current tends to slow secondary fluid flow velocity while accelerating primary flow of the velocity. We observed that the values obtained for velocity, concentration and temperature are in concurrence with the actual flow of the MHD fluid.

References

- 1 Abo-Eldahab E.M., Elbarbary E.M.E., Hall current effect on magneto hydrodynamic free-convection flow past a semi-infinite vertical plate with mass transfer, *Int. J. Engg. Sci.*, 39, 2001, pp.1641-1652.
- 2 Attia H.A., Ion slip effect on unsteady couette flow with heat transfer under exponential decaying pressure gradient, *Tamkang Journal of Science and Engineering*, 12(2), 2009, pp 209-214.
- 3 Ibrahim S.Y., Makinde O.D., Chemically reacting MHD boundary layer flow of heat and mass transfer over a moving vertical plate with suction, *Scientific Research and Essays*, 5(19), 2010, pp 2875-2882.
- 4 Raptis A., Kafousias N.G., Magnetohydrodynamic free convection flow and mass transfer through porous medium bounded by an infinite vertical porous plate with constant heat flux, *Can. J. Phys.*, 60(12), 1982, pp. 1725-1729.
- 5 Rajput U.S., Kumar G., Chemical reaction effect on unsteady MHD flow past an impulsively started oscillating inclined plate with variable temperature and mass diffusion in the presence of Hall current, *Applied Research Journal*, 2(5), 2016, pp. 244-253.
- 6 Rajput U.S., Kumar G., Unsteady MHD flow past an impulsively started inclined plate with variable temperature and mass diffusion in the presence of Hall currents, *Applications and Applied Mathematics: An International Journal (AAM)*, 11(2), 2016, pp 693-703.
- 7 Rajput U.S., Kumar G., Effects of radiation and chemical reaction on MHD flow past a vertical plate with variable temperature and mass diffusion, *Journal of Naval Architecture and Marine Engineering*, 16, 2019, pp. 99-108.
- 8 Sahin A., Chamkha A.J., Effects of chemical reaction, heat and mass transfer and radiation on the MHD flow along a vertical porous wall in the presence of induced magnetic field, *Int. Journal of Industrial Mathematics*, 2(4), 2010, pp. 245-261.
- 9 Sharma P.R., Kumar N., Sharma P., Influence of chemical reaction and radiation on unsteady MHD free convection flow and mass transfer through viscous incompressible fluid past a heated vertical plate immersed in porous medium in the presence of heat source, *Appl. Math. Sciences*, 5(46), 2011, pp. 2249-2260.
- 10 Youn J. K., Heat and mass transfer in MHD micropolar flow over a vertical moving porous plate in a porous medium, *Transport in Porous Media*, 56(1), 2004, pp. 17-37.

Addresses:

- Mr. Manish Kumar, Department of Mathematics and Statistics, Integral University, Lucknow, India.
mkumarmath84@gmail.com
- Dr. Gaurav Kumar, Department of Mathematics and Computer Science, BBD University, Lucknow, U.P, India.
logontogauravsharma@gmail.com
(* *corresponding author*)
- Dr. Abdul Wadood Khan, Department of Mathematics and Statistics, Integral University, Lucknow, India.
awkhan@iul.ac.in

Study for a photovoltaic system to supply electricity to an isolated apiary

Eugen Răduca, Mihaela Molnar*, Cristinel Popescu, Cornel Hațiegan

Abstract *The paper presents, based on the study and the experience of the authors in the field, some considerations, especially from an application aspect, useful in building a photovoltaic system for supplying electricity to an isolated apiary, as well as simulations for such a system, made with the PVGIS program . The main high-performing electric machines of today with relatively high energy consumption from an isolated beehive are identified, as well as their specific mode of use, during a calendar year, an essential factor for establishing the installed power of such a photovoltaic system and a its effective technical-economic design.*

Keywords: *apiary, isolated, system, photovoltaic*

1. Introduction

Apiary is the generic name for an agricultural formation that includes several hives with bees and a set of specific tools and equipment used by the beekeeper (the person who works in the apiary) to extract honey [1], [2] produced by bees and other adjacent products, such as: pollen, royal jelly, propolis, bee venom. [3]. Beekeeping, like other fields, has developed and continues to develop in order to obtain higher quality products and better economic efficiency. This development involves the use in the apiary of more complex and more efficient tools that are powered by electricity. At the same time, strategies for optimal use of work in an apiary must be devised

2. Structures of photovoltaic systems for an apiary

An apiary can be located both in areas inhabited by humans - in this situation there are certain legal restrictions [4] in quiet areas, far from human settlements, but also from areas where there is intense human activity such as factories, heavily trafficked roads and railways, i.e. generally where pollution is high.



To obtain honey and other bee products, the beekeeper uses a series of specific tools and machines [1], [5] some of which are simple, others more complex, more efficient, more productive. The latter are in most cases fed from a source of electricity, the voltages required for their supply being 230Vac (most) or 12Vdc/24Vdc. As a rule, where there are settlements and human activity, electricity from the national power grid is available, but in isolated areas, where the largest and most productive beehives are located, no power source is available, so electricity it must be produced in the place where the hive exists.

In the context of the production of increasingly cheaper and more efficient photovoltaic panels, the development of electricity production systems using photovoltaic panels has gained momentum. Currently, it is generally appreciated that such a system can be used for a period of 15-25 years with low / reasonable maintenance costs, and energy efficiency does not fall below 80%.

For an apiary located in an area where there is available electricity from the national energy system, electric machines have the overwhelming majority of cases, as the primary source of energy, electricity produced in the national energy system. However, in cases where the owner has a photovoltaic system and where it is also a prosumer, the machinery and other electrical equipment in the apiary can be supplied with alternative electricity from the system's inverter terminals (figure 1).

If there are machines in the apiary that require a 12Vdc/24Vdc power supply, they are powered by an electric rectifier connected to the output of the inverter (not shown in figure 1).

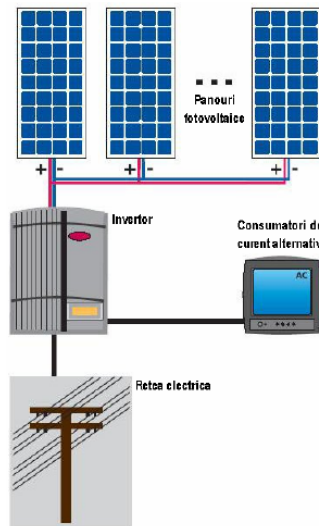


Figure 1. Photovoltaic on-grid system

For an isolated apiary, two structures of photovoltaic systems can be considered of interest, shown figure 2, figure 3 [6], [7].

The system shown in figure 2 can generate electric current, simultaneously alternating and continuous, both from the photovoltaic panels and from the diesel generator. The alternating current, of the desired voltage and frequency, is available at the output of the inverter and the direct current, at the output of the regulator. Photovoltaic panels generate electricity, of course, only during the day, when sunlight is available, direct or diffused, with a sufficient intensity to supply the power needed by consumers [8]. The primary source of energy, sunlight, is free. The Diesel generator generates electricity based on the diesel it is fueled with.

It has the advantage that it can work at any time, day or night, and also that it takes over the load peaks of the consumers connected to the inverter or regulator. In addition, the system can be dimensioned in such a way that the total capacity of the batteries in the system is lower, compared to the situation in which the generator would be missing, without significant restrictions on the use of the system. As disadvantages, we note that diesel fuel must be purchased against the cost, the noise produced by the diesel generator in operation is quite high, which can disturb the bees. We also note that environmental pollution occurs through the noxious substances it emits, a fact that could also affect the quality of the honey obtained. Last but not least, it should be mentioned that by using a diesel / gasoline generator, the complexity of the installation increases, so its reliability decreases and, as a rule, the efficiency of the initial investment in the electricity production system.

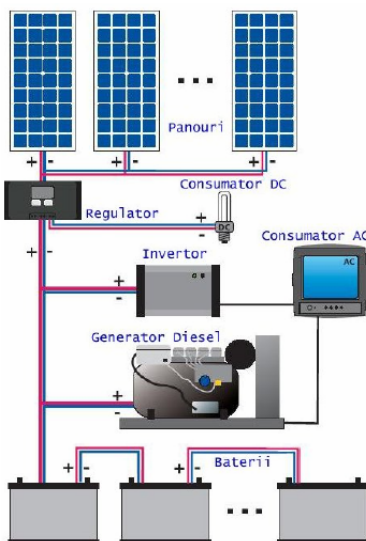


Figure 2. Isolated hybrid system with photovoltaic off-grid system

The system shown in figure 3 can also generate, simultaneously, alternating and direct current due to the presence of photovoltaic panels. It eliminates the disadvantages of using a diesel / gasoline generator, but the number of batteries used, compared to the previous system, is slightly higher, depending on the work schedule that the user sets. This is the type of photovoltaic system recommended for powering machinery and auxiliary consumers from an isolated apiary [7].

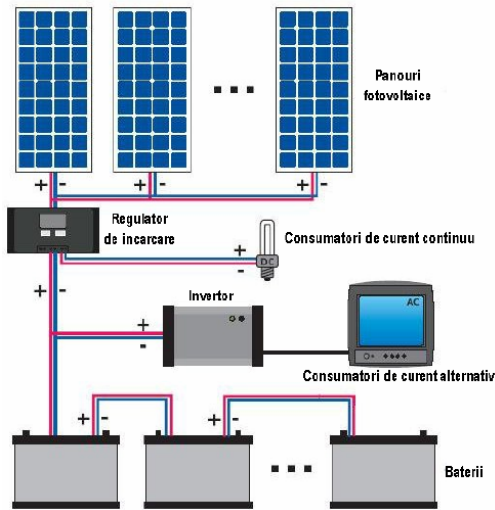


Figure 3. Isolated system with photovoltaic off-grid system

3. Considerations for the sizing of a photovoltaic system for supplying electricity to an apiary

The sizing of a photovoltaic system for supplying electricity to the devices/equipment used and auxiliary consumers in an apiary involves several stages [5], which can be summarized as follows:

- a – establishing the variant of photovoltaic system used and the main component elements;
- b. – establishing in the field the place where the photovoltaic system will be located;
- c.- establishing the machinery and auxiliary consumers that will be powered from the photovoltaic system and the powers required by them for each major work cycle;
- d- dimensioning of the photovoltaic system.

3.1. Establishing the used photovoltaic system variant and the main component elements

The variant of photovoltaic system used is essentially determined by the area where the apiary is located, with or without access to the national electrical energy system [6]. In the first case, a system like the one in fig.1 will be used, in the second a system like the one in figure 2 or figure 3.

3.2. Establishing the location of the photovoltaic system

The photovoltaic system is usually located in a compact space, without large differences in level, preferably as flat as possible, protected from possible natural calamities such as floods, landslides. In this phase, the size of the chosen land is, of course, approximate. However, it can be approximated quite well, under the logical assumptions that the installed electrical power of the photovoltaic system is known from the beginning and considering that photovoltaic panels occupy the largest area of the land, where the dimensions of a photovoltaic panel in the photovoltaic system are known.

The land must be chosen so that the photovoltaic panels can be oriented to the South or with small deviations to the West from this azimuth. They must not be obstructed by any kind of obstacles (buildings, trees, other forms of relief, etc.) when the sun moves across the sky from East to West. It is preferable that the distance from the apiary, respectively the bee house, does not exceed 50 meters, but also not less than 7-8 meters from the apiary. The exact space and location of the system components will be done after all the components are concretely known.

3.3. Establishing the machinery and auxiliary consumers that will be powered from the photovoltaic system and the powers required by them for each major work cycle

An inventory is made of the apiary machines that must be supplied with electricity, but also of the auxiliary consumers. The most frequently used ones are those for lighting, necessary in the beehive, knowing that a series of operations can also take place when the light is weaker, (in the evening or sometimes even at night, when the hives are additionally fed, with syrup, for example, to eliminate stealth). Other consumers, of the auxiliary type, can be an electric water pump, an electric heating resistance or even a small refrigerator in the beekeeping hut, for temporary storage, for example, of products for the treatment of bees.

3.4. Principles in sizing the photovoltaic system

The sizing of the photovoltaic system is the most complex part of the realization and is specific to the system variant chosen [7].

Considering that the most used system is the one in figure 3, some elements related to it will be briefly presented.

As said, the electricity provided by the photovoltaic system must mainly power the electrical machinery/devices used in the apiary. There are several machines/apparatus that should exist in any medium/large size apiary (containing from a few dozen hives to several hundred hives) for the productive activity to be normal and efficient. These would be: the centrifugal machine, used to extract the honey deposited by the bees on the frames in the hive; the stripping bench, used for stripping existing honey cells on the hive frames; the dehumidifier, used by the beekeeper to reduce the amount of water (if any) in the honey up to a percentage of 18%, (standardized for the commercialization process); bottling machine, used for bottling honey for commercial purposes, ; the heater, used at the same time as the bottling machine because the honey bottling process requires the honey to have a lower viscosity suitable for bottling.

Each of these devices have an electrical power of several hundred watts to several kW [9], [10].

If all of these would work simultaneously, the required useful electrical power would be:

$$P_{TOT} = P_{cen\ mac} + P_{hon\ dec} + P_{deh} + P_{bot\ mac} + P_{hea} \quad (1)$$

The photovoltaic system must, theoretically, produce this energy plus that to compensate for losses in the system and that required for auxiliary sources, the latter reaching, as the case may be, around 1 kW.

In practice, however, the 5 machines do not work simultaneously, but:

the centrifugal machine and the stripping bench are used intensively together in the months of May-June, when the bees collect pollen and nectar from which they obtain honey, i.e.:

$$P_1 = P_{cen\ mac} + P_{hon\ dec} \quad (2)$$

the heating and bottling machines are used as appropriate in autumn – winter, i.e.:

$$P_2 = P_{bot\ mac} + P_{hea} \quad (3)$$

and the dehumidifier is used in the period before bottling, i.e.:

$$P_3 = P_{deh} \quad (4)$$

It therefore follows that the photovoltaic system must be dimensioned for P_{SV} power:

$$P_{SV} = \max (P_1, P_2, P_3) \quad (5)$$

From the compared technical data of these 5 machines it can be concluded that, as a rule, for an established situation, it is possible to opt for P_1 to be at least

double compared to P_2 and P_3 respectively, an important and useful fact in dimensioning taking into account the energy that it can be captured by the panels in the months of May - June compared to December - January, when it is minimal. So P_{SV} will choose the value of P_1 .

As is known, the energy provided by a photovoltaic system is uneven throughout the year, being high in summer and low in winter. In addition, the energy given by the system depends on the geographic coordinates of the system's location. [8] but also the state of the weather, which is partly unpredictable, the forecasts being estimates.

We also add that the stupar's activity is asymmetrical over the course of a year. there are intense moments of activity, such as those during the picking, honey extraction, honey bottling, with some moderate in intensity, such as the preparation and maintenance of the beehives, but also temporary inactivity, such as late autumn and early winter. It also follows that the need/consumption of electrical power in the apiary has large variations at different times of the year.

The main elements of the system. [11], [12], [13] the photovoltaic panels, the solar accumulators, the inverter in particular, must be chosen correlated, in terms of number and technical performance, in order to obtain a functional and reliable system for a long time and to ensure the recovery of the investment in the shortest possible time.

4. Simulations for sizing the photovoltaic system

Currently, an optimal sizing of photovoltaic systems requires the use of appropriate software [14], [15], [11], [16] Several simulations were carried out with the PV GIS program [17, 33] for the dimensioning of a photovoltaic system, for the south-west area of Romania, for several power variants required from the system. For one of the cases it was considered that:

$$P_{SV} = P_1 = 22800 \text{ W} \quad (6)$$

Simulations were made for various elevation angles (20° , 30° , 35° , 45°), the panels being oriented to the south (azimuth 0°), for several powers of the photovoltaic panels (by default a different number of panels of the same type), different energy as the value stored in the solar accumulators (by default a different number of accumulators of the same type present in the system).

The program provided results that show the solar energy received by the photovoltaic system, the energy stored in the accumulators, but indirectly, and if the realized system provides at any time the necessary energy requested by the consumers of the apiary. Thus, for example in figure 7, the 100% presence of the indication of the lack of energy in the accumulators shows that the system is undersized (here the observation is made that the one who interprets the results must extract from the diagram only the time interval associated with P_{SV}).

Next, figure 4, figure 5, figure 6, figure 7 show some of the results of the simulations made.

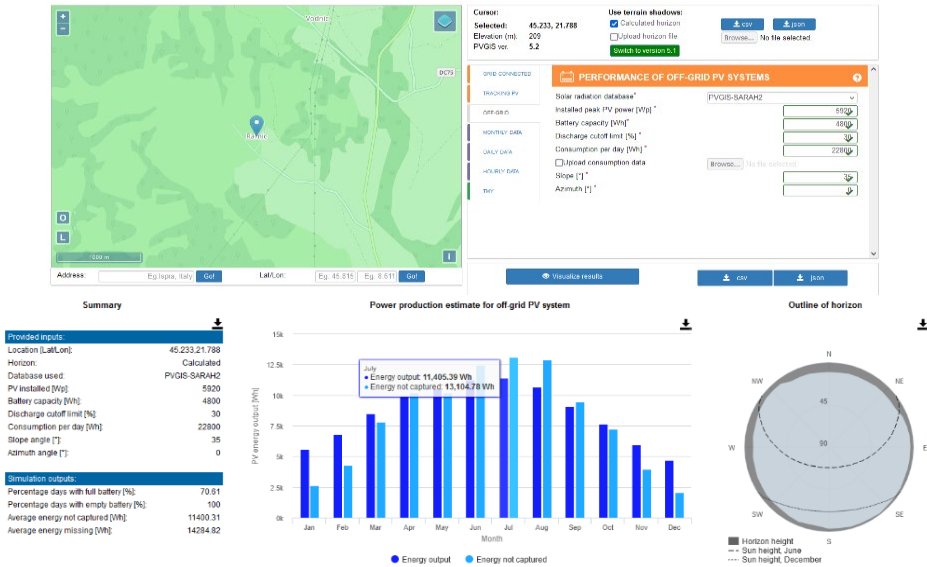


Figure 4. Simulation number 1

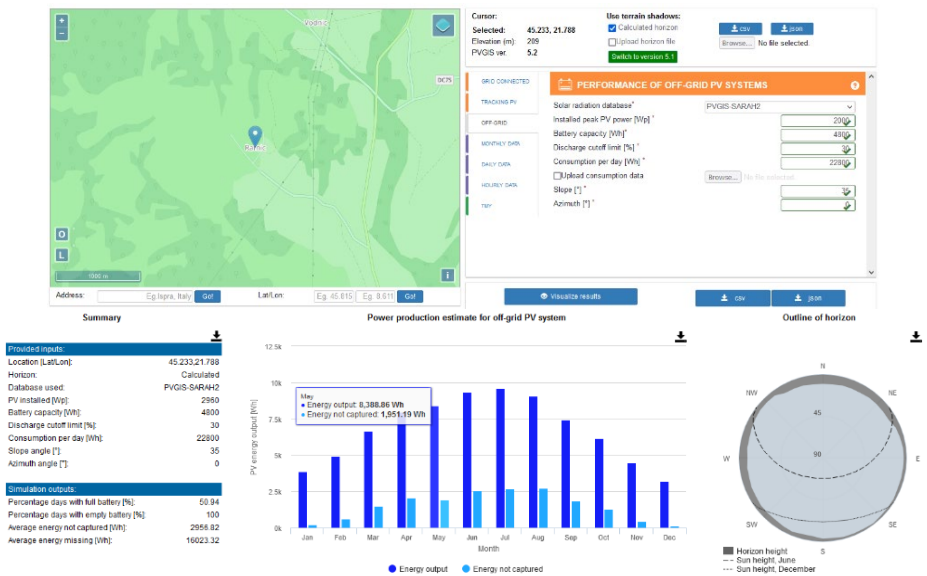


Figure 5. Simulation number 2

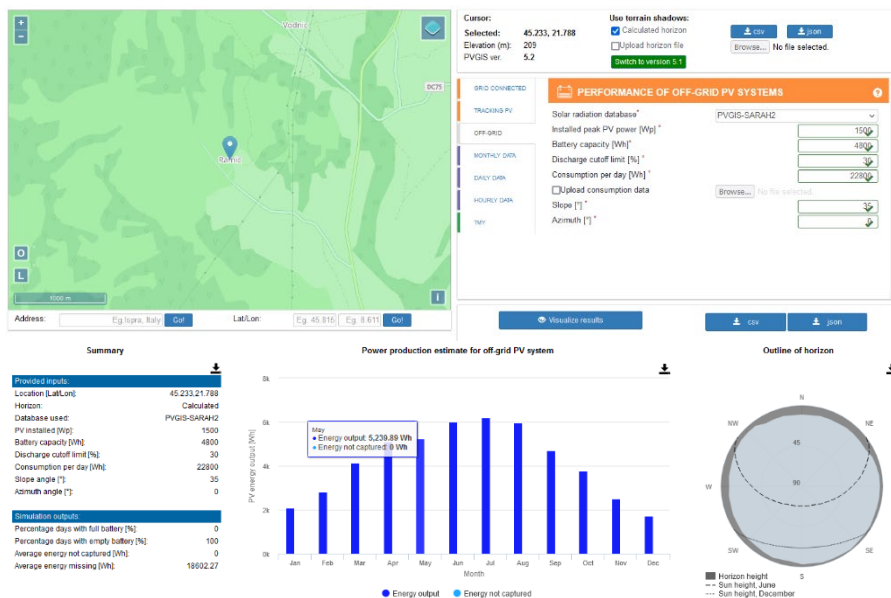


Figure 6. Simulation number 3

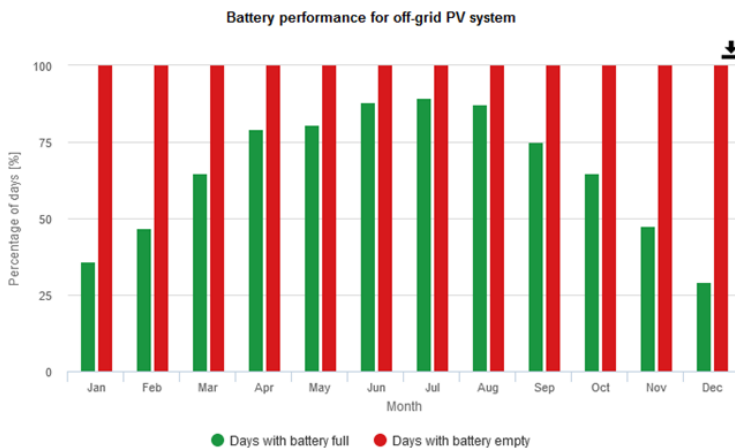


Figure 7 Battery performance for off grid PV system

The term of probability, from figure 7 reveals precisely the uncertainty of the results caused especially by the impossibility of knowing the meteorological situation in advance. The existence of 100% probability in the prediction of the battery state of charge clearly indicates that there will be at least one day in the month when the energy demand is insufficient.

5. Conclusion

The need for the presence and use of electricity in an apiary is determined by the fact that, on the one hand, there has been an increase in the complexity of the activity in such an agricultural household, which has led to the appearance and use of more complex machines powered by energy electrical, and on the other hand, the automation of some operations in the apiary was imposed in order to increase labor productivity and economic efficiency.

Larger hives are usually located in isolated areas without access to the national energy system, and therefore, the production of electricity is a local activity. At present, the production of electricity in beehives is mostly carried out with generator sets with diesel or gasoline, which are polluting solutions with toxic gases for the environment, but also noisy, and the current and maintenance expenses are high. The use of photovoltaic systems eliminates these disadvantages.

Some considerations and recommendations of an applicative nature, taking into account the experience of some of the authors in the field of beekeeping, useful in the design and realization of a photovoltaic system for supplying electricity to an apiary located in an isolated place. are :

- the structures that can be used for photovoltaic systems to supply electricity to an isolated beehive are the ones often used in many applications [6], [7]. Their installed electrical powers are currently of the order of kilowatts or more, differing significantly depending on the number of hives in the apiary that we estimate would be suitable to be equipped with such a system, and which, indicatively, can be 50 - 300 beehives;

- the main types of high-performing electric machines from today with high relative energy consumption from a hive were established, and their specific way of use was indicated, according to the needs, during a calendar year, so as not to affect the technical-economic performances in an isolated apiary;

- the simulations carried out with the PVGIS program show that in cases where the positioning of the photovoltaic panels at elevation angles in the 20^0 - 45^0 range or the azimuth with $\pm 10^0$ relative to the South position, leads to variations in the estimated amount of electricity supplied by the photovoltaic system with a maximum of 2-3%.

References

- 1 Asociația crescătorilor de albine din Romania, *Manualul apicultorului*, ediția a VI-a, Apimondia București, 2002.
- 2 <https://www.stuparul.ro/unelte-apicole-pentru-extractia-mierii/>
- 3 Jarvis D.C., *Mierea si alte produse naturale*, Apimondia București, 1976.
- 4 Legea apiculturii nr.383 din 2013, Monitorul Oficial, Partea I nr. 14 din 09 ianuarie 2014, București

- 5 Mateescu C., Siceanu A., a.o., *Ghid de bune practici în apicultură*, LVS Crepuscul, Ploiesti, 2011.
- 6 <https://sunprojekt.ro/tipuri-de-sisteme-fotovoltaice-on-grid-off-grid-si-hybrid/>
- 7 <https://starbay.ro/tipuri-de-sisteme-fotovoltaice-componente-avantaje-si-dezavantaje/>
- 8 Ineichen P., *Global irradiation: average and typical year, and year to year annual variability*, Solar world congress 2011, Kassel, Germania, ResearchGate
- 9 <https://www.stuparul.ro/unelte-apicole-pentru-extractia-mierii/>
- 10 <https://www.apis-blaj.ro/>
- 11 Mermoud A., *Conception et Dimensionnement de Systèmes Photovoltaïques , Introduction des Modules PV en couches minces dans le logiciel PVsyst*, Université de Geneve, 2005 <https://docplayer.fr/76649263>
- 12 <https://www.unfpa.md/cele-mai-bune-panouri-fotovoltaice-monocristaline/>
- 13 <https://solarcenter.ro/panouri-fotovoltaice-amorfe-avantaje-si-dezavantaje/>
- 14 Gerstmeier T., S.van Riesen, a.o., *Software Modeling of FLATCON© CPV Systems*, 6th International Conference on Concentrating Photovoltaic Systems: CPV-6. 2010, Freiburg, Germany AIP Conference Proceedings, 1277(1), pp.183-186
- 15 Mermoud A., Lejeune T., a.o., 2010, *Performance assessment of a simulation model for pv modules of any available, technology*, 25th European Photovoltaic Solar Energy Conference, 6-10 Sept. 2010, Valencia, Spain, Material Science, p.p. 4786-4791, DOI 10.4229/25thEUPVSEC2010-4BV.1.114
- 16 <https://www.pvsyst.com/>
- 17 https://joint-research-centre.ec.europa.eu/photovoltaic-geographical-information-system-pvgis_en

Addresses:

- Prof. Dr. Eng. Eugen Răduca, Department of Engineering Science, Babeş-Bolyai University, Cluj-Napoca, Romania, Faculty of Engineering, Piața Traian Vuia, nr. 1-4, 320085, Reșița, Romania
eugen.raduca@ubbcluj.ro
- Prof. Assist. Dr. Eng. Mihaela Molnar, Department of Engineering Science, Babeş-Bolyai University, Cluj-Napoca, Romania, Faculty of Engineering, Piața Traian Vuia, nr. 1-4, 320085, Reșița, Romania
mihaela.molnar@ubbcluj.ro
(* corresponding author)
- Prof. Dr. Eng. Cristinel Popescu, University „Constantin Brancuși of Tg. Jiu“, Faculty of Engineering, Calea Eroilor nr.30, 210135, Tg. Jiu, Romania
cristi67pop@yahoo.com
- Lect. Dr. Eng. Fiz. Cornel Hatiegan, Department of Engineering Science, Babeş-Bolyai University, Cluj-Napoca, Romania, Faculty of Engineering, Piața Traian Vuia, nr. 1-4, 320085, Reșița, Romania
cornel.hatiegan@ubbcluj.ro

The strain energy in loosening the clamped end of a beam (part I)

Patric-Timotei Stan, Zeno-Iosif Praisach*, Gilbert-Rainer Gillich,
Tiberiu Mănescu, Cristian Tufiși

Abstract. *Using analytical equations, the paper aims to solve the dynamic behavior of beams where a clamped end of the beam does not respect the ideal boundary conditions by introducing a weakening coefficient. In the paper, the characteristic equation for determining the eigenvalues and the relationship of the modal function and strain energy are derived. The results show the first six vibration modes for different values of the weakening coefficient which is considered in the clamped end and the evolution of the strain energy.*

Keywords: *weak clamped end, mode shapes, strain energy*

1. Introduction

Different types of failures it can be occurred in mechanical structures and they can be caused by a lots of factors, such as: loosening of joints due to excessive vibrations and shocks, degradation caused by environmental conditions, material fatigue and exceeding the expected operating demands, improper manufacturing conditions [1].

From dynamic behavior, the analysis of beams with fixed ends involves the consideration of displacements and slopes perfect boundary conditions. Most researchers use a measurement of natural frequencies to characterize imperfect boundary conditions, while others consider modal shapes to detect deviation from ideal conditions [2]. The precise calculation of the natural frequencies is significantly influenced by the correct positioning of the supports, respectively by the correct choice of the boundary conditions [3, 4].

The loss of integrity of structures can be attributed not only to the presence of cracks but also to joint failure, especially for beam-type structures. Methods used of modal parameters prove reliable for the detection and evaluation of damage in beams by applying several techniques like flexibility coefficients, derived stiffness matrix, the frequency response function FRF [5 – 7].



Because real beams have non-ideal boundary conditions, it is necessary to use advanced models to determine the real modal parameters [8].

In this paper, the authors present an analytical solution regarding the dynamic behavior of a beam for which the clamped end is defined by a weakening coefficient $k_1 \in [0, \dots, 1]$, which allows us to have both bending moment and slope at this support [9]. So, that for the zero value of k_1 the support is considered to be a hinge, and for the 1 value of k_1 , the support becomes clamped.

2. Analytical approach

It is analyzed the dynamic behavior of a normalized beam ($L=1$) under the action of its dead weight (q) with constant cross-section. It is considered the case of a simply supported beam (Fig. 1) where a bending moment equal to the moment is introduced on the left hinge bending moment of a clamped end multiplied by a stiffness coefficient k_1 which can have values between $[0, \dots, 1]$. The right support has the stiffness coefficient $k_2=0$, so, at this point we have a hinge.



Figure 1. A schematic diagram with left end hinge is subjected to a bending moment (left) equal to that in the clamp end (right)

It is known from the strength of materials that for a hinge support (H) located at $x=0$ the slope has the expression:

$$W'_H(0) = \frac{q \cdot L^3}{24E \cdot I} \quad (1)$$

and for the clamped end (C) at $x=0$ the bending moment can be written as:

$$W''_C(0) = -\frac{q \cdot L^2}{8E \cdot I} \quad (2)$$

where,

q [N/m] – is the load per unit of length (dead load);

L [m] – is the beam length;

E [N/m²] – is the Young's modulus;

I [m⁴] – is the moment of the inertia of the cross section of the beam.

If the bending moment from relation (2) is applied to the hinged at $x=0$ (Fig. 1 – left), it becomes a clamped end (Fig. 1 – right), and the slope from relation (1) becomes negative. The connection between the slope and the bending moment from (2) can be written:

$$W_H'(0) = -\frac{q \cdot L^3}{24E \cdot I} = -\frac{L}{3} \left(\frac{q \cdot L^2}{8E \cdot I} \right) = -\frac{L}{3} \left(-W_C''(0) \right) = \frac{L}{3} W_C''(0) \quad (3)$$

or, expressing the bending moment from (3) and taking into account the stiffness k_1 :

$$k_1 W_C''(0) = k_1 \frac{3}{L} W_H'(0) \quad (4)$$

Under these conditions and taking into considerations the weakened coefficient, the bending moment from the clamped end must be equal to the bending moment applied to the hinge:

$$k_1 W_C''(0) = (1 - k_1) W_H''(0) \quad (5)$$

also taking into account (4), in the left support we get:

$$(1 - k_1) W_H''(0) - k_1 W_C''(0) = 0 = (1 - k_1) W_H''(0) - k_1 \frac{3}{L} W_H'(0) \quad (6)$$

From relation (6) it can be seen that for $k_1=0$, the bending moment is zero ($W_H''(0)=0$), so in $x=0$ we have a hinge, and for $k_1=1$, the slope is zero ($W_H'(0)=0$), so we have a clamped end. For any other values of $k_1 \in [0, \dots, 1]$, in the left support we will find both bending moment and slope.

3. Modal analysis and the strain energy

It can be started from the spatial solution of the differential equation of bending vibrations, free and undamped using Euler-Bernoulli model:

$$W(x) = A \sin(\alpha x) + B \cos(\alpha x) + C \sinh(\alpha x) + D \cosh(\alpha x) \quad (7)$$

where,

$W(x)$ – is the modal motion function;

A, B, C, D – are integration constants that are obtained from the boundary conditions;

α – is the eigenvalue;

x – is the variable length of the normalized beam.

Boundary condition for clamped end (C) and hinged end (H), at $x=0$:

$$\begin{cases} W_H(0) = W_C(0) = 0 = B + D \Rightarrow D = -B \\ W_C'(0) = 0 = \alpha(A + C) \\ W_H''(0) = -2\alpha^2 B \end{cases} \quad (8)$$

Boundary condition for hinged end (H), at $x=L=1$:

$$\begin{cases} W(L) = W(1) = 0 = A\sin\alpha + B(\cos\alpha - \cosh\alpha) + C\sinh\alpha \\ W''(L) = W''(1) = 0 = \alpha^2[-A\sin\alpha - B(\cos\alpha + \cosh\alpha) + C\sinh\alpha] \end{cases} \quad (9)$$

and the integration constants B and C are obtained from system (9) are:

$$\begin{cases} B = -A \frac{\sin\alpha}{\cos\alpha} \\ C = -A \frac{\sin\alpha \cdot \cosh\alpha}{\cos\alpha \cdot \sinh\alpha} \end{cases} \quad (10)$$

By introducing the constants B , C and D in relation (6), the characteristic equation (11) is obtained. Solutions (11) give us the eigenvalues for each vibration mode.

$$2\alpha(1 - k_1)\sin\alpha \cdot \sinh\alpha + k_1 \frac{3}{L}(\sin\alpha \cdot \cosh\alpha - \cos\alpha \cdot \sinh\alpha) = 0 \quad (11)$$

The eigenvalues α_n for the first six vibration modes ($n=6$) and different values of k_1 , solutions of relationship (11) for $L = 1$, can be found in table 1.

Table 1. Eigenvalues for the $n=6$ vibration modes and different values of stiffness coefficient k_1

k_1	Vibration mode (n)					
	1	2	3	4	5	6
0.0	π	$2\cdot\pi$	$3\cdot\pi$	$4\cdot\pi$	$5\cdot\pi$	$6\cdot\pi$
0.1	3.191179	6.308917	9.442121	12.57945	15.71845	18.85832
0.2	3.244789	6.338981	9.462877	12.59527	15.73124	18.86904
0.3	3.303022	6.374539	9.488147	12.61482	15.74717	18.88247
0.4	3.366603	6.417199	9.519554	12.63956	15.76753	18.89977
0.5	3.436416	6.469232	9.559584	12.67182	15.79448	18.92287
0.6	3.513548	6.533943	9.612229	12.71560	15.83176	18.95527
0.7	3.599335	6.616272	9.684261	12.77816	15.88658	19.00385
0.8	3.695415	6.723820	9.787957	12.87416	15.97451	19.08434
0.9	3.803753	6.868497	9.947185	13.03697	16.13541	19.24065
1.0	3.926602	7.068583	10.21018	13.35177	16.49336	19.63495

The expression of the modal function for the bending vibration modes is represented in relationship (12):

$$W(x) = A \left[\sin(\alpha x) - \frac{\sin \alpha}{\cos \alpha} (\cos(\alpha x) - \cosh(\alpha x)) - \frac{\sin \alpha \cdot \cosh \alpha}{\cos \alpha \cdot \sinh \alpha} \sinh(\alpha x) \right] \quad (12)$$

The strain energy, or potential energy, is a function of the square of the curvature of the modal function, and is defined as:

$$E_{p_n} = \frac{1}{2} \int_0^L E \cdot I \cdot W''(x)^2 dx \quad (13)$$

From relation (12) we obtain the curvature expression, which its squared is directly proportional to the normalized strain energy:

$$W''(x)^2 = \left\{ A \alpha^2 \left[-\sin(\alpha x) + \frac{\sin \alpha}{\cos \alpha} (\cos(\alpha x) + \cosh(\alpha x)) - \frac{\sin \alpha \cdot \cosh \alpha}{\cos \alpha \cdot \sinh \alpha} \sinh(\alpha x) \right] \right\}^2 \quad (14)$$

4. Results

Below are presented the first $n=6$ (six) normalized vibration modes and the normalized strain energy for the following values of $k_1=0.0, 0.25, 0.50, 0.75, 0.85, 0.95$ and $1, 00$ ($k_2=0$). The obtained results are illustrated in figures 2-8.

5. Conclusions

The paper presents the eigenvalues, modal shapes and strain energy for bending vibration modes for the case where the left clamped end of the beam is weakened by the coefficient $k \in [0, \dots, 1]$ and the right end of the beam is a hinge.

For the extreme cases: $k_1=0$, the eigenvalues (Table 1) were obtained for the simply supported beam (hinged at both ends); respectively for $k_1=1$, we find the eigenvalues for the beam clamped at one end and hinged at the other.

From the analysis of the figures from figures 2 – 4, it can be observed that for stiffness values of $k_1 < 0.5$, from the point of view of the mode shapes, the soft clamped end has a behaviour very close to that of a hinged support.

Instead, the normalized strain energy in the left support, which in the hinge has zero value ($k_1=0$), with the increase of k_1 , its value increases, reaching $\sim 7\%$ of the maximum value for $k_1=0.25$ and $\sim 37\%$ of the maximum value for $k_1=0.5$, at first vibration mode. For the second vibration mode, the normalized strain energy has smaller values in this point, respectively, $\sim 2\%$ for $k_1=0.25$ and $\sim 14\%$ for $k_1=0.5$ and the trend continues for the other vibration modes.

For stiffness values $k_1 > 0.75$ (figures 5 – 8), the mode shapes of the beam are significantly affected and although the relation (6) that describes the soft clamped end of the beam is a linear expression of k_1 , the effect of k_1 in the modal function does not have a linear behavior. At the point $x=0$, the normalized strain energy becomes maximum for $k_1=0.74$ at the first vibration mode, $k_1=0.86$ at the 2nd vibration mode, $k_1=0.9$ at the 3rd vibration mode, $k_1=0, 925$ at vibration mode 4, $k_1=0, 94$ at vibration mode 5 and $k_1=0, 95$ at vibration mode 6.

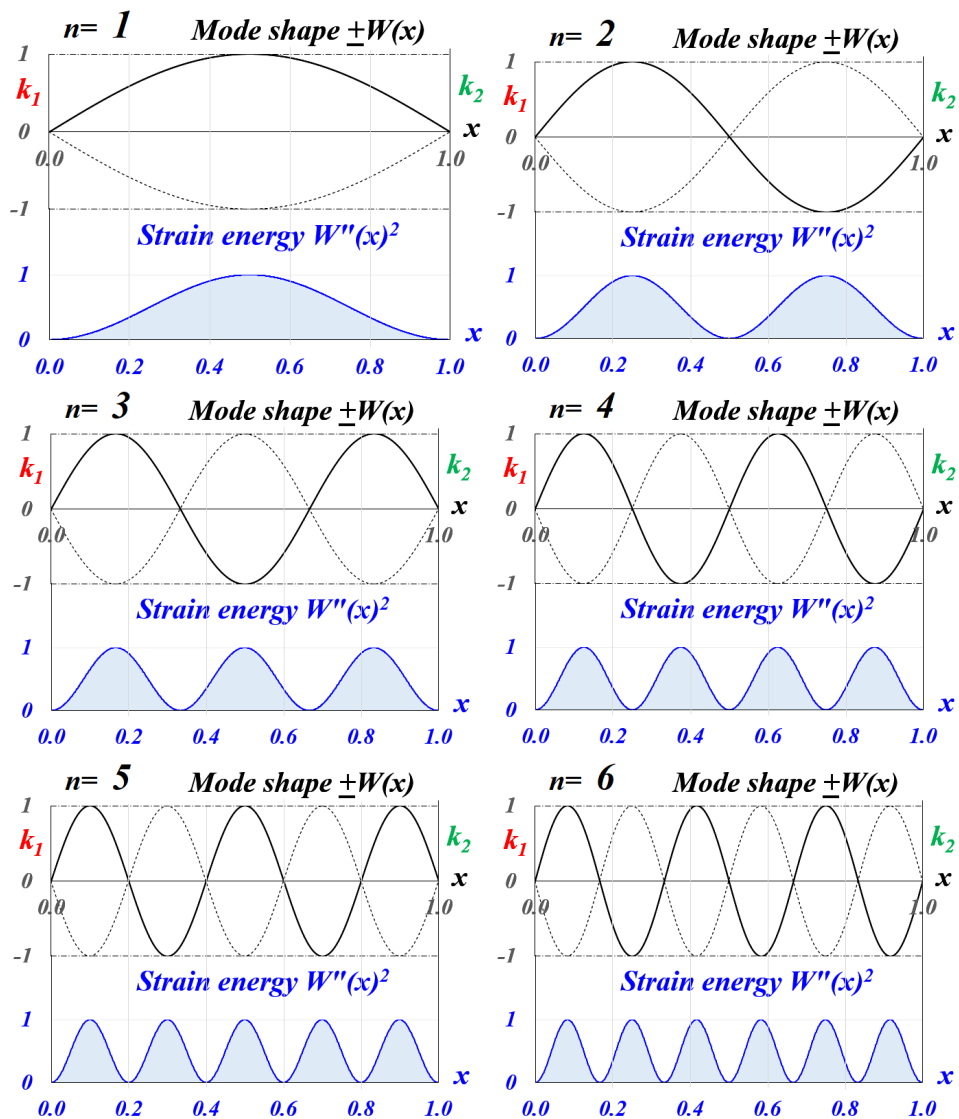


Figure 2. Normalized mode shapes ($\pm W(x)$) and normalized strain energy ($W''(x)^2$) for the first $n=6$ vibration modes and $k_1=0.0$

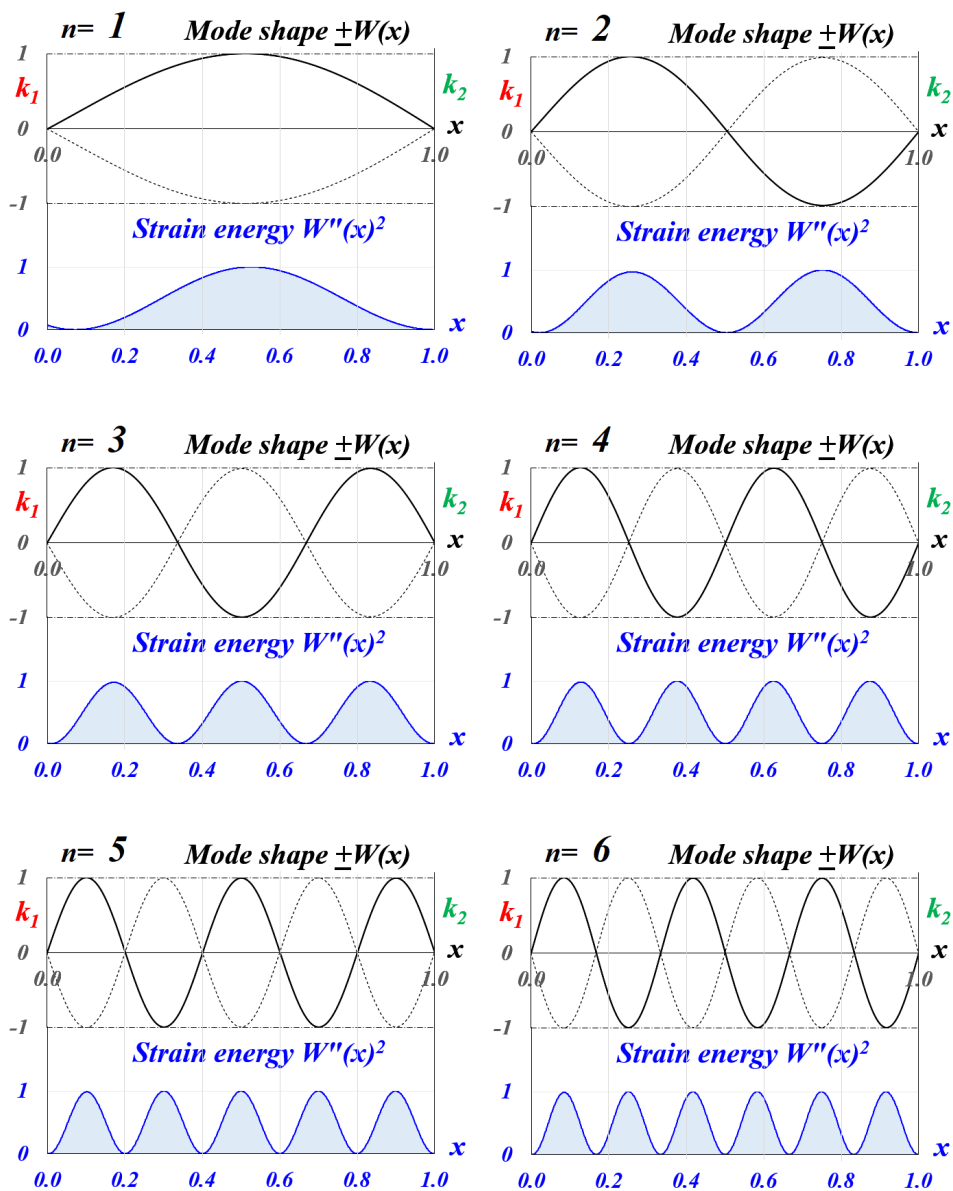


Figure 3. Normalized mode shapes ($\pm W(x)$) and normalized strain energy ($W'''(x)^2$) for the first $n=6$ vibration modes and $k_1=0.25$

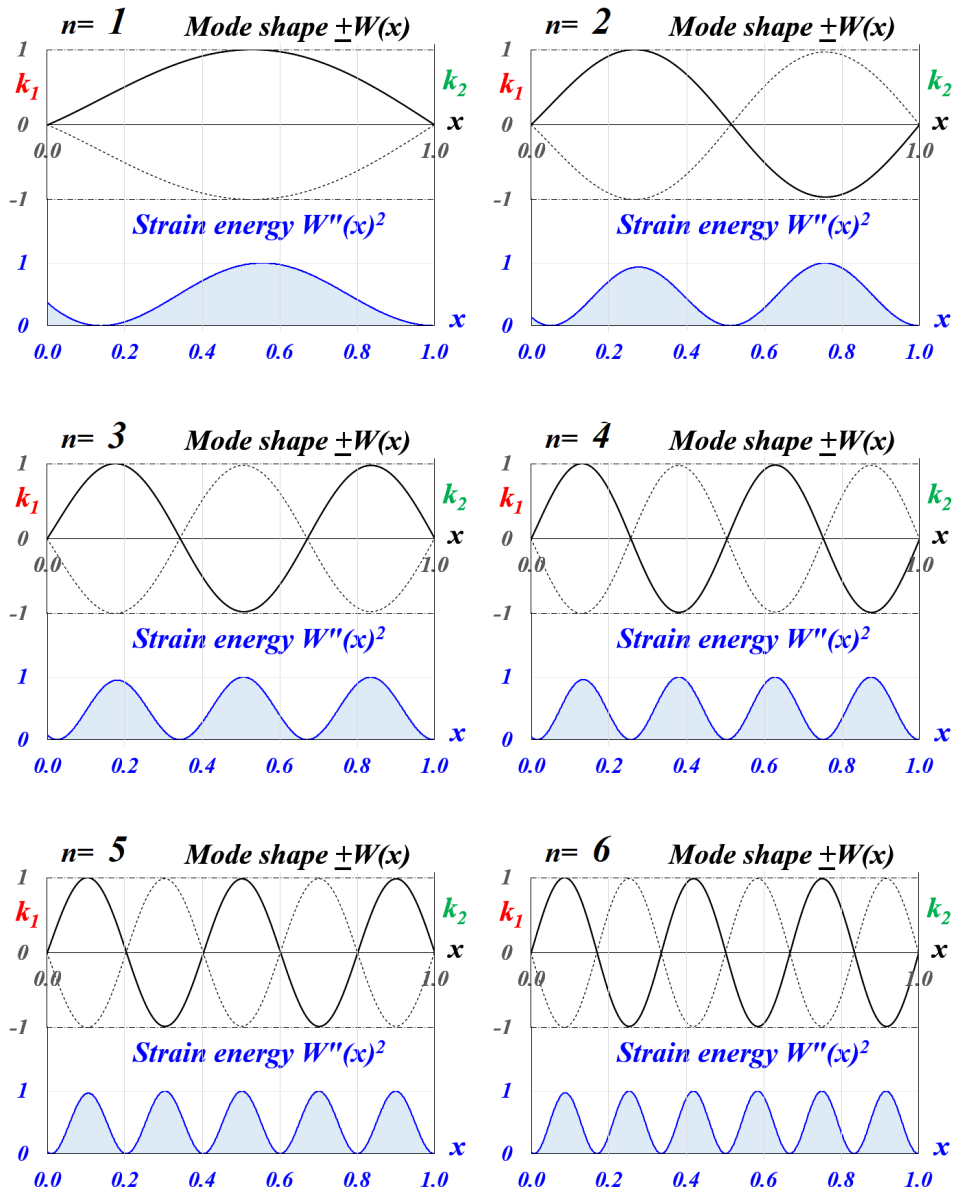


Figure 4. Normalized mode shapes ($\pm W(x)$) and normalized strain energy ($W'''(x)^2$) for the first $n=6$ vibration modes and $k_1=0.50$

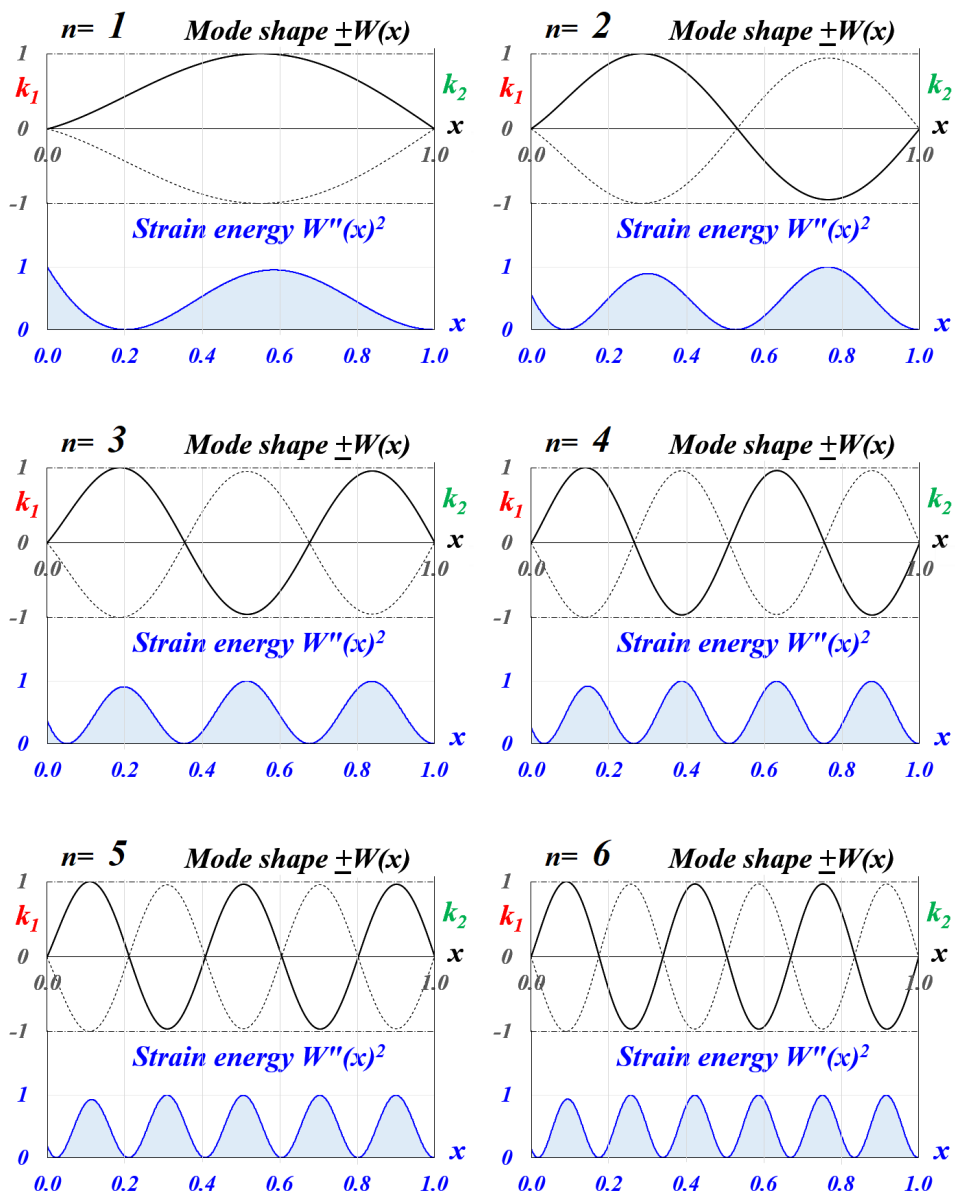


Figure 5. Normalized mode shapes ($\pm W(x)$) and normalized strain energy ($W''(x)^2$) for the first $n=6$ vibration modes and $k_1=0.75$

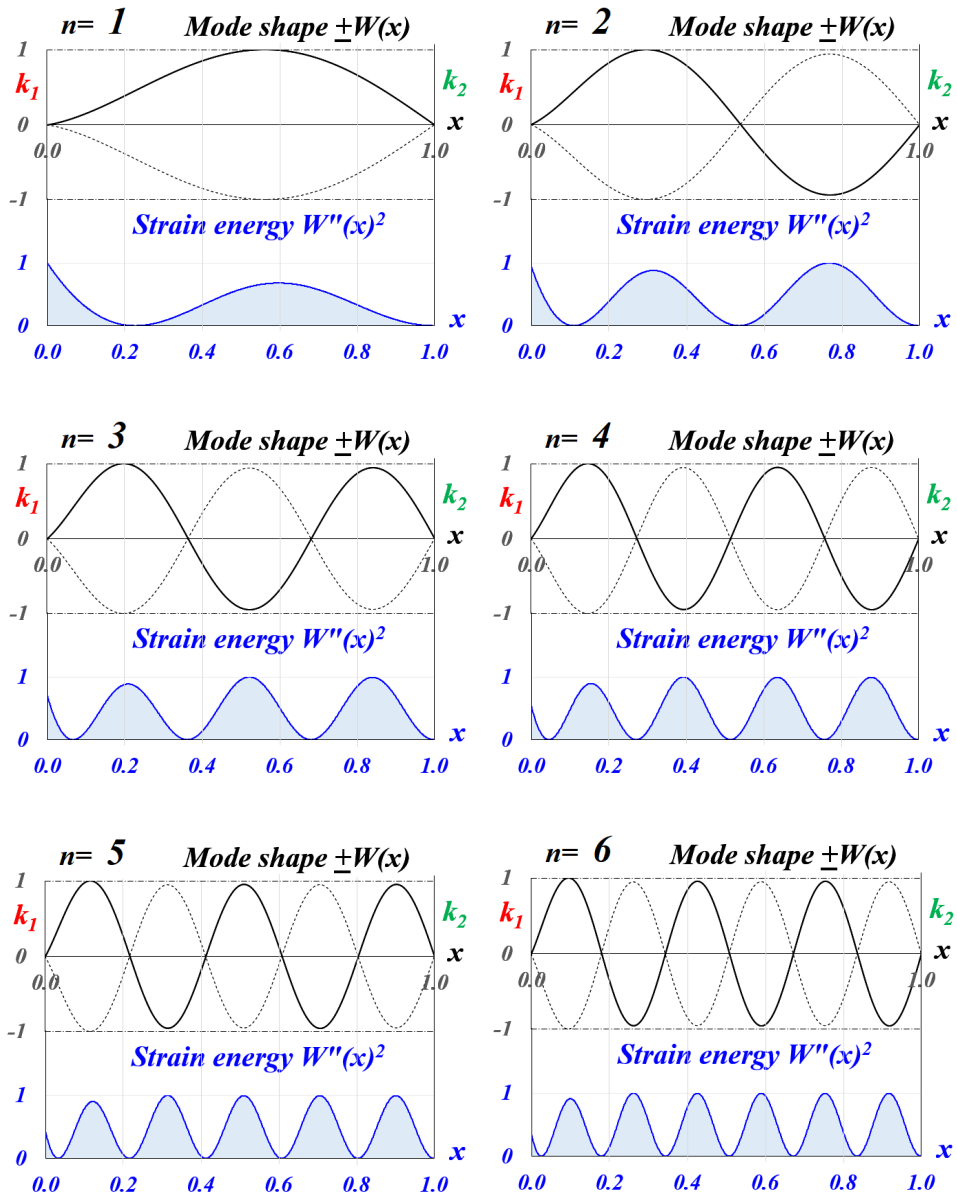


Figure 6. Normalized mode shapes ($\pm W(x)$) and normalized strain energy ($W''(x)^2$) for the first $n=6$ vibration modes and $k_1=0.85$

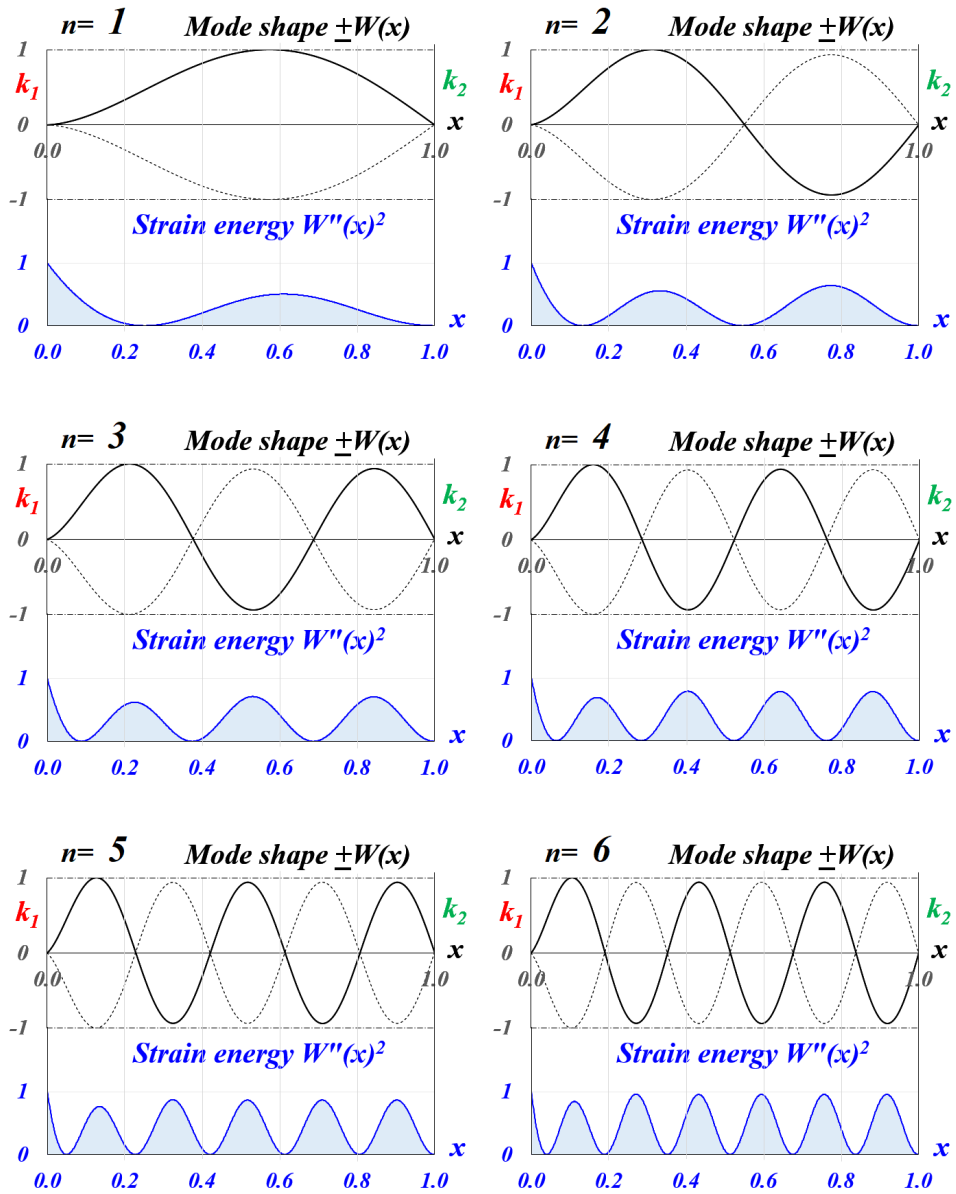


Figure 7. Normalized mode shapes ($\pm W(x)$) and normalized strain energy ($W''(x)^2$) for the first $n=6$ vibration modes and $k_1=0.95$

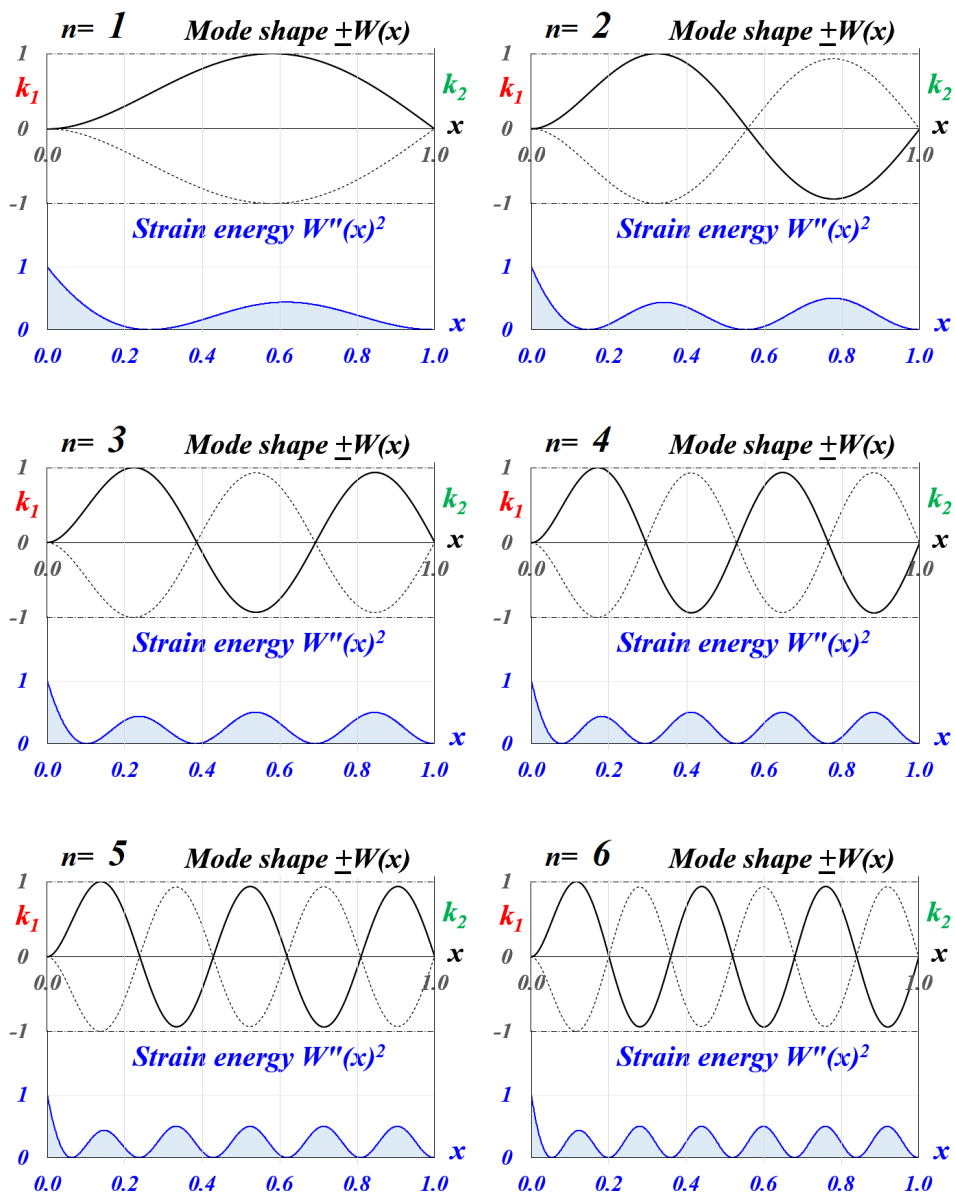


Figure 8. Normalized mode shapes ($\pm W(x)$) and normalized strain energy ($W''(x)^2$) for the first $n=6$ vibration modes and $k_1=1.0$

References

- 1 Lupu D., Tufiși C., Gillich G.R., Ardeljan M., Detection of transverse cracks in prismatic cantilever beams affected by weak clamping using a machine learning method, *Analecta Technica Szegedinesia*, 16(01), 2022, pp. 122-128.
- 2 Lupu D., Gillich G.R., Nedelcu D., Gillich N., Mănescu T., *A method to detect cracks in the beams with imperfect boundary conditions*, International Conference on Applied Science (ICAS 2020), Journal of Physics: Conference Series 1781(2021), 012012, IOP Publishing, pp. 1-13.
- 3 Praisach Z.I., Ardeljan D., Pîrșan D.A., Gillich G.R., A new approach for imperfect boundary conditions on the dynamic behavior, *Analecta Technica Szegedinesia*, 16(01), 2022, pp. 56-61.
- 4 Gillich G.R., Praisach Z.I., Exact solution for the natural frequencies of slender beams with an abrupt stiffness decrease, *Journal of Engineering Sciences and Innovation*, 2(1), 2017, A. Mechanics, Mechanical and Industrial Engineering, Mechatronics, pp. 13-21.
- 5 Karthikeyan M., Tiwari R., Talukdar S., *Identification of crack model parameters in a beam from modal parameters*, in 12th National Conference on Machines and Mechanisms (NaCoMM-2005), 2005.
- 6 Nahvi H., Jabbari M., Crack detection in beams using experimental modal data and finite element model, *International Journal of Mechanical Sciences*, 47(10), 2005, pp. 1477–1497.
- 7 Dems K., Turant J., Structural damage identification using frequency and modal changes, *Bulletin of the Polish Academy of Sciences Technical Sciences*, 59(1), 2011, pp. 23–32.
- 8 Gillich G.R., Nedelcu D., Wahab M.A., Pop M.V., Hamat C.O., A new mathematical model for cracked beams with uncertain boundary conditions, *International Conference on Noise and Vibration Engineering (ISMA 2020)*, Leuven, Belgium, pp. 3871-3883.
- 9 Shi D., Tian Y., Choe K.N., Wang Q., A weak solution for free vibration of multi-span beams with general elastic boundary and coupling condition, *JVE International Ltd. Vibroengineering PROCEDIA*, 2016, vol. 10, pp. 298–303.

Addresses:

- Phd. stud. Eng. Patric-Timotei Stan, Doctoral School of Engineering, Babeș-Bolyai University, Cluj-Napoca, Romania, Faculty of Engineering, Piața Traian Vuia, nr. 1-4, 320085, Reșița
patric.stan@stud.ubbcluj.ro

- Lect. PhD. Habil. Zeno-Iosif Praisach, Department of Engineering Science, Faculty of Engineering, Babeş-Bolyai University, Cluj-Napoca, Romania, Faculty of Engineering, Piața Traian Vuia, nr. 1-4, 320085, Reșița,
zeno.praisach@ubbcluj.ro
(* *corresponding author*)
- Prof. PhD. Gilbert-Rainer Gillich, Department of Engineering Science, Faculty of Engineering, Babeş-Bolyai University Cluj-Napoca, Romania, Faculty of Engineering, Piața Traian Vuia, nr. 1-4, 320085, Reșița,
gilbert.gillich@ubbcluj.ro
- Assoc. Prof. PhD Habil. Tiberiu Mănescu, Aurel Vlaicu University, Bd. Revoluției, nr. 77, Arad, Romania
manescu.tiberiu@gmail.com
- Lect. PhD. Cristian Tufiși, Department of Engineering Science, Faculty of Engineering, Babeş-Bolyai University Cluj-Napoca, Romania, Piața Traian Vuia, nr. 1-4, 320085, Reșița,
cristian.tufisi@ubbcluj.ro

The strain energy in loosening the clamped end of a beam (part II)

Dan-Alexandru Pîrșan, Zeno-Iosif Praisach*, Gilbert-Rainer Gillich,
Cornel Hațiegan

Abstract. *In the second part of the paper, the dynamic behavior of a doubly clamped beam is presented, where the right clamped end of the beam is weakened by introducing a weakening coefficient. The analytical calculation is based on the determination of the bending moment from the weakened clamped end expressed as a function of slope, after which the modal function, strain energy, and the characteristic equation are determined to obtain the eigenvalues of the first six vibration modes depending on the weakened coefficient of the clamped end. The obtained mode shapes and strain energies are determined for seven values of the weakened coefficient.*

Keywords: *weak clamped end, mode shapes, strain energy*

1. Introduction

The second part of the paper is a continuation of part 1 and aims to analytically solve a weakened clamped end for a doubly clamped beam in terms of its dynamic behavior. For these reasons, the bibliographic citations are presented in the introduction chapter of first part. For this analysis case, it is considered that the weakened coefficient $k_1=1$ (left clamped support) and the dynamic behavior of the beam is analyzed for the right support with the weakened coefficient $k_2 \in [0, \dots, 1]$ which allows us to have both bending moment and slope at this support. So, that for the zero value of k_2 the support is considered to be a hinge, and for the 1 value of k_2 , the support becomes clamped.

2. Analytical approach

For the normalized beam ($L=1$) of constant cross-section and loaded with dead weight (q), in accordance with the relations provided by the strength of the materials, for the right clamped (C) end (fig. 1 left), the bending moment can be expressed:



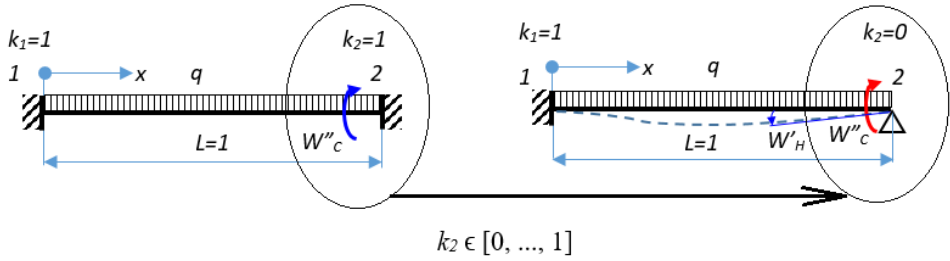


Figure 1. A schematic diagram with right end hinge is subjected to a bending moment (right) equal to that in the clamp end (left)

$$W''_C(L) = -\frac{q \cdot L^2}{12E \cdot I} \quad (1)$$

and for the hinge end (H) at $x=L$ the slope can be written as:

$$W'_H(L) = -\frac{q \cdot L^3}{48E \cdot I} \quad (2)$$

where,

q [N/m] – is the load per unit of length (dead load);

L [m] – is the beam length;

E [N/m²] – is the modulus of elasticity of the beam material;

I [m⁴] – is the moment of the inertia of the cross section of the beam.

If the bending moment (1) is applied to the hinge, the slope becomes positive, and the relationship (2) depending on the bending moment (1) becomes:

$$W'_H(L) = \frac{q \cdot L^3}{48E \cdot I} = -\frac{L}{4} \left(-\frac{q \cdot L^2}{8E \cdot I} \right) = -\frac{L}{4} W''_C(L) \quad (3)$$

or, expressing the bending moment from (3) and taking into account the stiffness k_2 :

$$k_2 W''_C(L) = -k_2 \frac{4}{L} W'_H(L) \quad (4)$$

Taking into considerations the weakened coefficient k_2 , the bending moment from the clamped end must be equal to the bending moment applied to the hinge:

$$k_2 W''_C(L) = (1 - k_2) W''_H(L) \quad (5)$$

also taking into account (4), in the right support it will obtained:

$$(1 - k_2) W''_H(L) - k_2 W''_C(L) = 0 = (1 - k_2) W''_H(L) + k_2 \frac{4}{L} W'_H(L) \quad (6)$$

From relation (6) if $k_2=0$, the bending moment is zero ($W''_{\text{H}}(L)=0$), that means for $x=L$ we have a hinge, and if $k_2=1$, the slope is zero ($W'_{\text{H}}(L)=0$), so we have a clamped end. For any other values of $k_2 \in [0, \dots, 1]$, the right support becomes a weakened clamped end and in this point we will find both bending moment and slope.

3. Eigenvalues, modal function and strain energy function

Using the procedure presented in the first part of the paper, the spatial solution of the differential equation of bending vibrations, free and undamped using Euler-Bernoulli model:

$$W(x) = A\sin(\alpha x) + B\cos(\alpha x) + C\sinh(\alpha x) + D\cosh(\alpha x) \quad (7)$$

where,

$W(x)$ – is the modal motion function;

A, B, C, D – are integration constants that are obtained from the boundary conditions;

α – is the eigenvalue;

x – is the variable length of the normalized beam.

Boundary condition for clamped end (C), at $x=0$:

$$\begin{cases} W_C(0) = 0 = B + D \Rightarrow D = -B \\ W'_C(0) = 0 = \alpha(A + C) \Rightarrow C = -A \end{cases} \quad (8)$$

In the right support, the deflection is zero both for the hinge end and for the clamped end. Taking into account the results obtained in (8), introduced in (7) for $x=L=1$, the integration constant B is obtained:

$$\begin{cases} W(1) = 0 = A(\sin\alpha - \sinh\alpha) + B(\cos\alpha - \cosh\alpha) \\ \Rightarrow B = -A \frac{\sin\alpha - \sinh\alpha}{\cos\alpha - \cosh\alpha} \end{cases} \quad (9)$$

By introducing the constants B, C and D in relation (6), the characteristic equation (10) is obtained. Solutions (10) give us the eigenvalues for each vibration mode.

$$\alpha(1 - k_2)(\sin\alpha \cdot \cosh\alpha - \cos\alpha \cdot \sinh\alpha) + k_2 \frac{4}{L}(1 - \cos\alpha \cdot \cosh\alpha) = 0 \quad (10)$$

The expression of the modal function for the bending vibration modes is represented in relationship (11):

$$W(x) = A \left[\sin(\alpha x) - \sinh(\alpha x) - \frac{\sin\alpha - \sinh\alpha}{\cos\alpha - \cosh\alpha} (\cos(\alpha x) - \cosh(\alpha x)) \right] \quad (11)$$

The strain energy depends of the square of the curvature of the modal function, and is defined as:

$$E_{p_n} = \frac{1}{2} \int_0^L E \cdot I \cdot W''(x)^2 dx \quad (12)$$

From relation (11) we obtain the curvature expression, which its squared is directly proportional to the normalized strain energy:

$$W''(x)^2 = \left\{ A\alpha^2 \left[\frac{\sin\alpha - \sinh\alpha}{\cos\alpha - \cosh\alpha} (\cos(\alpha x) + \cosh(\alpha x)) - \sin(\alpha x) - \sinh(\alpha x) \right] \right\}^2 \quad (13)$$

4. Results

The eigenvalues α_n for the first six vibration modes (n=6) and different values of k_2 , solutions of relationship (10) for $L = 1$, can be found in table 1.

Table 1. Eigenvalues for the n=6 vibration modes and different values of stiffness coefficient k_2

k_2	Vibration mode (n)					
	1	2	3	4	5	6
0.0	3.926602	7.068583	10.21018	13.35177	16.49336	19.63495
0.1	3.982267	7.098856	10.23143	13.36812	16.50664	19.64614
0.2	4.041832	7.133840	10.25663	13.38776	16.52273	19.65975
0.3	4.105765	7.174669	10.28695	13.41177	16.54258	19.67667
0.4	4.174604	7.222855	10.32407	13.44177	16.56771	19.69827
0.5	4.248967	7.280433	10.37048	13.48025	16.60047	19.72675
0.6	4.329552	7.350196	10.42997	13.53129	16.64490	19.76597
0.7	4.417137	7.436006	10.50854	13.60187	16.70831	19.82325
0.8	4.512551	7.543231	10.61608	13.70490	16.80534	19.91407
0.9	4.616622	7.679200	10.76929	13.86595	16.96874	20.07655
1.0	4.730041	7.853205	10.99561	14.13717	17.27876	20.42035

The first n=6 (six) normalized vibration modes ($\pm W(x)$ – relationship (11)) and the normalized strain energy ($W''(x)^2$ – relationship (13)) for the following values of $k_2=0.0, 0.25, 0.50, 0.75, 0.85, 0.95$ and $1, 00$ are illustrated in the figures 2 - 8.

For this analyzed cases the weakened coefficient k_1 is considered to be 1.

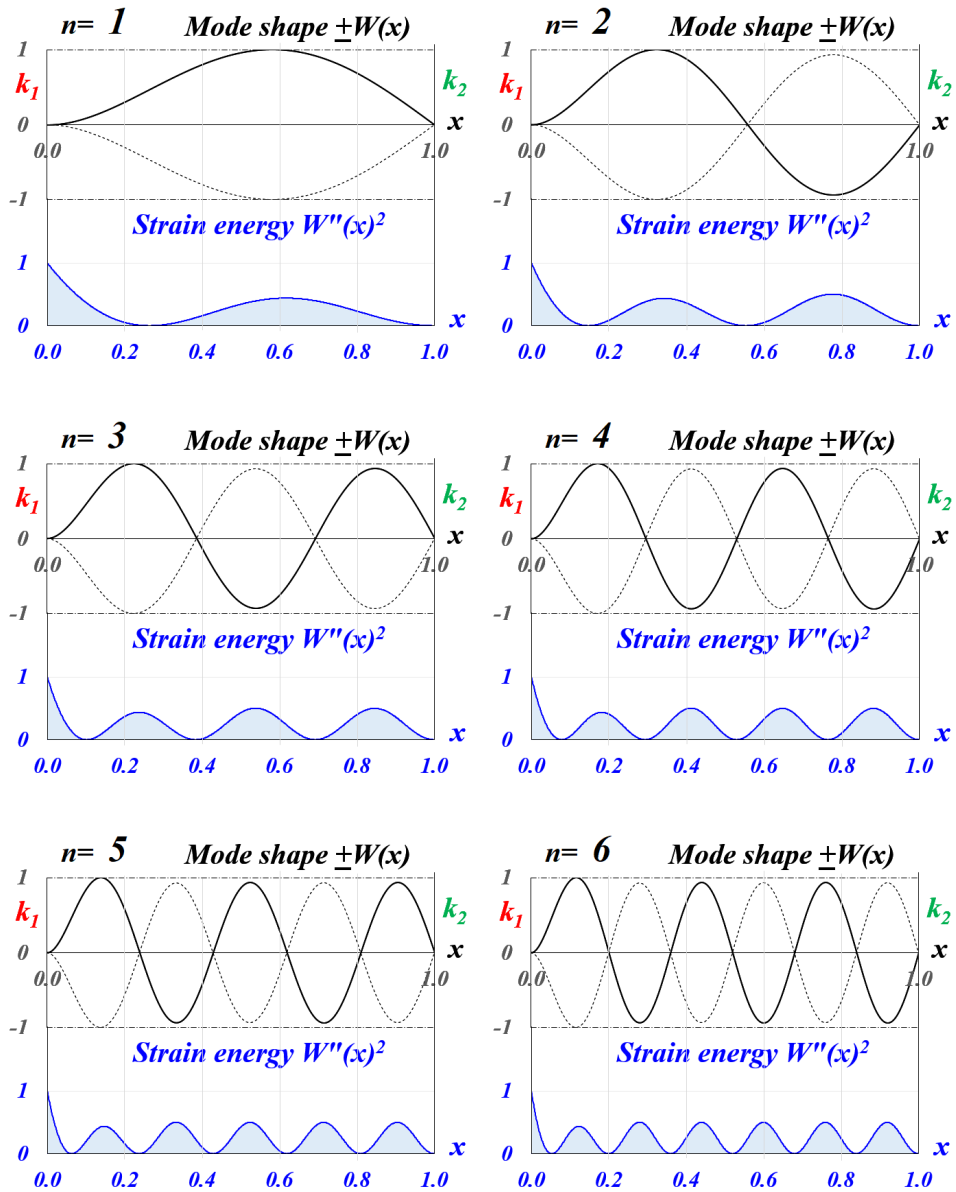


Figure 2. Normalized mode shapes ($\pm W(x)$) and normalized strain energy ($W''(x)^2$) for the first $n=6$ vibration modes and $k_2=0.0$

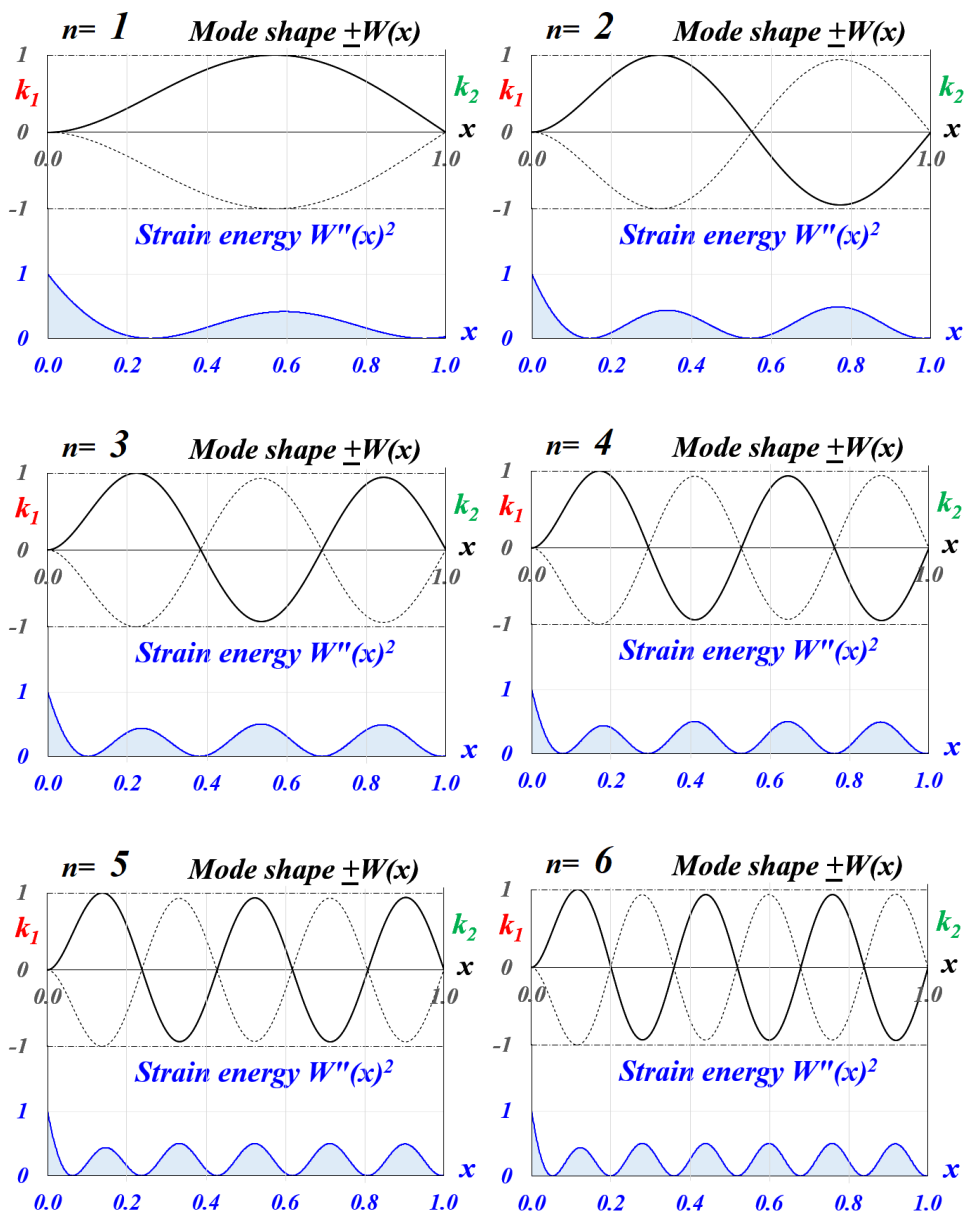


Figure 3. Normalized mode shapes ($\pm W(x)$) and normalized strain energy ($W''(x)^2$) for the first $n=6$ vibration modes and $k_2=0.25$

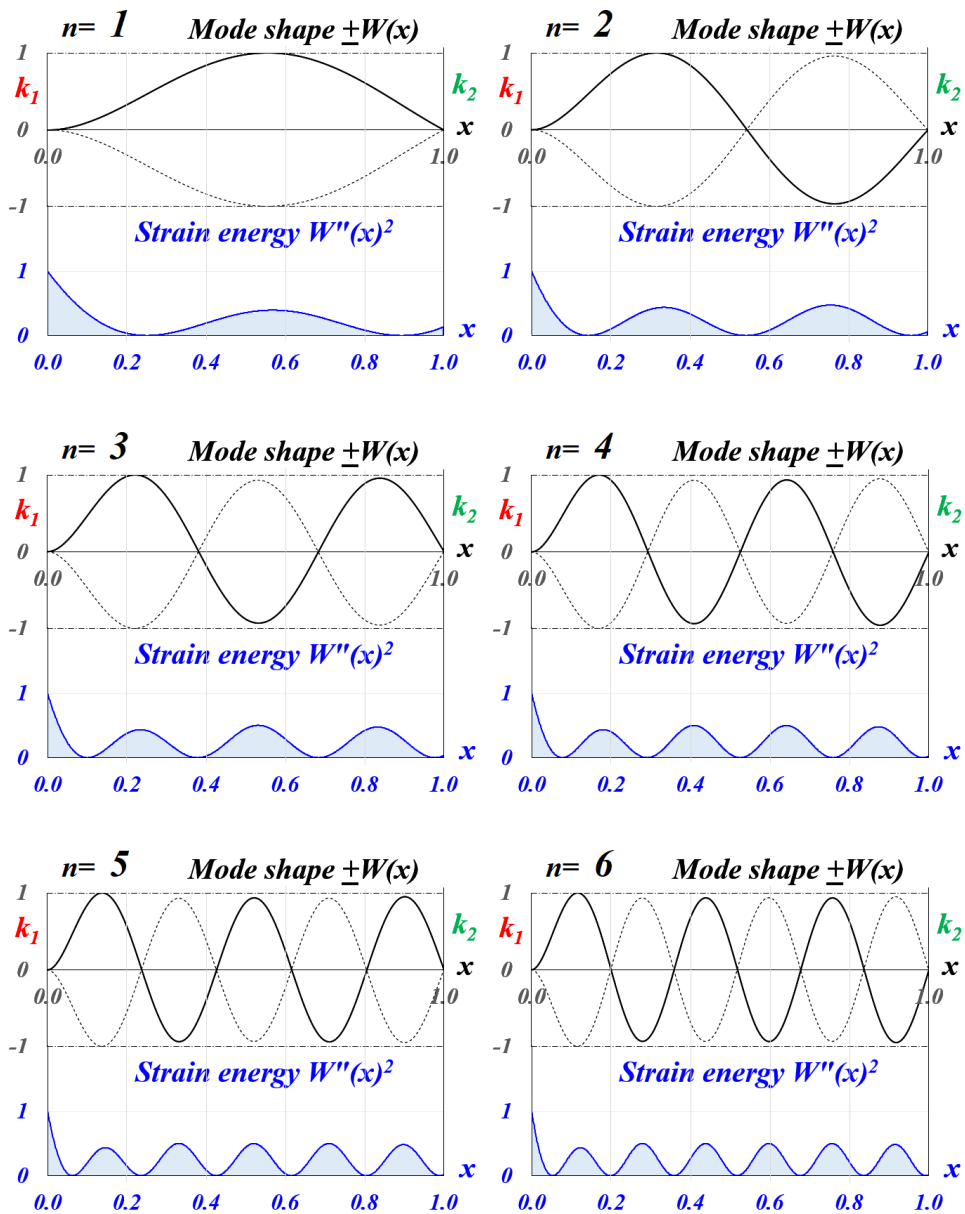


Figure 4. Normalized mode shapes ($\pm W(x)$) and normalized strain energy ($W''(x)^2$) for the first $n=6$ vibration modes and $k_2=0.50$

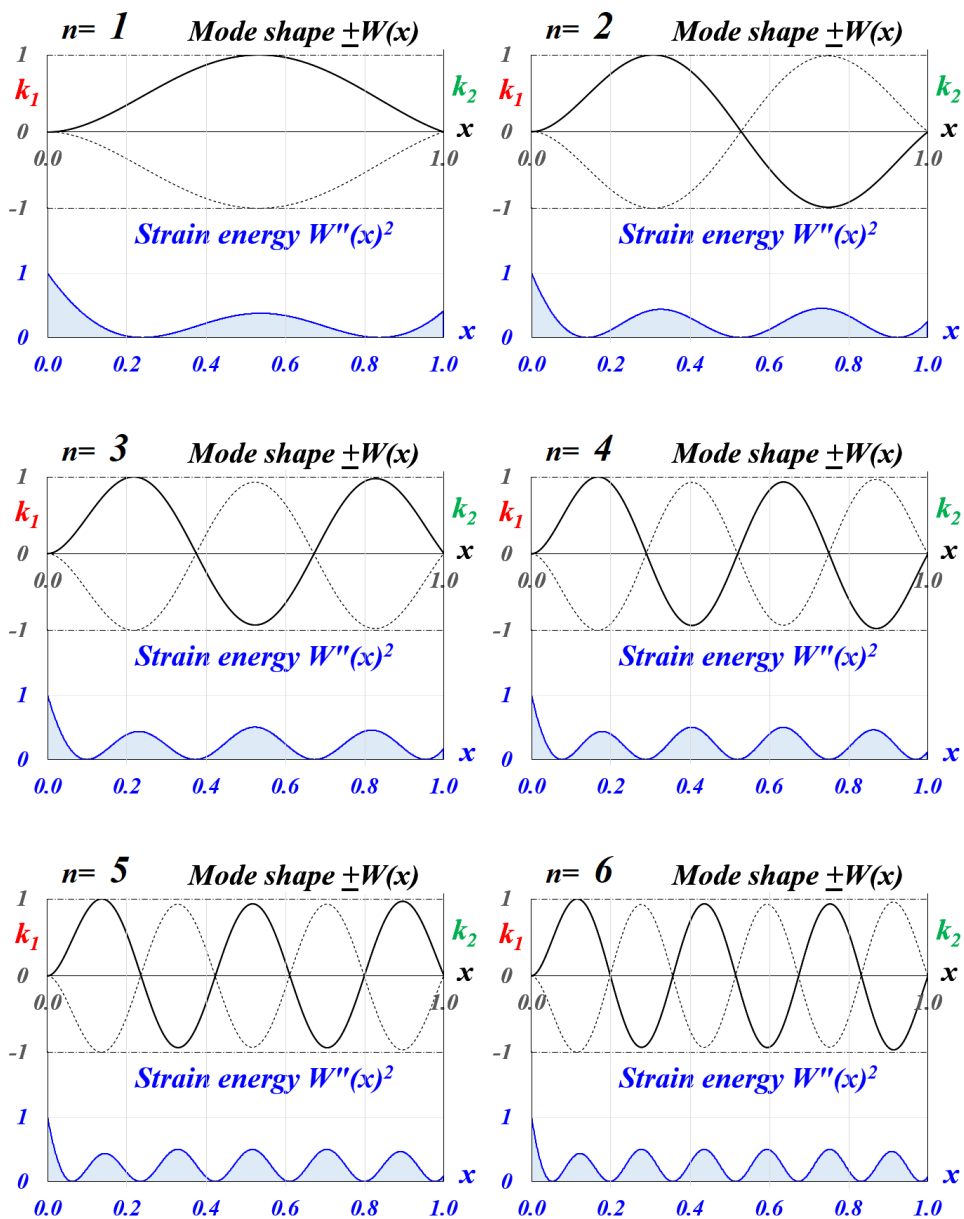


Figure 5. Normalized mode shapes ($\pm W(x)$) and normalized strain energy ($W''(x)^2$) for the first $n=6$ vibration modes and $k_2=0.75$

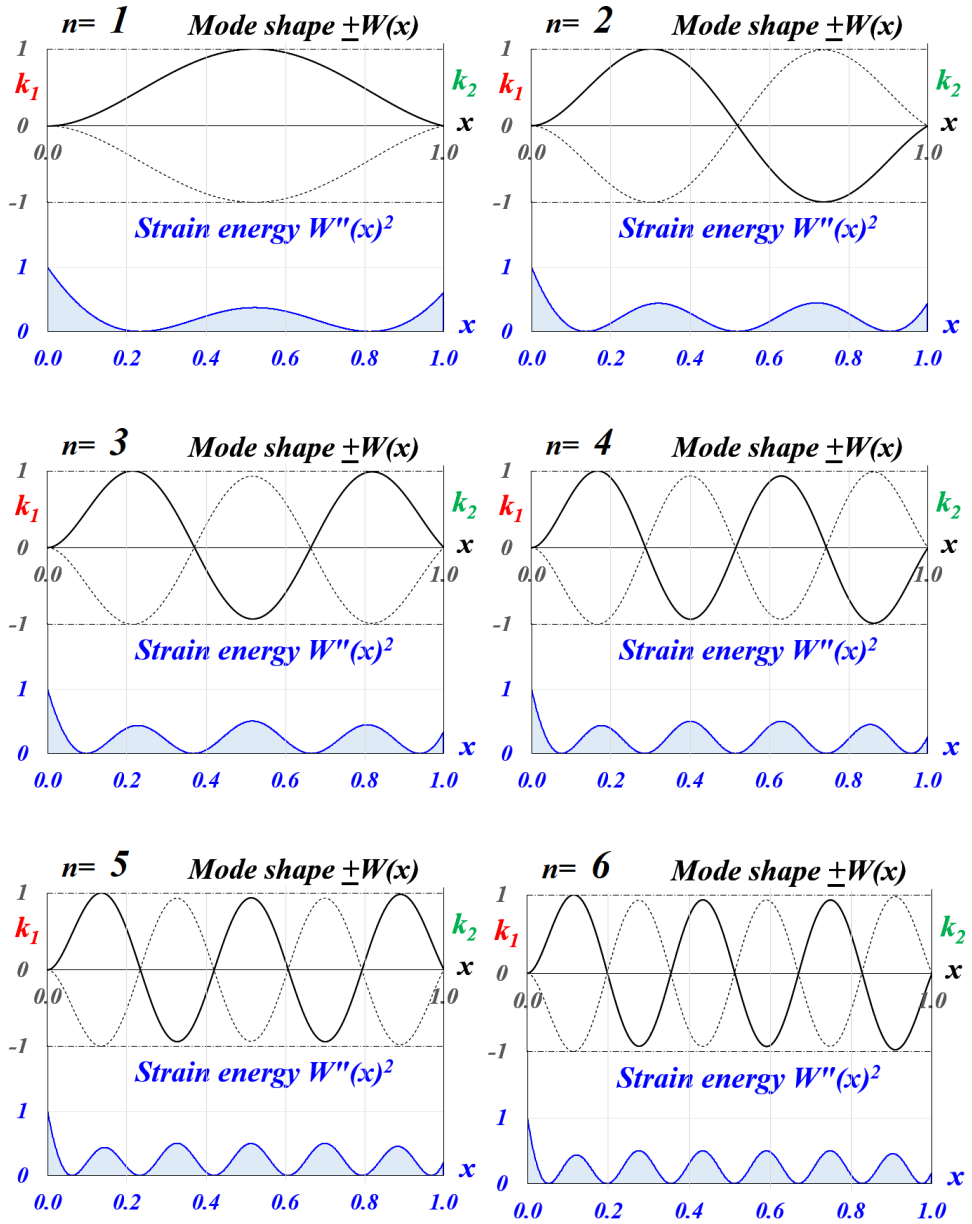


Figure 6. Normalized mode shapes ($\pm W(x)$) and normalized strain energy ($W''(x)^2$) for the first $n=6$ vibration modes and $k_2=0.85$

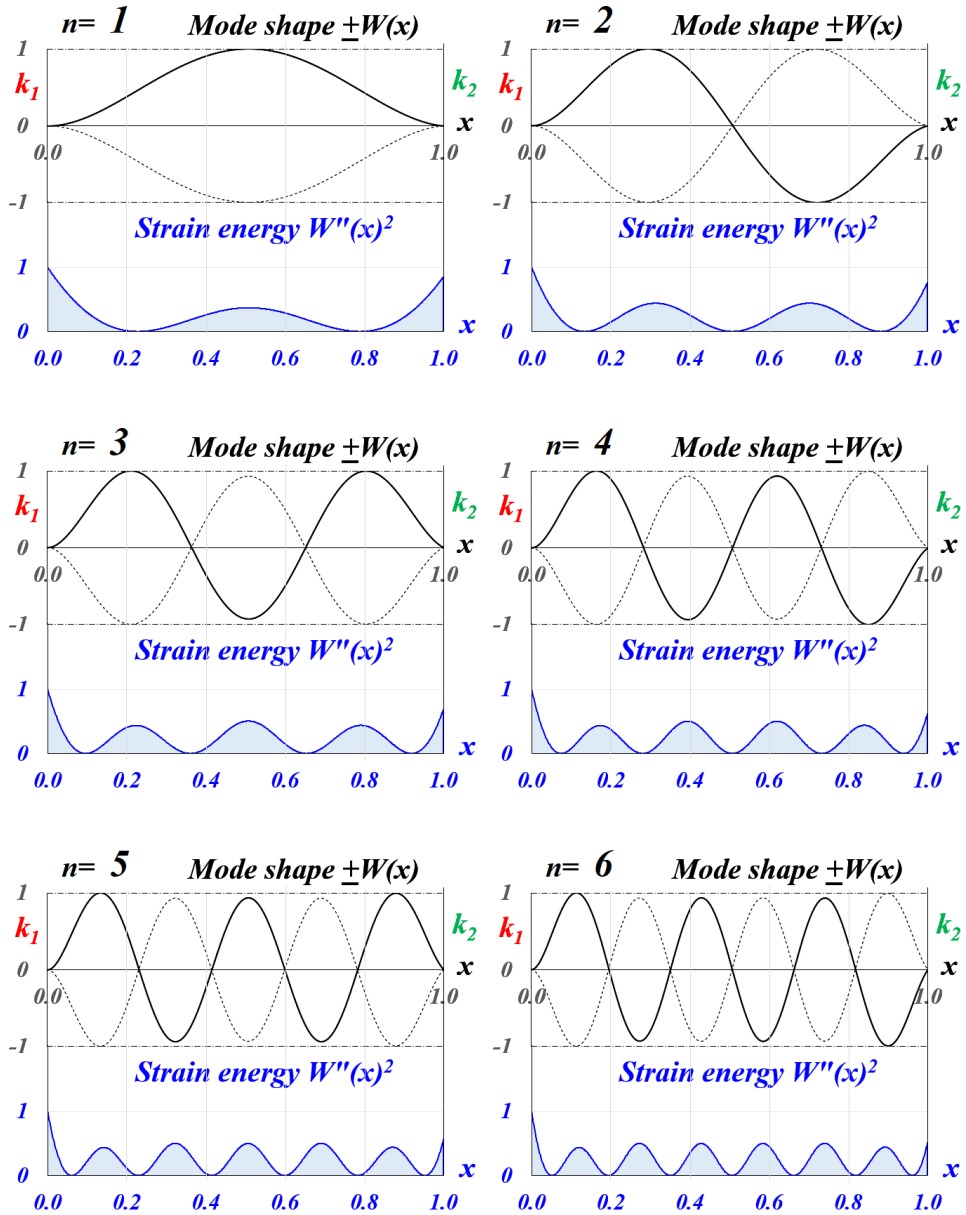


Figure 7. Normalized mode shapes ($\pm W(x)$) and normalized strain energy ($W''(x)^2$) for the first $n=6$ vibration modes and $k_2=0.95$

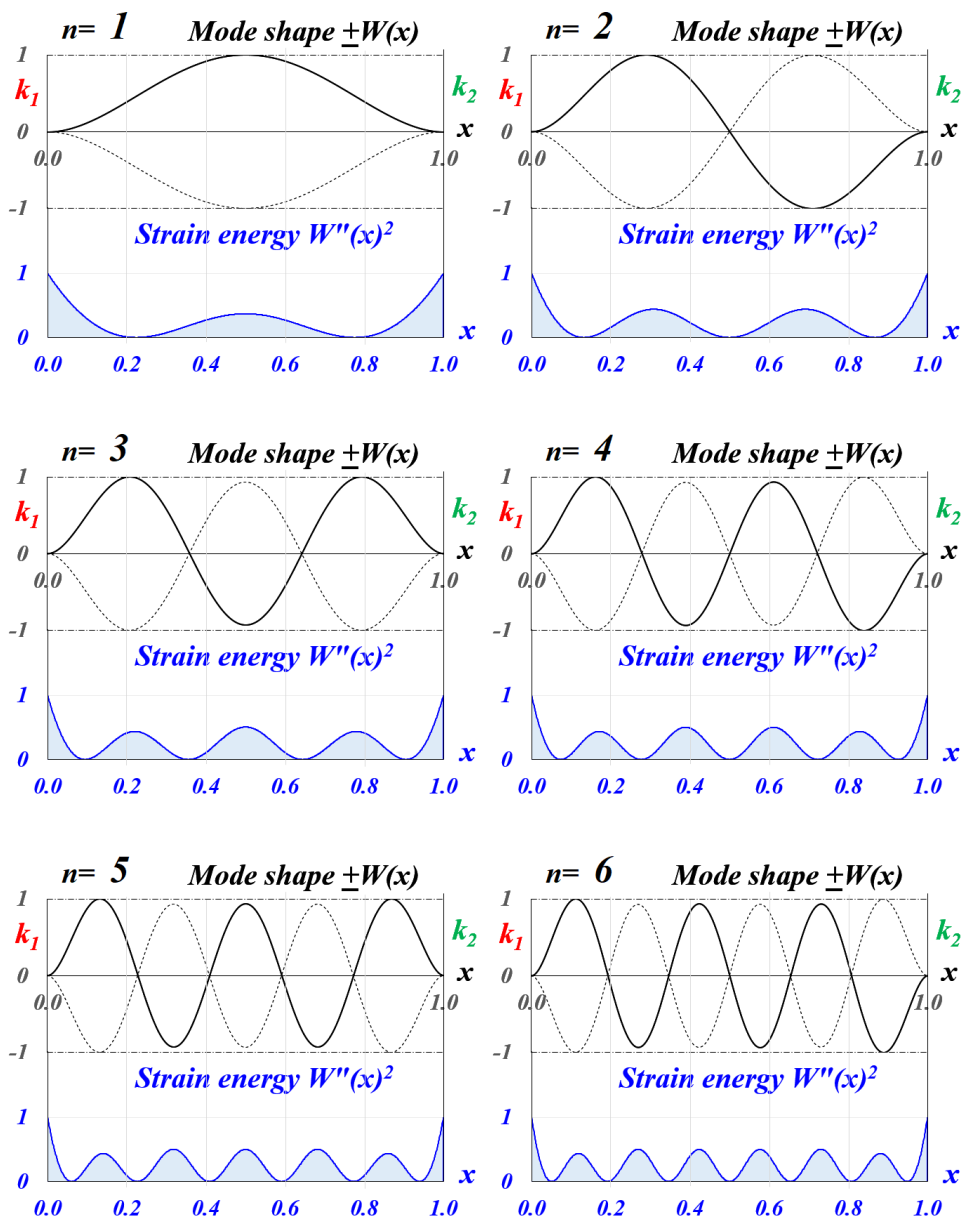


Figure 8. Normalized mode shapes ($\pm W(x)$) and normalized strain energy ($W''(x)^2$) for the first $n=6$ vibration modes and $k_2=1.0$

5. Conclusions

The paper presents the eigenvalues, modal shapes and strain energy for the six bending vibration modes for the case where the right clamped end of the beam is weakened by the coefficient $k_2 \in [0, \dots, 1]$ and the left end of the beam is clamped.

For the extreme cases: $k_2=0$, the eigenvalues (Table 1) were obtained for the beam clamped at one end and hinged at the other; respectively for $k_2=1$, we find the eigenvalues for the double clamped beam.

From the analysis of the figures from figures 2 – 5, it can be observed that for stiffness values of $k_2 < 0.75$, from the point of view of the mode shapes, the soft clamped end has a behavior very close to that of a hinged support.

Instead, the normalized strain energy in the right support, which in the hinge has zero value ($k_2=0$), with the increase of k_2 , its value increases, reaching $\sim 2.5\%$ of the maximum value for $k_2=0.25$, $\sim 13.4\%$ of the maximum value for $k_2=0.5$ and $\sim 41\%$ of the maximum value for $k_2=0.75$, at first vibration mode.

For the second vibration mode, the normalized strain energy has smaller values in this point, respectively, $\sim 0.8\%$ for $k_2=0.25$, and $\sim 5.7\%$ for $k_2=0.5$ and $\sim 25\%$ for $k_2=0.75$ and the trend continues for the other vibration modes.

For stiffness values $k_2 > 0.85$ (figures 6 – 8), the mode shapes of the beam are significantly affected and although the relation (6) that describes the soft clamped end of the beam is a linear expression of k_2 , the effect of k_2 in the modal function does not have a linear behavior. At the point $x=L$, the normalized strain energy becomes maximum for $k_2=1.0$ for all vibration modes.

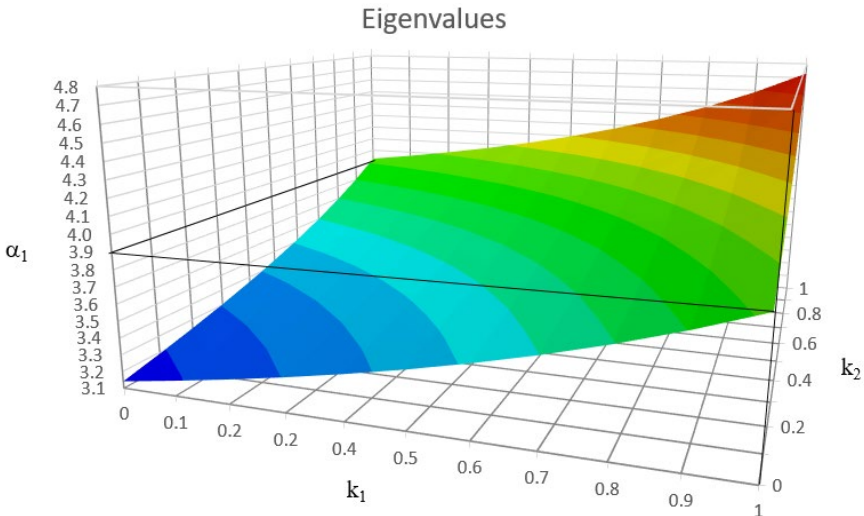


Figure 9. First vibration mode eigenvalues for $k_1 \in [0, \dots, 1]$ and $k_2 \in [0, \dots, 1]$

Taking into account the results presented in the first and second part of the paper, in figure 9 it can be seen in 3D representation, the eigenvalues for the first mode of vibration for all the evolution of the weakened coefficients k_1 and k_2 .

The minimum value $\alpha_1=\pi$ corresponds to the simply supported case, the peaks for $k_1=1, k_2=0$, respectively $k_1=0, k_2=1$, correspond to the clamp-hinge, respectively hinge-clamp cases, with the eigenvalue of $\alpha_1=3.926602$, and the maximum value $\alpha_1=4.730041$ corresponds to the double clamped beam.

References

- 1 Lupu D., Tufiș C., Gillich G.R., Ardeljan M., Detection of transverse cracks in prismatic cantilever beams affected by weak clamping using a machine learning method, *Analecta Technica Szegedinensesia*, 16(1), 2022, pp. 122-128.
- 2 Lupu D., Gillich G.R., Nedelcu D., Gillich N., Mănescu T., *A method to detect cracks in the beams with imperfect boundary conditions*, International Conference on Applied Science (ICAS 2020), Journal of Physics: Conference Series 1781(2021) 012012, IOP Publishing, pp. 1-13.
- 3 Praisach Z.I., Ardeljan D., Pîrșan D.A., Gillich G.R., A new approach for imperfect boundary conditions on the dynamic behavior, *Analecta Technica Szegedinensesia*, 16(1), 2022, pp. 56-61.
- 4 Gillich G.R., Praisach Z.I., Exact solution for the natural frequencies of slender beams with an abrupt stiffness decrease, *Journal of Engineering Sciences and Innovation*, 2(1) 2017, *A. Mechanics, Mechanical and Industrial Engineering, Mechatronics*, pp. 13-21.
- 5 Karthikeyan M., Tiwari R., Talukdar S., *Identification of crack model parameters in a beam from modal parameters*, in 12th National Conference on Machines and Mechanisms (NaCoMM-2005), 2005.
- 6 Nahvi H., Jabbari M., Crack detection in beams using experimental modal data and finite element model, *International Journal of Mechanical Sciences*, 47(10), 2005, pp. 1477–1497.
- 7 Dems K., Turant J., Structural damage identification using frequency and modal changes, *Bulletin of the Polish Academy of Sciences Technical Sciences*, 59(1), 2011, pp. 23–32.
- 8 Gillich G.R., Nedelcu D., Wahab M.A., Pop M.V., Hamat C.O., *A new mathematical model for cracked beams with uncertain boundary conditions*, International Conference on Noise and Vibration Engineering (ISMA 2020), Leuven, Belgium, pp. 3871-3883.

- 9 Shi D., Tian Y., Choe K.N., Wang Q., A weak solution for free vibration of multi-span beams with general elastic boundary and coupling condition, *JVE International Ltd. Vibroengineering PROCEDIA*, vol. 10, 2016, pp. 298–303.

Addresses:

- Phd stud. Eng. Dan-Alexandru Pîrşan, Doctoral School of Engineering, Babeş-Bolyai University, Cluj-Napoca, Romania, Faculty of Engineering, Piaţa Traian Vuia, nr. 1-4, 320085, Reşiţa, Romania
dan.pirsan@ubbcluj.ro
- Lect. PhD. Habil. Zeno-Iosif Praisach, Department of Engineering Science, Babeş-Bolyai University, Cluj-Napoca, Romania, Faculty of Engineering, Piaţa Traian Vuia, nr. 1-4, 320085, Reşiţa, Romania
zeno.praisach@ubbcluj.ro
(* *corresponding author*)
- Prof. PhD. Gilbert-Rainer Gillich, Department of Engineering Science, Babeş-Bolyai University, Cluj-Napoca, Romania, Faculty of Engineering, Piaţa Traian Vuia, nr. 1-4, 320085, Reşiţa, Romania
gilbert.gillich@ubbcluj.ro
- Lect. PhD. Cornel Haţiegan, Department of Engineering Science, Babeş-Bolyai University, Cluj-Napoca, Romania, Faculty of Engineering, Piaţa Traian Vuia, nr. 1-4, 320085, Reşiţa, Romania
cornel.hatiegan@ubbcluj.ro

Dynamic behavior of a clamped circular plate and strain energy representation (part I)

Lucian-Nestor Manu, Zeno-Iosif Praisach*, Gilbert-Rainer Gillich, Cristian Tufișu

Abstract. *The first part of the paper presents a study regarding the dynamics behavior of thin circular plate clamped all around. An analytical investigation is performed and the results in terms of mode shapes are used to highlight the plate's dynamics. The modal shapes are obtained using Bessel functions and their graphic representation is presented in 3D by using MS Excel software.*

Keywords: *circular plate, mode shape, Bessel functions*

1. Introduction

In mechanical and civil engineering structures, the circular plates are often used. Their support types are imposed by different conditions and often are imposed by the structures functions and exploitation [1].

Circular plates are plane and thinned structures which are characterized by the thickness h . The thickness is small compared to the radius R [2].

Many researchers have been obtained analytical solutions. Their research has focus on the topic of natural frequencies of the plates [3-6].

The first researches regarding vibrations of plates were published at the end of the 18th century by researchers as Euler and Bernoulli. Their research was continued by Tanaka, Chladni, Konig, Rayleigh, Ritz etc.

In the recent times: Timoshenko and Leissa for instance brought important progresses in this domain [7-11], by development of methods in order to solve the plates and establish some solutions of their differential equations of equilibrium.

In the paper, the modal functions for a circular plate clamped all around are derived by using Bessel functions and the normalized modal shapes are illustrated in 3D by using MS Excel.



2. Analytical approach

Following the methodology described in [2] the differential equation of motion for the transverse displacement w of a circular plate is given by:

$$D\nabla^4 w + \rho \frac{\partial^2 w}{\partial t^2} \quad (1)$$

where,

D [Nm] is the flexural rigidity and is defined by:

$$D = \frac{Eh^3}{12(1-\nu^2)} \quad (2)$$

E [N/m²] is Young's modulus

h [m] is the plate thickness

ν is Poisson's ratio

ρ [m] is mass density per unit area of the plate

t [s] is time

$\nabla^4 = (\nabla^2)^2$ and ∇^2 is the Laplacian operator.

Free vibrations are assumed and the motion is expressed as:

$$w = W \cos(\omega t) \quad (3)$$

where,

ω [rad/s] is the circular frequency

W is a function only of the position coordinates.

Then, by substituting the equation (3) into equation (1) we obtained:

$$(\nabla^4 - k^4)W = (\nabla^2 + k^2)(\nabla^2 - k^2)W \quad (4)$$

where the dimensionless wave number k defined as:

$$k^4 = \frac{\rho \omega^2}{D} \quad (5)$$

By superimposing the solutions, the complete solution to equation (4) become:

$$\begin{cases} \nabla^2 W_1 + k^2 W_1 = 0 \\ \nabla^2 W_2 - k^2 W_2 = 0 \end{cases} \quad (6)$$

It is assumed that the Fourier components are in θ and the solutions (6) becomes:

$$W(r, \theta) = \sum_{n=0}^{\infty} W_n(r) \cos(n\theta) + \sum_{n=1}^{\infty} W_n^*(r) \sin(n\theta) \quad (7)$$

The origin of a polar coordinate system of the circular plate clamped all around is taken to coincide with the center of the circular plate. For the analyzed case, the plate has no internal holes. The symmetry of the boundary conditions respect to one

or more diameters of the circular plate exist. In this case the terms involving $\sin(n\theta)$ are not needed [11].

Taking in consideration the Bessel functions, by substituting the equation (7) into equation (6), the general solution in polar coordinates for the circular plate becomes:

$$W_n(r, \theta) = [A_n J_n(kr) + C_n I_n(kr)] \cos(n\theta) \quad (8)$$

where,

$n = 0 \dots \infty$ represents the number of nodal diameters

A_n, B_n are the coefficients obtained from boundary conditions

J_n is the Bessel function of the first kind

I_n is the modified Bessel function of the first kind.

The boundary conditions for a circular plate clamped all around with radius R :

$$\begin{cases} W(R) = 0 \\ \frac{\partial W(R)}{\partial r} = 0 \end{cases} \quad (9)$$

When equation (9) is substituted into equation (8), the existence of a nontrivial solution yields the characteristic determinant:

$$\begin{vmatrix} J_n(\lambda) & I_n(\lambda) \\ J'_n(\lambda) & I'_n(\lambda) \end{vmatrix} = 0 \quad (10)$$

where, $\lambda = kR$.

Next, the recursion relations will be used:

$$\begin{cases} \lambda J'_n(\lambda) = nJ_n(\lambda) - \lambda J_{n+1}(\lambda) \\ \lambda I'_n(\lambda) = nI_n(\lambda) + \lambda J_{n+1}(\lambda) \end{cases} \quad (11)$$

The frequency equation is obtained by expanding equation (10):

$$J_n(\lambda)J_{n+1}(\lambda) + I_n(\lambda)J_{n+1}(\lambda) = 0 \quad (12)$$

The solutions of the frequency equation give us the dimensionless wave numbers λ^2 , where, n represents the number of nodal diameters, and s the number of nodal circles and does not include the contour circle.

The normalized mode shape function is:

$$\begin{cases} W(r, \theta)_{n,s} = \left[J_n \left(\lambda_{n,s}, \frac{r}{R} \right) - \frac{I_n(\lambda_{n,s})}{I_n(\lambda_{n,s})} I_n \left(\lambda_{n,s}, \frac{r}{R} \right) \right] \cos(n\theta) \\ W(r, \theta)_{n,s} = \left[J_n \left(\lambda_{n,s}, \frac{r}{R} \right) - \frac{J_n(\lambda_{n,s})}{I_n(\lambda_{n,s})} I_n \left(\lambda_{n,s}, \frac{r}{R} \right) \right] \sin(n\theta) \end{cases} \quad (13)$$

3. Results

The dimensionless wave numbers $\lambda_{n,s}^2$ depending on the number of nodal diameters n , respectively the number of nodal circles s are presented in table 1.

Table 1. Dimensionless wave numbers $\lambda_{n,s}^2$

s	Nodal diameters n					
	0	1	2	3	4	5
0	10.21583	21.2604	34.87704	51.03004	69.66583	90.73899
1	39.77115	60.82867	84.58265	111.0214	140.1079	171.8030
2	89.10414	120.0792	153.8151	190.3038	229.5186	271.4282
3	158.1842	199.0534	242.7206	289.1799	338.4112	390.3895
4	247.0064	297.7601	351.3360	407.7295	466.9250	528.9021
5	355.5693	416.2026	479.6751	545.9830	615.1140	687.0511
6	483.8722	554.3824	627.7441	703.9546	783.0036	864.8769

The mode shapes for the circular plate clamped all around is presented in the figures 1 - 7.

Fig. 1 present the first six vibration modes for nodal circle $s=0$ and nodal diameters $n=0, 1, 2, 3, 4$ and 5 .

Fig. 2 present the first six vibration modes for nodal circle $s=1$ and nodal diameters $n=0, 1, 2, 3, 4$ and 5 .

Fig. 3 present the first six vibration modes for nodal circle $s=2$ and nodal diameters $n=0, 1, 2, 3, 4$ and 5 .

Fig. 4 present the first six vibration modes for nodal circle $s=3$ and nodal diameters $n=0, 1, 2, 3, 4$ and 5 .

Fig. 5 present the first six vibration modes for nodal circle $s=4$ and nodal diameters $n=0, 1, 2, 3, 4$ and 5 .

Fig. 6 present the first six vibration modes for nodal circle $s=5$ and nodal diameters $n=0, 1, 2, 3, 4$ and 5 .

Fig. 7 present the first six vibration modes for nodal circle $s=6$ and nodal diameters $n=0, 1, 2, 3, 4$ and 5 .

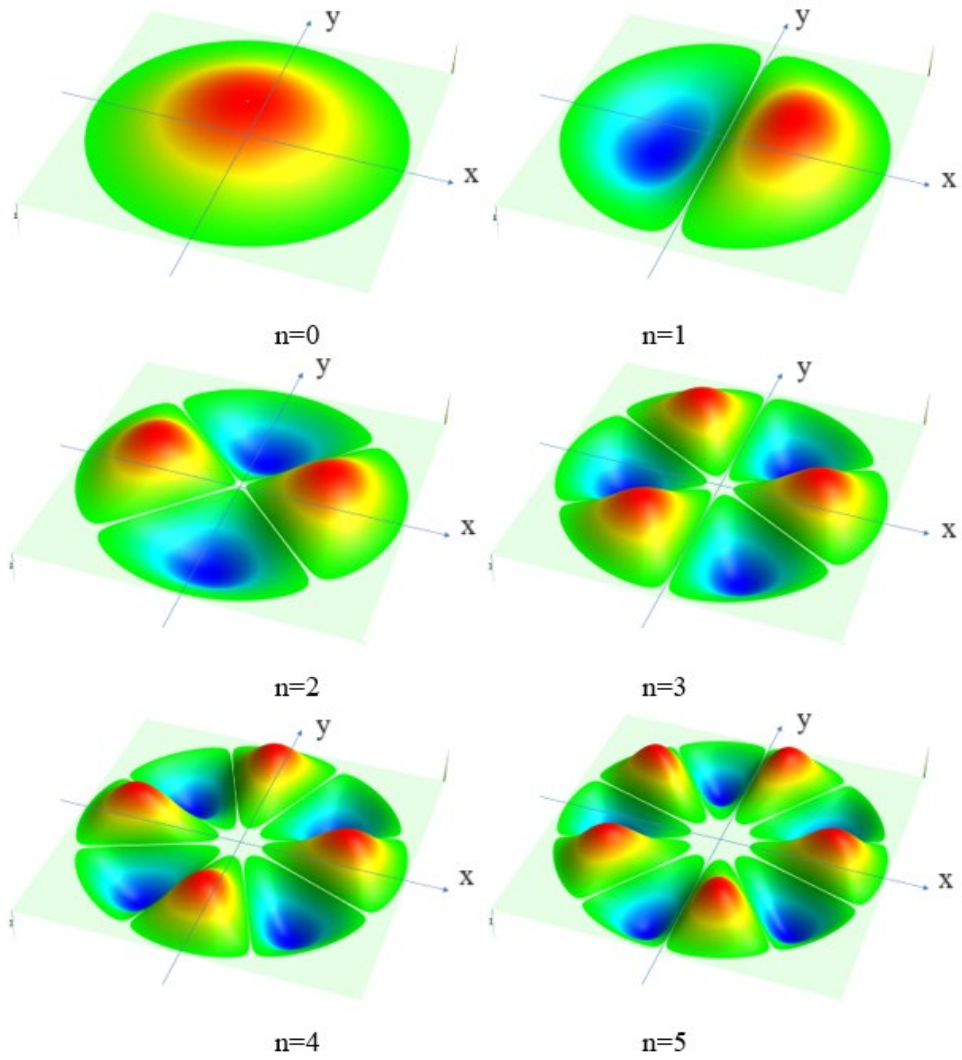


Figure 1. Mode shapes for the circular plate clamped all around; nodal circle $s=0$, nodal diameters $n=0, \dots, 5$.

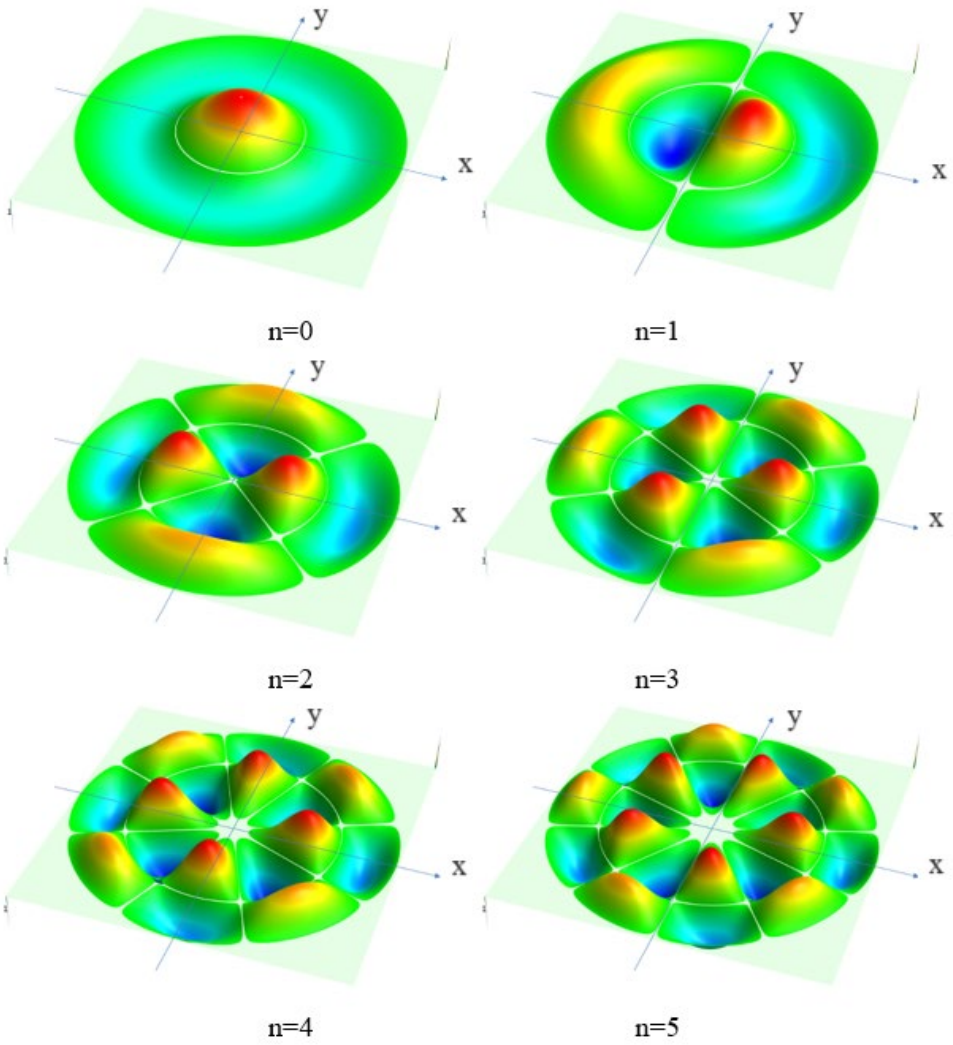


Figure 2. Mode shapes for the circular plate clamped all around; nodal circle $s=1$, nodal diameters $n=0, \dots, 5$.

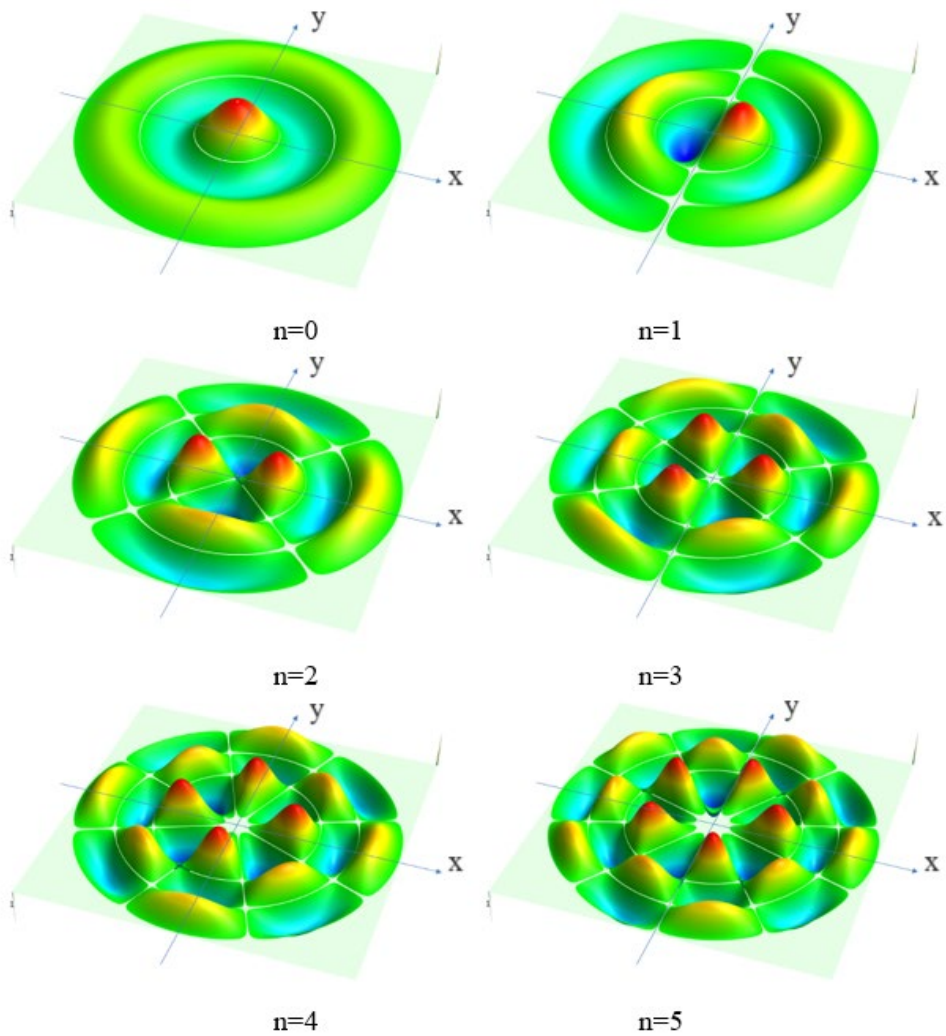


Figure 3. Mode shapes for the circular plate clamped all around; nodal circle $s=2$, nodal diameters $n=0, \dots, 5$.

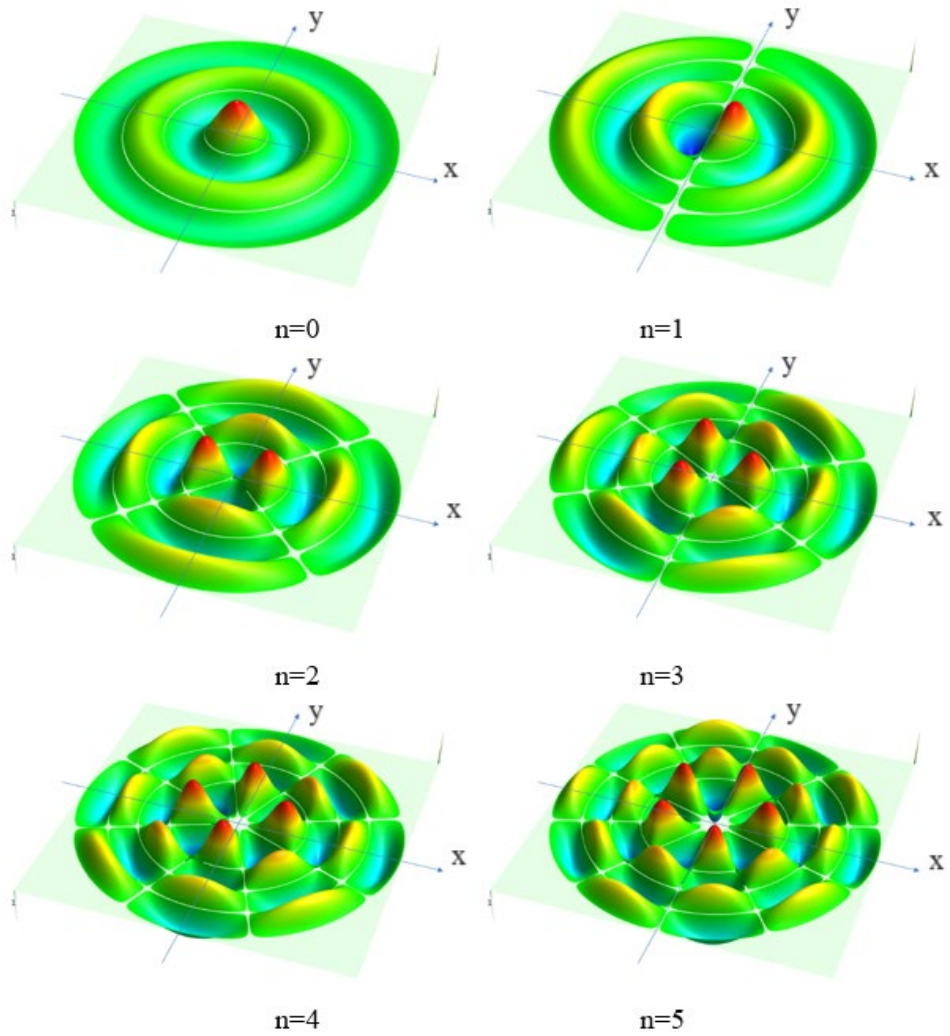


Figure 4. Mode shapes for the circular plate clamped all around; nodal circle $s=3$, nodal diameters $n=0, \dots, 5$.

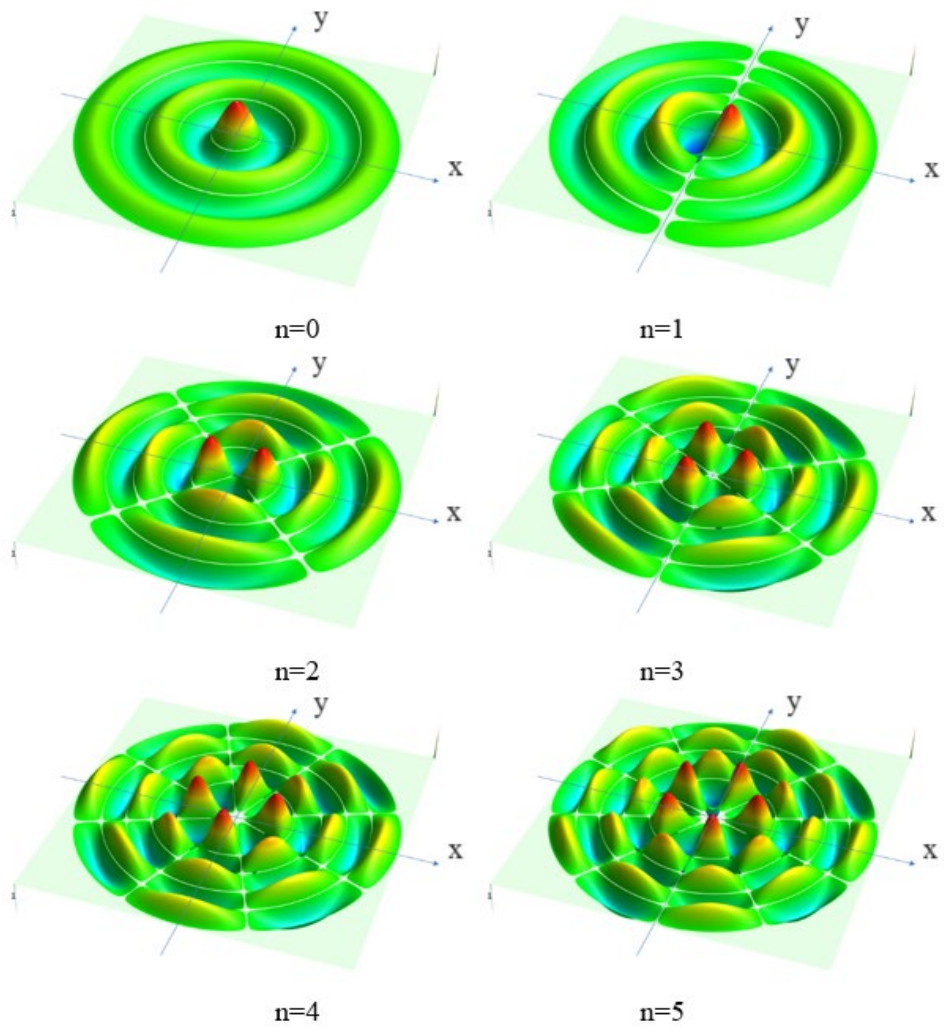


Figure 5. Mode shapes for the circular plate clamped all around; nodal circle $s=4$, nodal diameters $n=0, \dots, 5$.

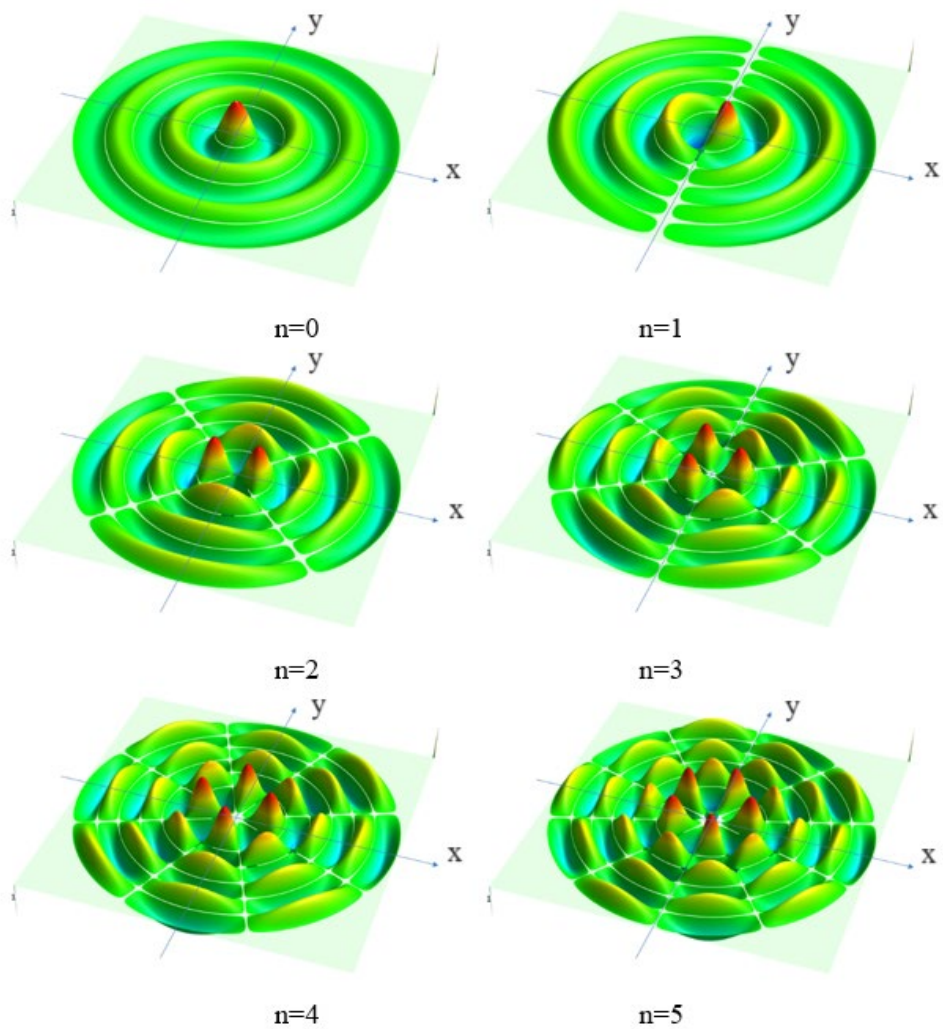


Figure 6. Mode shapes for the circular plate clamped all around; nodal circle $s=5$, nodal diameters $n=0, \dots, 5$.

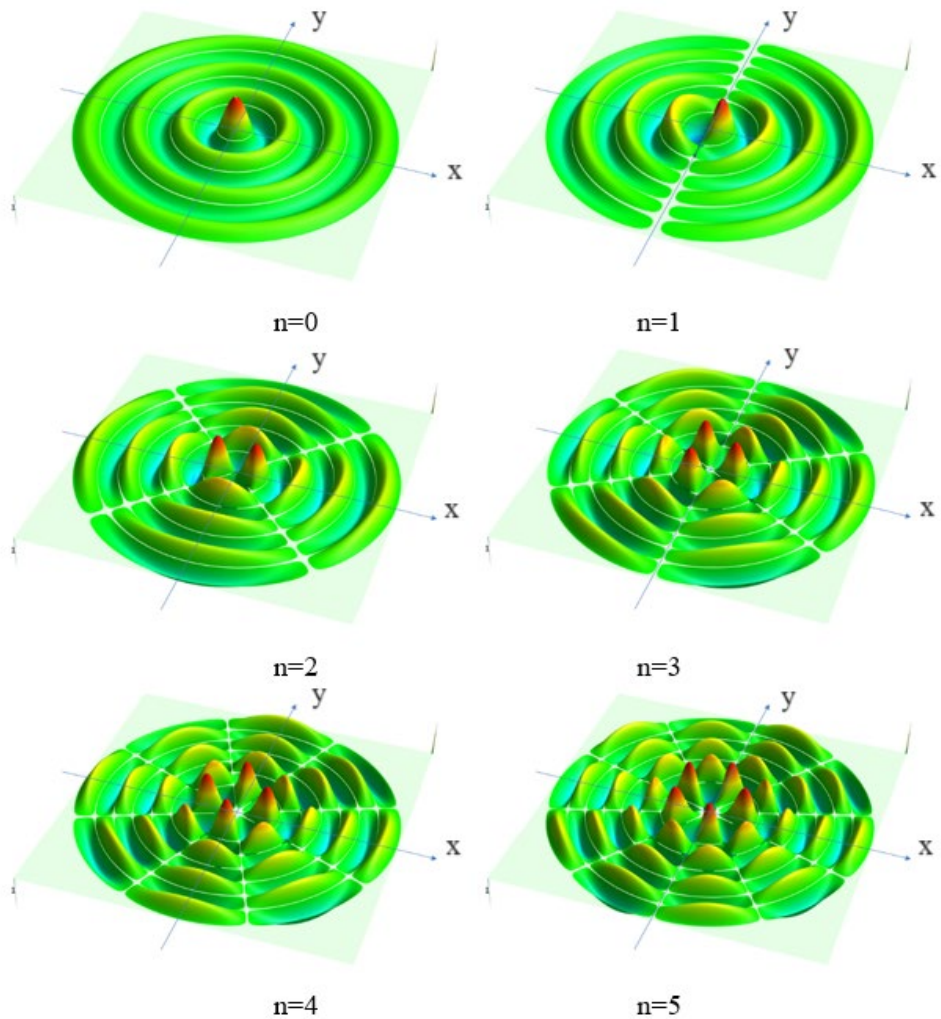


Figure 7. Mode shapes for the circular plate clamped all around; nodal circle $s=5$, nodal diameters $n=0, \dots, 5$.

4. Conclusions

The paper presents the vibration modes for a circular plate clamped all around in a 3D representation using MS Excel software. Using the Bessel functions, the frequency equation and the modal function were analytically determined.

The dimensionless wave numbers $\lambda_{n,s}^2$ were calculated for six values of the nodal diameters $n=0, 1, \dots, 5$ and seven values of the nodal circles $s=0, 1, \dots, 6$ and presented in table 1.

For these values of nodal diameters and nodal circles, the modal shapes for a circular plate clamped all around in polar coordinates are illustrated in figures 1 – 7, by using the first relation of the system (13), respectively taking $\cos(n\theta)$ into account. In this case, the inflection points of the odd nodal diameters (n) pass through the y axis, and the modal function along this direction has zero value.

If the second relation of the system (13) is used, which takes $\sin(n\theta)$ into account, the representation of the modal shapes is rotated by 90 degrees, respectively, the inflection points of the modal shapes for odd nodal diameters (n) pass through the x axis (fig. 8 – 10).

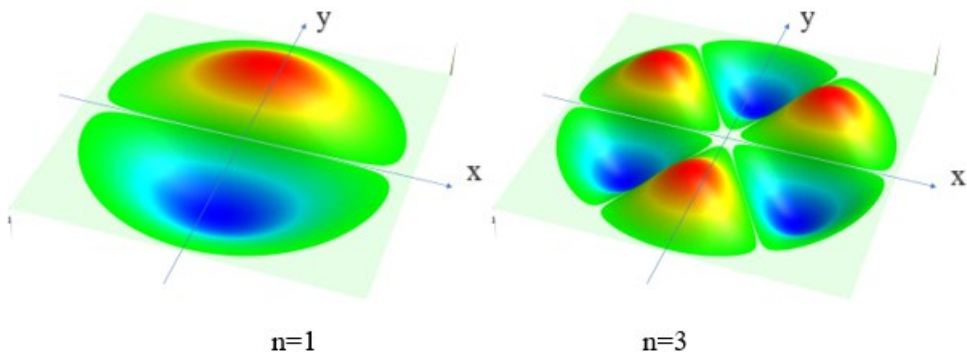


Figure 8. Mode shapes for the circular plate clamped all around with $\sin(n\theta)$; nodal circle $s=0$.

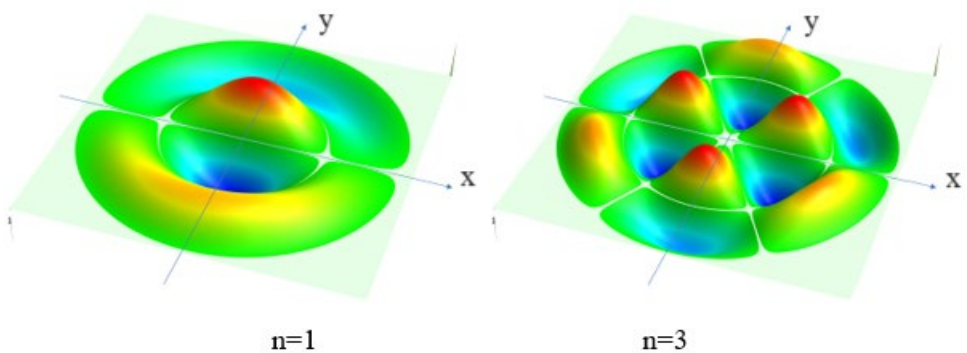


Figure 9. Mode shapes for the circular plate clamped all around with $\sin(n\theta)$; nodal circle $s=1$.

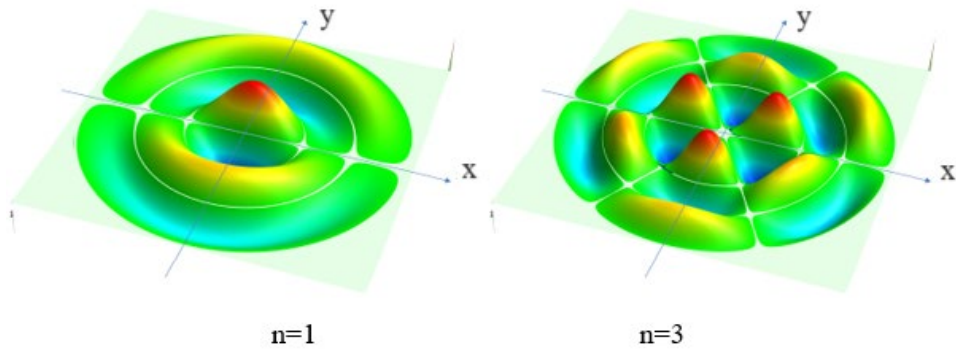


Figure 10. Mode shapes for the circular plate clamped all around with $\sin(n\theta)$; nodal circle $s=2$.

References

- 1 Gillich G.R., Praisach Z.I., Ntakpe J.L., Hațiegan C., An Analysis of the Dynamic Behavior of Circular Plates from a Damage Detection Perspective, *Romanian Journal of Acoustic and Vibrations*, 11(1), 2014, pp. 41-46,
- 2 Praisach Z.I., Micliuc. D.M., Gillich G.R., Korca, Z.I., Natural Frequency Shift of Damaged Circular Plate Clamped All Around, *ANNALS of Faculty Engineering Hunedoara – International Journal of Engineering*, 14(4), 2016, pp.57-62.
- 3 Senjanovic I., Hadzic,N., Vladimir N., Cho D.-S., Natural vibrations of thick circular plate based on the modified Mindlin theory, *Arch. Mech.*, 66(6), 2014, pp. 389-409.
- 4 Thakare S.B., Damale A.V., Free vibration of circular plates with holes and cutouts, *IOSR Journal of Mechanical and Civil Engineering (IOSR-JMCE)*, 8(2), 2013, pp. 46-54,
- 5 Wei G.W., Zhao,Y.B., Xiang Y., The determination of natural frequencies of rectangular plates with mixed boundary conditions by discrete singular convolution, *International Journal of Mechanical Sciences*, 43, 2001, pp. 1731-1746.
- 6 Matthews D., Sun H., Saltmarsh K., Wilkes D., Munyard A., Pan J., *A detailed experimental modal analysis of a clamped circular plate*, Inter.Noise, Melbourne, Australia, 2014.
- 7 Mindlin R.D., *An introduction to the mathematical theory of vibrations of elastic plates*, World Scientific Publishing, 2006.
- 8 Timoshenko S., Woinowsky-Krieger S., *Theory of plates and shells*, McGraw-Hill Publishing Co., N.Y., 1959.
- 9 Reddy J.N., *Theory and analysis of elastic plates*, Taylor and Francis, Philadelphia, 1999.

- 10 Renton J.D., *Elastic Beams and Frames*, Second edition, Woodhead Publishing, Philadelphia, USA, 2011.
- 11 Leissa A., *Vibration of plates*, NASA SP, Scientific and Technical Information Division, National Aeronautics and Space Administration, 1969.

Addresses:

- PhD. Stud. Eng. Lucian Nestor Manu, Doctoral School of Engineering, Babeş-Bolyai University, Cluj-Napoca, Romania, Faculty of Engineering, Piaţa Traian Vuia, nr. 1-4, 320085, Reşiţa, Romania
lucian.manu@ubbcluj.ro
- Lect. PhD. Habil. Eng. Zeno-Iosif Praisach, Department of Engineering Science, Babeş-Bolyai University. Cluj-Napoca, Romania, Faculty of Engineering, Piaţa Traian Vuia, nr. 1-4, 320085, Reşiţa, Romania
zeno.praisach@ubbcluj.ro
(* *corresponding author*)
- Prof. PhD. Eng. Gilbert-Rainer Gillich, Department of Engineering Science, Babeş-Bolyai University. Cluj-Napoca, Romania, Faculty of Engineering, Piaţa Traian Vuia, nr. 1-4, 320085, Reşiţa, Romania
gilbert.gillich@ubbcluj.ro
- Lect. PhD. Eng. Cristian Tufiş, Department of Engineering Science, Babeş-Bolyai University. Cluj-Napoca, Romania, Faculty of Engineering, Piaţa Traian Vuia, nr. 1-4, 320085, Reşiţa, Romania
cristian.tufisi@ubbcluj.ro

Dynamic behavior of a clamped circular plate and strain energy representation (part II)

Ionela Harea, Zeno-Iosif Praisach*, Gilbert-Rainer Gillich,
Cristian Tufiș

Abstract. *The paper presents the strain energy of the circular plate clamped all around through a relation obtained analytically and the graphic representation of the modal shapes and the maximum normalized strain energy along the x axis. Depending on the number of nodal circles s and the nodal diameters n , the maximum strain energy can be both in the center of the circular plate clamped all around, as well as the first ventral points from the center of the circular plate towards the outside of the plate.*

Keywords: *circular plate, Bessel functions, strain energy*

1. Introduction

In the second part of the paper, the authors present the strain energy of the circular plate clamped all around through a relation obtained analytically by using Bessel functions and the graphic representation of the modal shapes and the maximum normalized strain energy along the x axis, according to fig. 1 – 7 from first part of the paper.

In this context, the bibliographic references and the bibliography are identical to the one presented in the first part of the paper.

2. Strain energy

The strain energy of bending and twisting of the plate expressed in polar coordinates [11] is:

$$U = \frac{D}{2} \int_A \left(\begin{aligned} & \left(\frac{\partial^2 W}{\partial r^2} + \frac{1}{r} \frac{\partial W}{\partial r} + \frac{1}{r^2} \frac{\partial^2 W}{\partial \theta^2} \right)^2 - \\ & - 2(1 - \nu) \left\{ \frac{\partial^2 W}{\partial r^2} \left(\frac{1}{r} \frac{\partial W}{\partial r} + \frac{1}{r^2} \frac{\partial^2 W}{\partial \theta^2} \right) - \left[\frac{\partial}{\partial r} \left(\frac{1}{r} \frac{\partial W}{\partial \theta} \right) \right]^2 \right\} \end{aligned} \right) dA \quad (1)$$



where,

$dA=r \cdot dr \cdot d\theta$

D [Nm] is the flexural rigidity

ν is Poisson's ratio

r [m] is the plate radius

θ [rad] is the angle for polar coordinates

The strain energy is directly proportional to the second-order derivative of the modal function, respectively:

$$\begin{cases} \frac{\partial^2 W(r,\theta)_{n,s}}{\partial r^2} = -n^2 \left[\frac{\partial^2 J_n(\lambda, \frac{r}{R})}{\partial \lambda^2} - \frac{J_n(\lambda)}{I_n(\lambda)} \cdot \frac{\partial^2 I_n(\lambda, \frac{r}{R})}{\partial \lambda^2} \right] \cos(n\theta) \\ \frac{\partial^2 W(r,\theta)_{n,s}}{\partial r^2} = -n^2 \left[\frac{\partial^2 J_n(\lambda, \frac{r}{R})}{\partial \lambda^2} - \frac{J_n(\lambda)}{I_n(\lambda)} \cdot \frac{\partial^2 I_n(\lambda, \frac{r}{R})}{\partial \lambda^2} \right] \sin(n\theta) \end{cases} \quad (2)$$

The relations are used for the derivation of the Bessel functions:

$$\begin{cases} \frac{\partial J_n(\lambda, \frac{r}{R})}{\partial \lambda} = -J_{n+1}(\lambda) + \frac{n}{\lambda} J_n(\lambda) = J_{n-1}(\lambda) - \frac{n}{\lambda} J_n(\lambda) \\ \frac{\partial I_n(\lambda, \frac{r}{R})}{\partial \lambda} = I_{n+1}(\lambda) + \frac{n}{\lambda} I_n(\lambda) = I_{n-1}(\lambda) - \frac{n}{\lambda} I_n(\lambda) \end{cases} \quad (3)$$

and the strain energy function becomes:

$$\begin{cases} \frac{\partial^2 W(r,\theta)_{n,s}}{\partial r^2} = \left[\begin{array}{l} \frac{n^2-n-\lambda^2}{\lambda^2} J_n\left(\lambda, \frac{r}{R}\right) + \frac{1}{\lambda} J_{n+1}\left(\lambda, \frac{r}{R}\right) - \\ - \frac{J_n(\lambda)}{I_n(\lambda)} \left(\frac{n^2-n+\lambda^2}{\lambda^2} I_n\left(\lambda, \frac{r}{R}\right) - \frac{1}{\lambda} I_{n+1}\left(\lambda, \frac{r}{R}\right) \right) \end{array} \right] \cos(n\theta) \\ \frac{\partial^2 W(r,\theta)_{n,s}}{\partial r^2} = \left[\begin{array}{l} \frac{n^2-n-\lambda^2}{\lambda^2} J_n\left(\lambda, \frac{r}{R}\right) + \frac{1}{\lambda} J_{n+1}\left(\lambda, \frac{r}{R}\right) - \\ - \frac{J_n(\lambda)}{I_n(\lambda)} \left(\frac{n^2-n+\lambda^2}{\lambda^2} I_n\left(\lambda, \frac{r}{R}\right) - \frac{1}{\lambda} I_{n+1}\left(\lambda, \frac{r}{R}\right) \right) \end{array} \right] \sin(n\theta) \end{cases} \quad (4)$$

It can be seen from (4) that the strain energy function is a surface function of r/R and the angle θ .

3. Results

The maximum strain energy from the first relation (4) is obtained along the x direction with de notation from fig. 1 – 7 from first part of the paper.

For the dimensionless wave numbers presented in tab. 1 (part I of the paper), below, in figures 1 - 7 are presented the modal shapes and the maximum strain energy along the x direction.

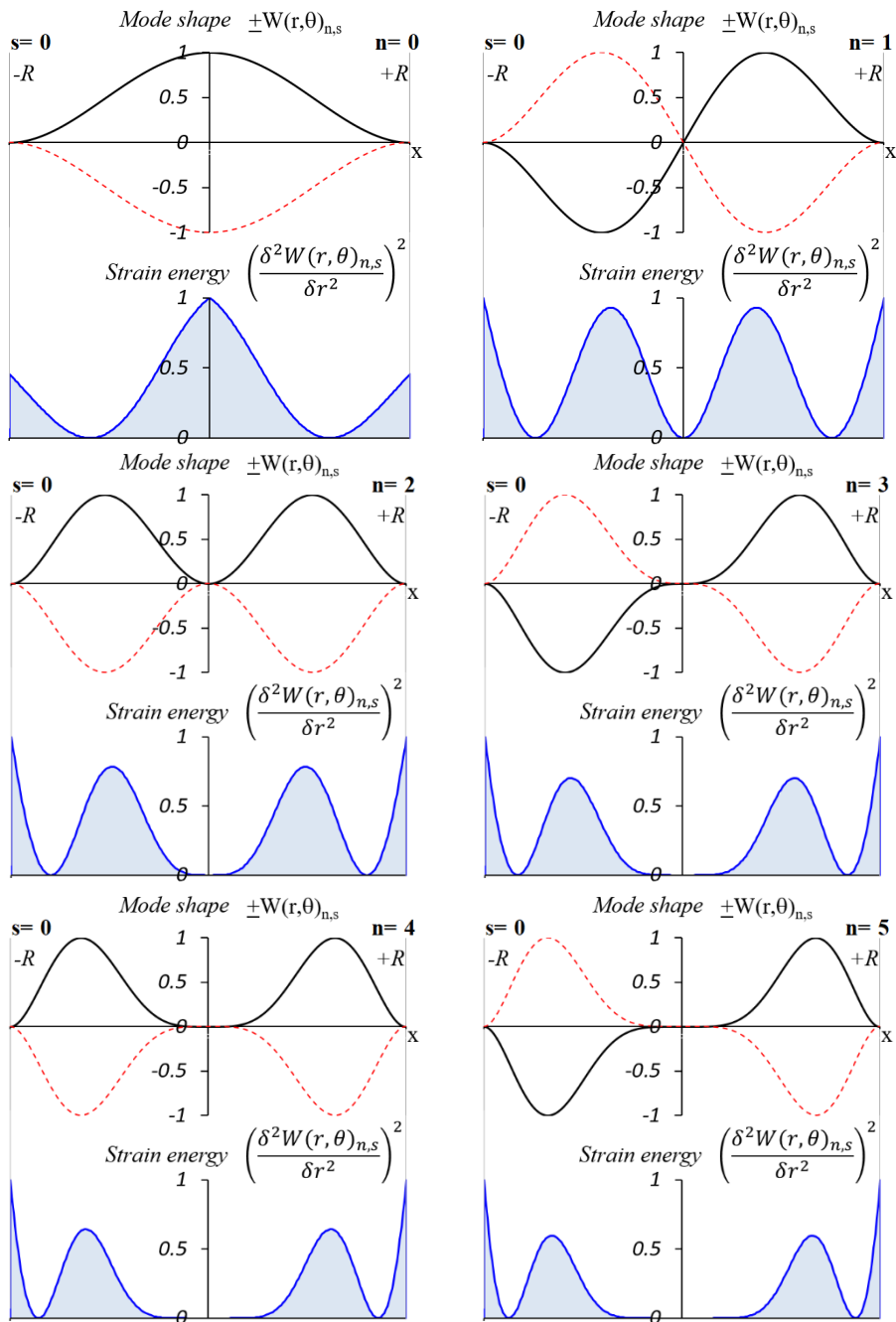


Figure 1. Normalized mode shape and strain energy for $s=0$ and $n=0, \dots, 5$.

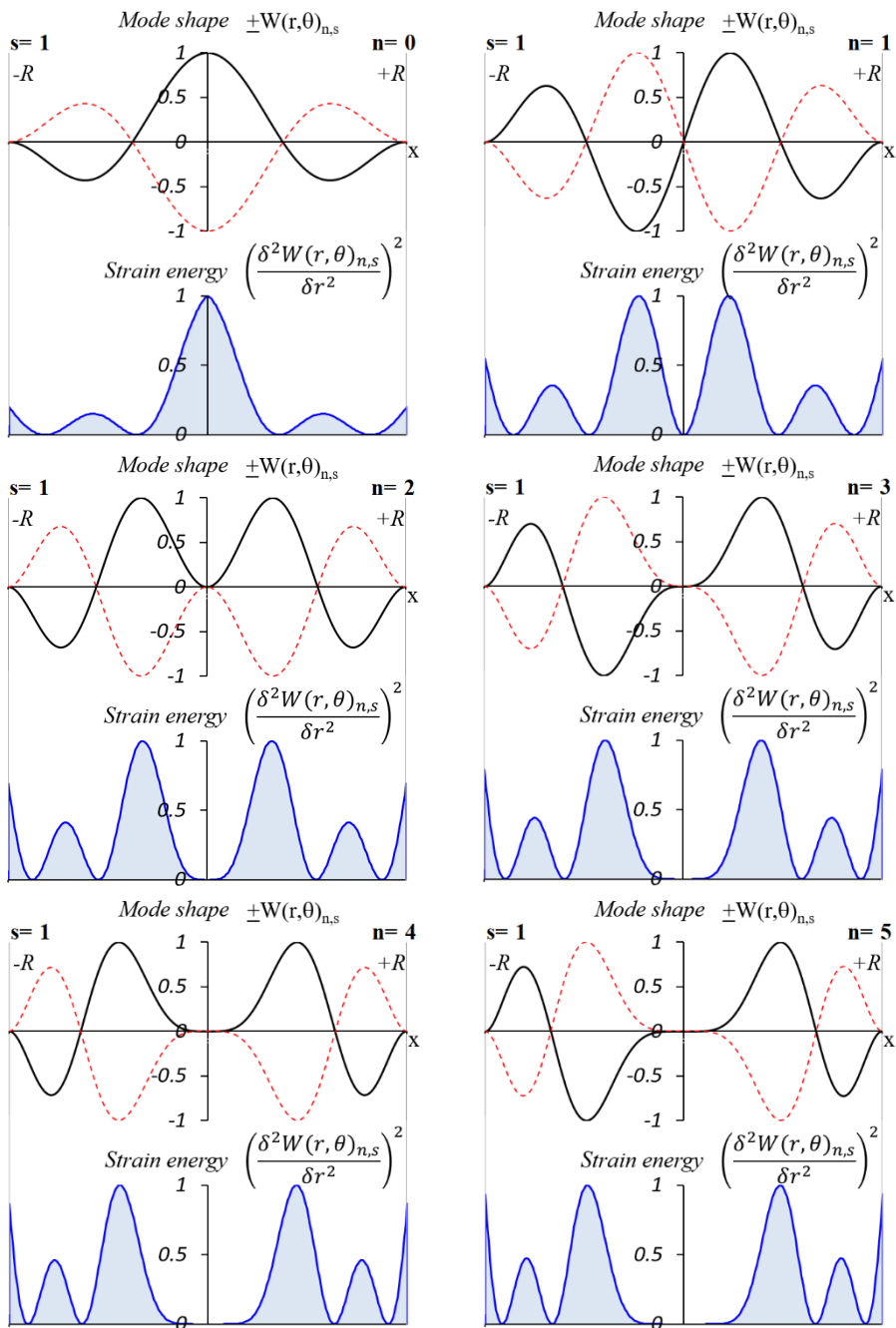


Figure 2. Normalized mode shape and strain energy for $s=1$ and $n=0, \dots, 5$.

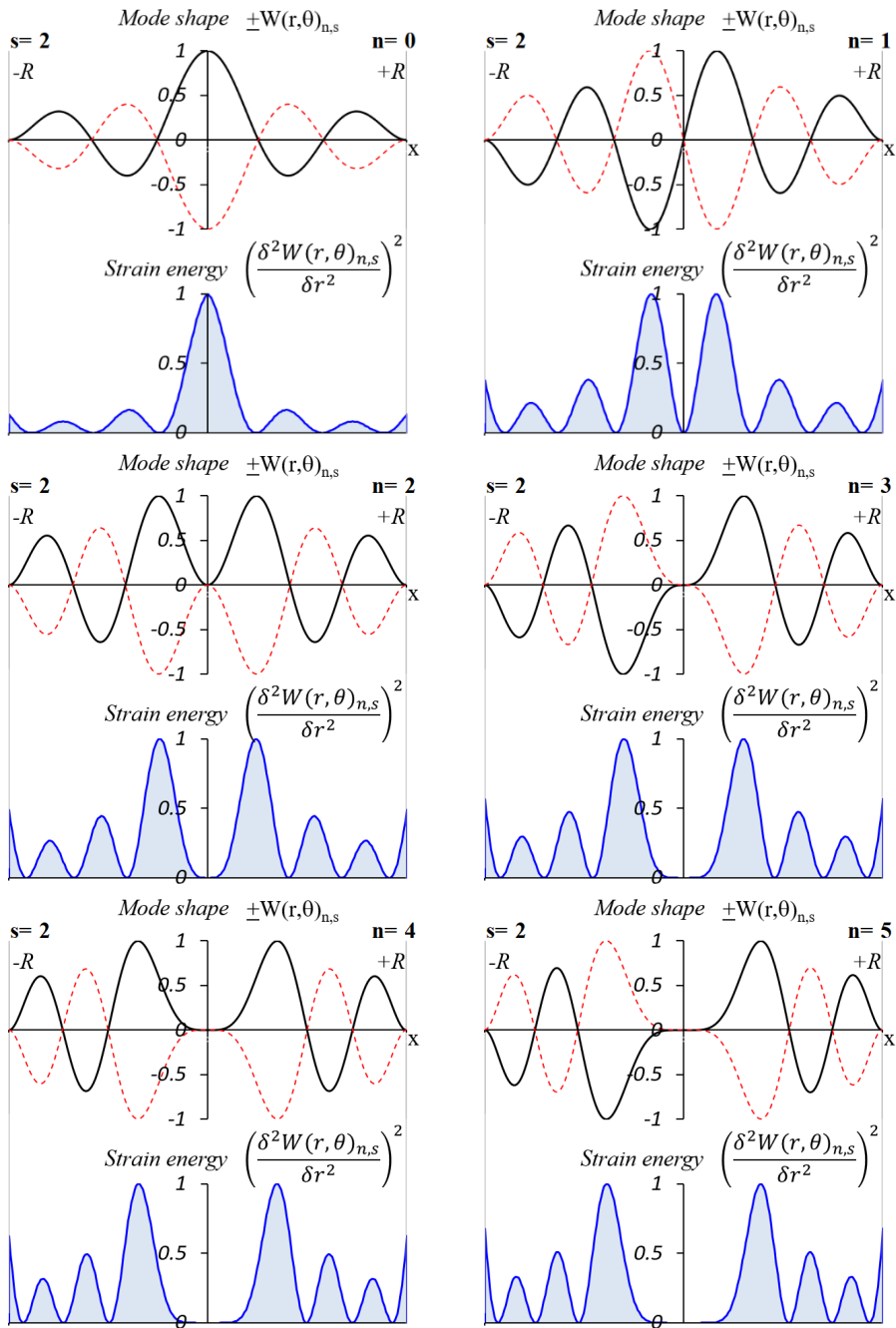


Figure 3. Normalized mode shape and strain energy for $s=2$ and $n=0, \dots, 5$.

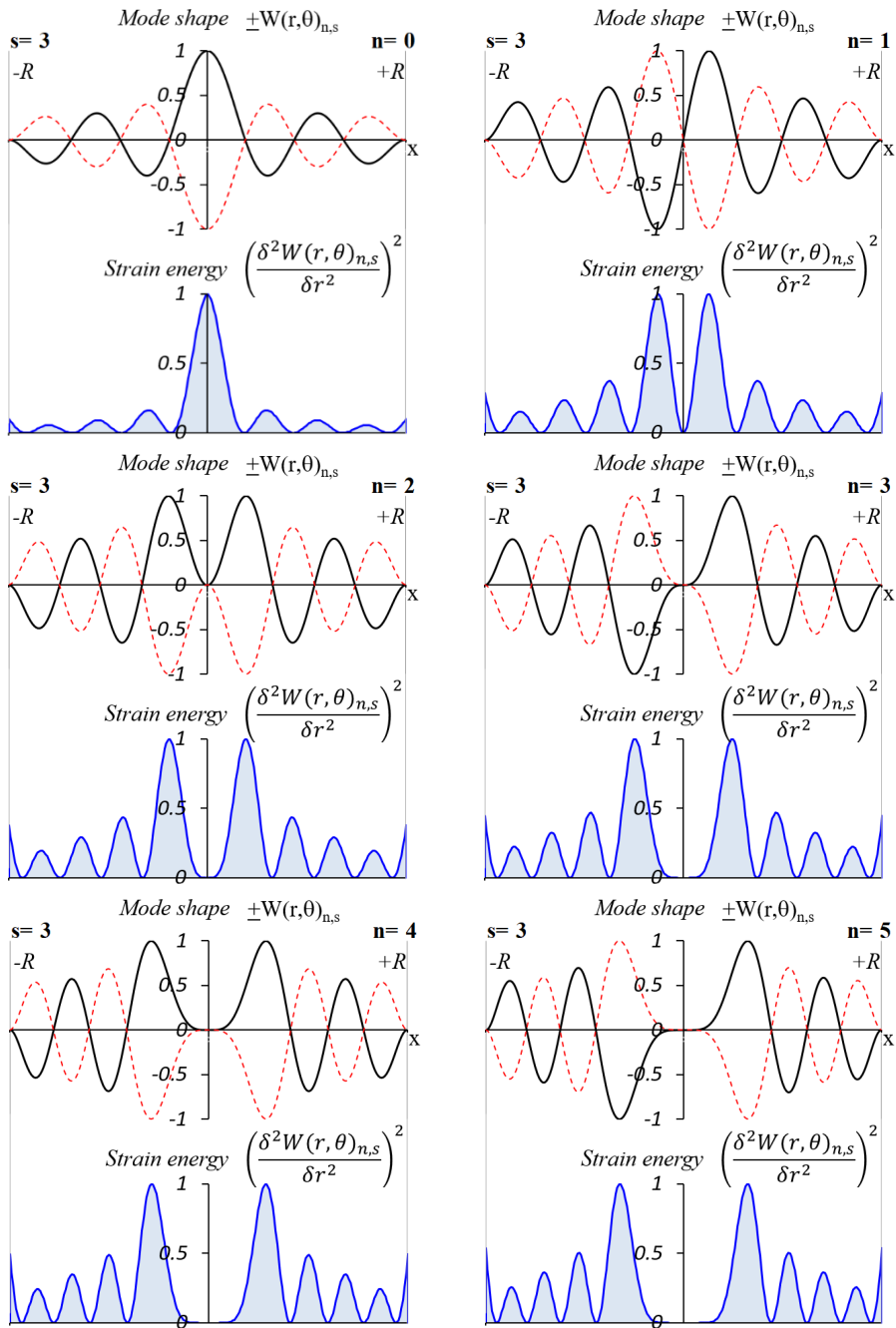


Figure 4. Normalized mode shape and strain energy for $s=3$ and $n=0, \dots, 5$.

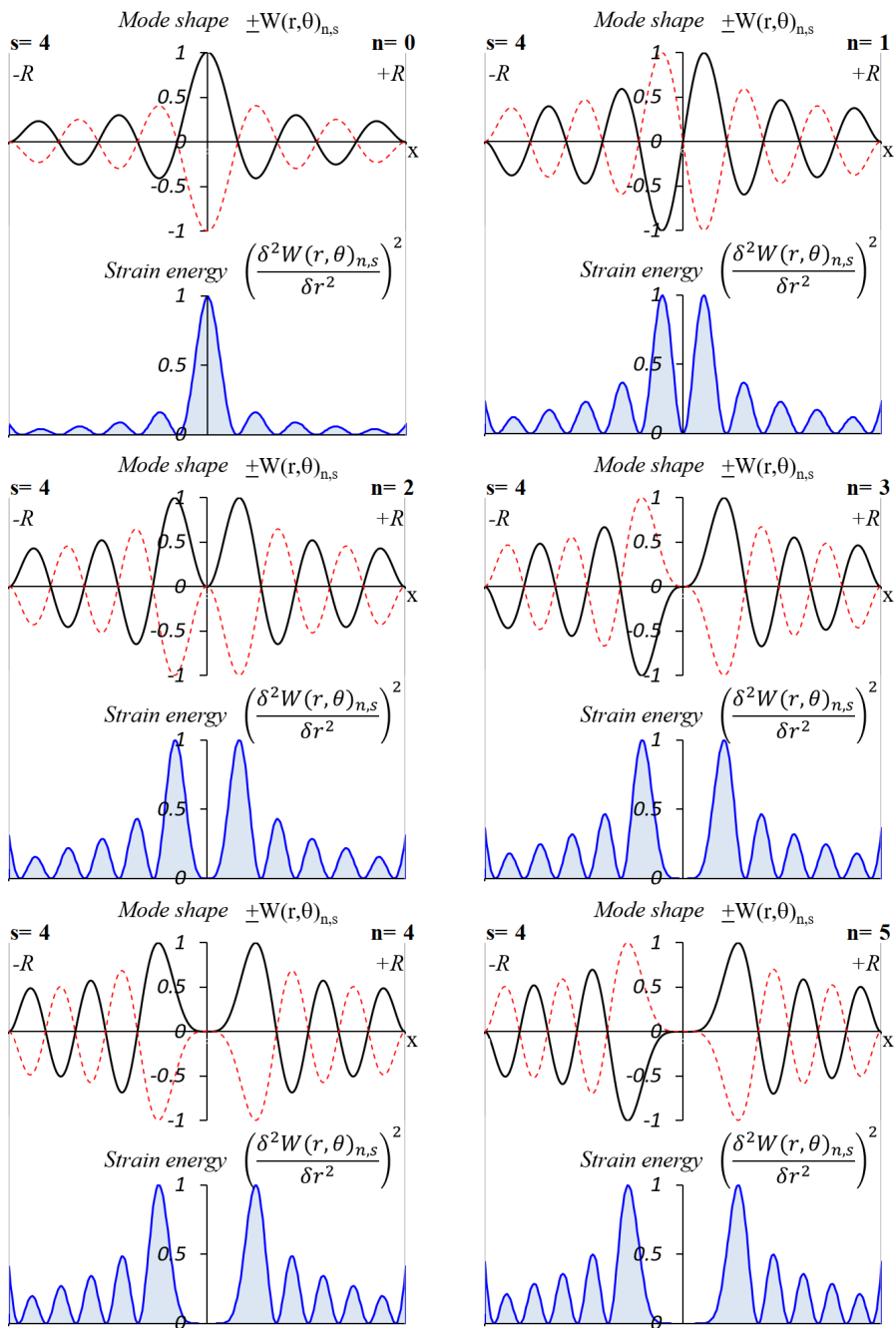


Figure 5. Normalized mode shape and strain energy for $s=4$ and $n=0, \dots, 5$.

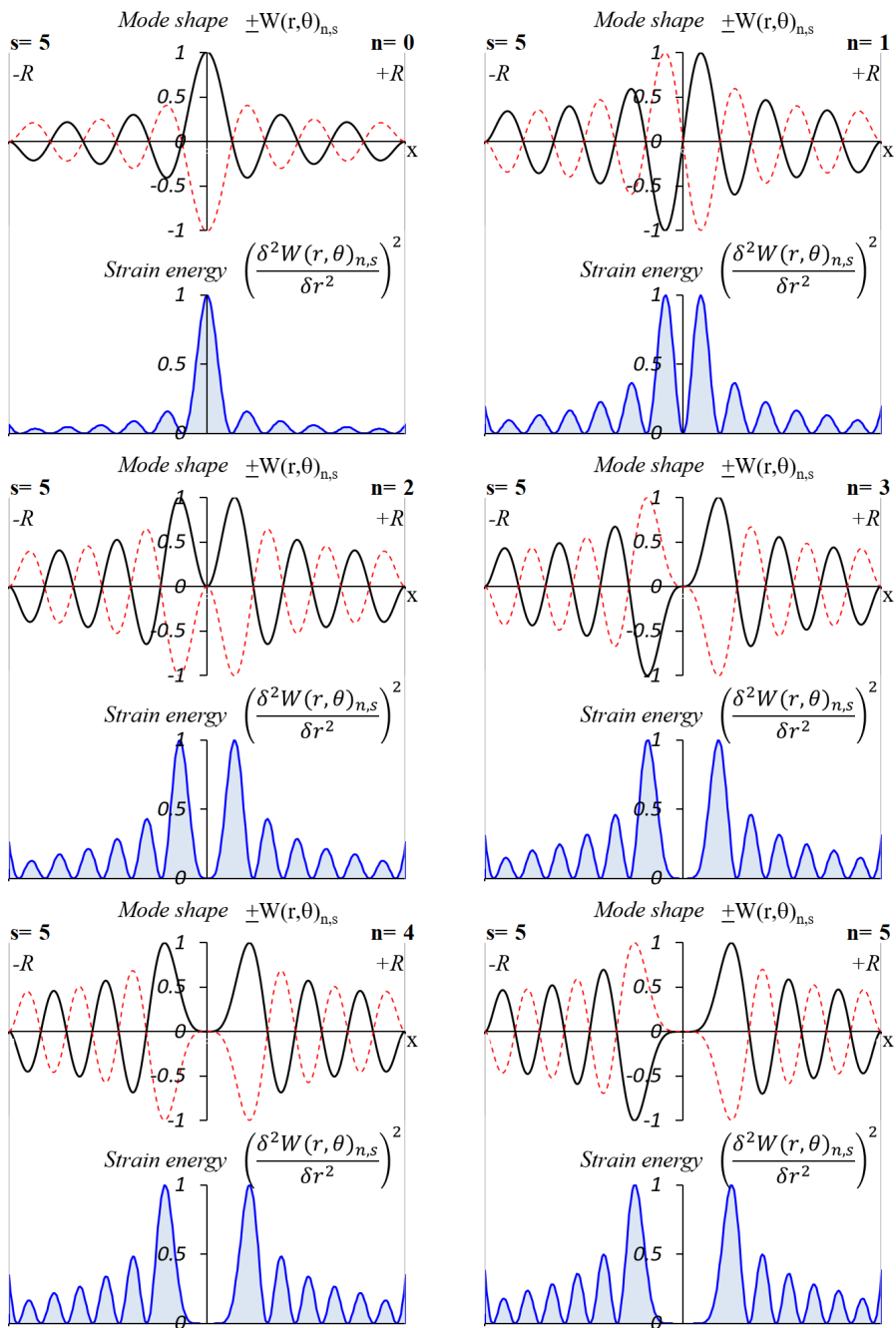


Figure 6. Normalized mode shape and strain energy for $s=5$ and $n=0, \dots, 5$.

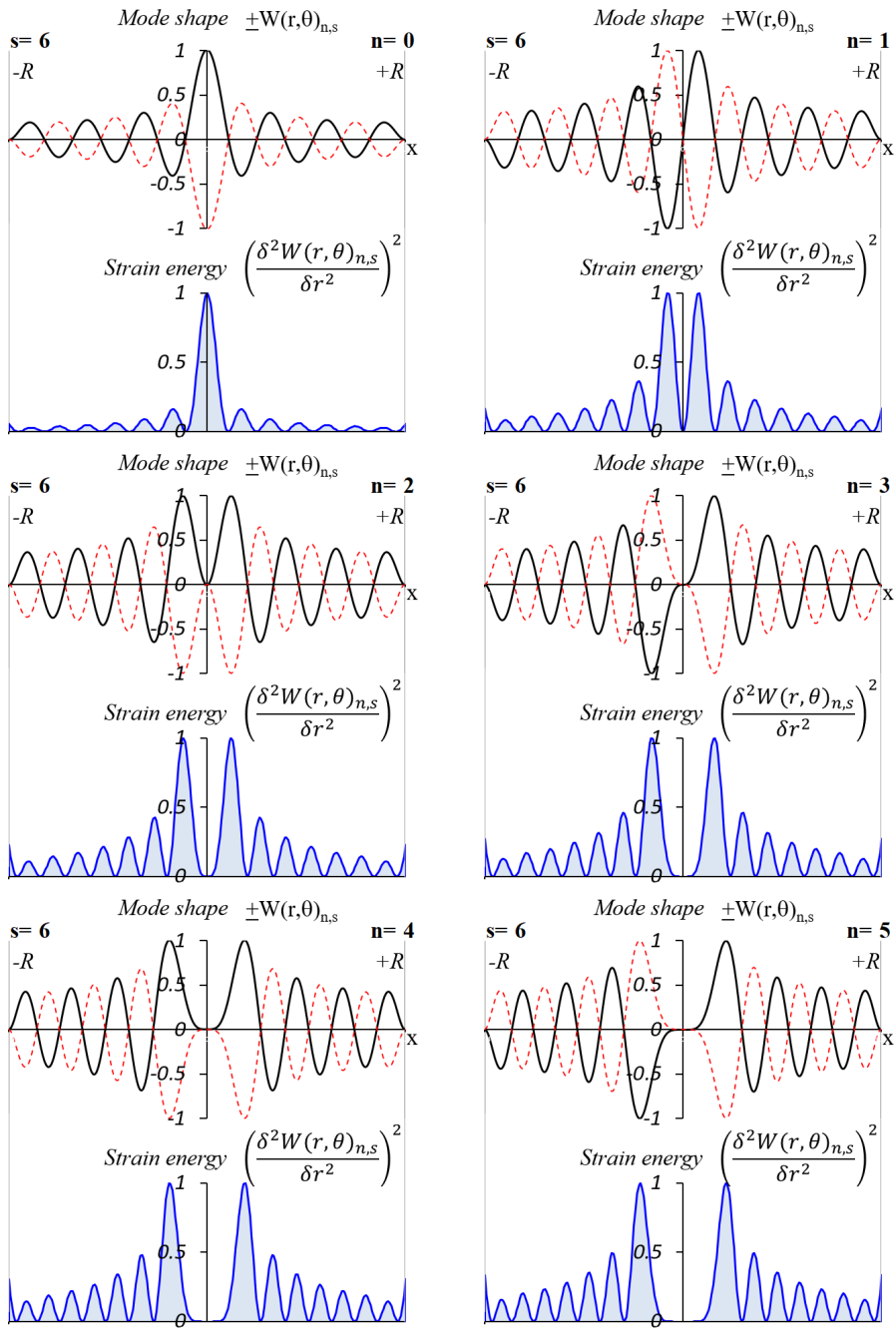


Figure 7. Normalized mode shape and strain energy for $s=6$ and $n=0, \dots, 5$.

Fig. 1 present the first six vibration modes and normalized strain energy for nodal circle $s=0$ and nodal diameters $n=0, 1, 2, 3, 4$ and 5 on x direction.

Fig. 2 present the first six vibration modes and normalized strain energy for nodal circle $s=1$ and nodal diameters $n=0, 1, 2, 3, 4$ and 5 on x direction.

Fig. 3 present the first six vibration modes and normalized strain energy for nodal circle $s=2$ and nodal diameters $n=0, 1, 2, 3, 4$ and 5 on x direction.

Fig. 4 present the first six vibration modes and normalized strain energy for nodal circle $s=3$ and nodal diameters $n=0, 1, 2, 3, 4$ and 5 on x direction.

Fig. 5 present the first six vibration modes and normalized strain energy for nodal circle $s=4$ and nodal diameters $n=0, 1, 2, 3, 4$ and 5 on x direction.

Fig. 6 present the first six vibration modes and normalized strain energy for nodal circle $s=5$ and nodal diameters $n=0, 1, 2, 3, 4$ and 5 on x direction.

Fig. 7 present the first six vibration modes and normalized strain energy for nodal circle $s=6$ and nodal diameters $n=0, 1, 2, 3, 4$ and 5 on x direction.

4. Conclusion

The paper presents the normalized vibration modes and strain energy for a circular plate clamped all around obtained for the maximum value of strain energy on x direction taking into consideration the first relationship (4). Using the Bessel functions of the first kind, the strain energy function was analytically determined.

The normalized mode shape and strain energy is illustrated in fig. 1 – 7 for the following dimensionless wave numbers $\lambda_{n,s}^2$: nodal circles $s=0, 1, \dots, 6$ and nodal diameters $n=0, 1, \dots, 5$.

From the analysis of figures 1 - 7 it can be found that the maximum normalized strain energy is in the center of the circular plate clamped all around, for the nodal diameter $n=0$ regardless of the number of nodal circles s . For values of nodal diameters $n>0$ the strain energy becomes zero in the center of the plate.

For $s=0$ and $n>0$, the strain energy is maximum at the clamped area of the circular plate.

For $s>0$ and $n>0$, the deformation energy is maximum at the first ventral point from the center of the plate, compared to the case of the doubly supported beam where the maximum strain energy is right at the clamped end. As the number of nodal diameters n increases, the maximum strain energy keeps moving away from the center of the circular plate.

Taking into account the 3D representation of the mode shapes (presented in part I), it is found that for $n=1$ we have one diameter of inflection, for $n=2$ we have 4 diameters of inflection, for $n=3$ there are 6 diameters of inflection, and so on, so we can say that for $n>1$, the number of inflection diameters is equal to $2n$. The number of inflection circles is equal to the number of nodal circles s .

References

- 1 Gillich G.R., Praisach Z.I., Ntakpe J.L., Hațiegan C., An Analysis of the Dynamic Behavior of Circular Plates from a Damage Detection Perspective, *Romanian Journal of Acoustic and Vibrations*, 11(1), 2014, pp. 41-46.
- 2 Praisach Z.I., Micliuc. D.M., Gillich G.R., Korca Z.I., Natural Frequency Shift of Damaged Circular Plate Clamped All Around, *ANNALS of Faculty Engineering Hunedoara – International Journal of Engineering*, 14(4), 2016, pp.57-62.
- 3 Senjanovic I., Hadzic N., Vladimir N., Cho D.-S., Natural vibrations of thick circular plate based on the modified Mindlin theory, *Arch. Mech.*, 66(6), 2014, pp. 389-409.
- 4 Thakare S.B., Damale A.V., Free vibration of circular plates with holes and cutouts, *IOSR Journal of Mechanical and Civil Engineering (IOSR-JMCE)*, 8(2), 2013, pp. 46-54.
- 5 Wei G.W., Zhao Y.B., Xiang Y., The determination of natural frequencies of rectangular plates with mixed boundary conditions by discrete singular convolution, *International Journal of Mechanical Sciences*, 43, 2001, pp. 1731-1746.
- 6 Matthews D., Sun H., Saltmarsh K., Wilkes D., Munyard A., Pan J., *A detailed experimental modal analysis of a clamped circular plate*, Inter. Noise, Melbourne, Australia, 2014.
- 7 Mindlin R.D., *An introduction to the mathematical theory of vibrations of elastic plates*, World Scientific Publishing, 2006.
- 8 Timoshenko S., Woinowsky-Krieger S., *Theory of plates and shells*, McGraw-Hill Publishing Co., N.Y., 1959.
- 9 Reddy J.N., *Theory and analysis of elastic plates*, Taylor and Francis, Philadelphia, 1999.
- 10 Renton J.D., *Elastic Beams and Frames*, Second edition, Woodhead Publishing, Philadelphia, USA, 2011.
- 11 Leissa A., *Vibration of plates*, NASA SP, Scientific and Technical Information Division, National Aeronautics and Space Administration, 1969.

Addresses:

- PhD. Stud. Eng. Ionela Harea, Doctoral School of Engineering, Babeş-Bolyai University, Cluj-Napoca, Romania, Faculty of Engineering, Piața Traian Vuia, nr. 1-4, 320085, Reșița, Romania
ionela.harea@ubbcluj.ro

- Lect. PhD. Habil. Eng. Zeno-Iosif Praisach, Department of Engineering Science, Babeş-Bolyai University. Cluj-Napoca, Romania, Faculty of Engineering, Piața Traian Vuia, nr. 1-4, 320085, Reșița, Romania
zeno.praisach@ubbcluj.ro
(* *corresponding author*)
- Prof. PhD. Eng. Gilbert-Rainer Gillich, Department of Engineering Science, Babeş-Bolyai University. Cluj-Napoca, Romania, Faculty of Engineering, Piața Traian Vuia, nr. 1-4, 320085, Reșița, Romania
gilbert.gillich@ubbcluj.ro
- Lect. PhD. Eng. Cristian Tufiși, Department of Engineering Science, Babeş-Bolyai University. Cluj-Napoca, Romania, Faculty of Engineering, Piața Traian Vuia, nr. 1-4, 320085, Reșița, Romania
cristian.tufisi@ubbcluj.ro